2004

Robust control design for an electrohydraulic wheel loader system with a human-in-the-loop assessment in a virtual environment

Roger Fales
Iowa State University

Robust control design for an electrohydraulic wheel loader system with a human-in-the-loop assessment in a virtual environment

by

Roger Fales

A dissertation submitted to the graduate faculty

in partial fulfillment of the requirements for the degree of

DOCTOR OF PHILOSOPHY

Major: Mechanical Engineering

Program of Study Committee:
Atul G. Kelkar, Major Professor
James Bernard
Greg Luecke
Brian Steward
Judy Vance

Iowa State University

Ames, Iowa

2004

Graduate College
Iowa State University

This is to certify that the doctoral dissertation of

Roger Fales

has met the dissertation requirements of Iowa State University

Signature was redacted for privacy.

Committee Member

Signature was redacted for privacy.

Committee Member

Signature was redacted for privacy.

Committee Member

Signature was redacted for privacy.

Committee Member

Signature was redacted for privacy.

Major Professor

Signature was redacted for privacy.

For the Major Program

DEDICATION

I dedicate this dissertation to my parents.

TABLE OF CONTENTS

LIST OF TABLES

LIST OF FIGURES

CHAPTER 1. INTRODUCTION AND LITERATURE REVIEW

1.1 Introduction

This dissertation presents a comprehensive report on the research activity that primarily focused on developing a high-fidelity dynamic simulation for an off-highway machine with embedded ability to do advanced control system analysis and design and to assess operator response in the real-time Virtual Reality (VR) environment. The off-highway machine used as the focus configuration was a 744 Model of Deere's wheel loader (see Fig. 1.1). Wheel loaders are used for material handling and excavation for construction, industrial, and agricultural purposes. The wheel loader has a linkage attached to the front of the machine used for manipulating a bucket or other work tool. The machine has four large wheels and has an articulation joint in the middle for steering. The linkage, steering, and drive systems draw power from an engine driven hydraulic pump.

Mobile hydraulic systems are different from systems known as hydraulic servo systems (HSS) which are used in aerospace and industrial applications. Mobile hydraulic systems are optimized for high energy efficiency, tolerance to contamination, and low cost compared to other applications of hydraulics. Energy efficiency is the main reason for use of load sensing pumps and overlapped valves in mobile systems. Low cost is achieved by using inexpensive proportional flow valves as opposed to servo valves used in other applications.

One of the purposes of this work is to model the dynamics and control system of a wheel loader so that machine characteristics can be evaluated in VR with high fidelity models without building a physical prototype. A dynamic model of the machine could include several aspects such as the engine, engine controls, digging forces, tires, drive train, traction, etc. However,

for the work represented in this paper, the dynamic system is assumed to be limited to the wheel loader electro-hydraulics and linkage.

Control system design for construction machinery poses many challenges. The dynamics of electro-hydraulically controlled wheel loader is highly nonlinear and complex due to several nonlinearities arising from the hydraulic subsystem. Furthermore, the operating conditions span over a wide range which leads to a wide variety of loading conditions. This necessitates consideration of robust performance and stability in the design of control system. The stability and performance robustness directly relate to safety and customer satisfaction, and therefore become important from industry's perspective. The coupling of the system further complicates the control design process. The existing control design practice in industry is primarily based on single-input single-output (SISO) classical frequency-domain techniques. Such methodology has inherent limitations due to limited design freedom and lack of robust synthesis methods.

In this dissertation, the control design focus is on designing PI, LQG, H_∞, and nonlinear controllers for a hydraulic front loader and comparing these designs for possible implementation on a real-life machine. The objective of the control system design is to track a coordinated linkage motion reference called "level lift". The control designs based on linear techniques are developed using a linearized model of the nonlinear dynamics about a typical operating point. The nonlinear control designs employ a technique which eliminates many of the nonlinear characteristics from the system model. Simulation results are presented to demonstrate the effectiveness of each controller using a realistic nonlinear loader model.

In the design process for construction and earth moving machines, an important step is to test the prototypes with human interaction. As a part of this step, operators give valuable feedback to designers about their perception of machine performance, layout, and ergonomics. However, building prototypes is expensive and time consuming. Therefore, one must build fewer prototypes and rely more on computer simulations. To get valuable feedback from operators without the expense of prototypes, VR machine simulations can be used very effectively.

The three main objectives of the research presented in this paper are as follows. First, we demonstrate a real-time dynamic simulation in VR using the wheel loader as a test case. Next,

electrohydraulic (EH) control algorithms are developed for linkage coordination. Finally, a *closed-loop* control system simulation with the operator-in-the-loop is developed in the virtual reality environment.

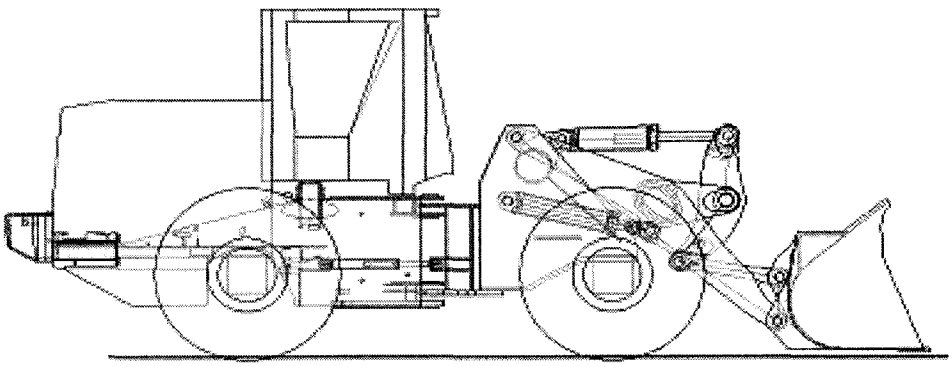

Figure 1.1 Side view of wheel Loader

1.2 Literature Review

This section attempts to summarize some of the existing literature that relates to the research work presented in this dissertation. From the literature review, it is concluded that modeling, control design, and VR simulations are rarely discussed together. The literature review revealed relatively few publications concerning modeling, control design, and VR simulations. Subsequent paragraphs give brief overview of the literature search in these three areas.

1.2.1 Modeling

Standardized software techniques exist for modeling the dynamics of off highway machinery. There exists several commercial modeling and simulation programs such as Dymola [21], Dynasty, Easy5, Hydraulics Block-Set, and others which have hydraulic system modeling capability along with the capability to model other types of systems such as linkages and electrical systems. Most efforts at modeling hydraulic systems were based on techniques from a 1967

book by H. E. Merritt[14]. Merritt's work is cited in most of the papers pertaining to hydraulics in the bibliography of this work.

1.2.2 Control Design

There exists some literature on advanced control of construction type machinery. The work done is primarily by the academic community in the area of advanced control design for such machinery[11]. For example, H_2 and H_∞ control designs were presented for a hydraulic power train in [10]. However, these efforts focussed on systems which lack some of the characteristics that are found in typical mobile hydraulic machines such as the load sensing pump presented in this work. There is work based on control of realistic systems with load sensing pumps[26][27]. Though they concentrate on stability of the system, these works are not based on recent robust control theory as in this dissertation. A control design based on feedback linearization was developed for a load sensing hydraulic system[25]. However that system was for the control of a single rotary motor using a servo valve.

The nonlinear control technique known as feedback linearization was evaluated by some researchers in recent years for use with hydraulic control systems [18]. Feedback linearization is a nonlinear design method by which the nonlinearities of the system are cancelled by using a compensator on the input with feedback such that the system appears to be linear. A particularly promising technique related to feedback linearization known as load force control was used to eliminate the nonlinearities in the pressure dynamics of a SISO system which consisted of a valve controlled hydraulic servo systems. As an example the nonlinearity due to fluid flow through an orifice which is related to the square root of the pressure difference between the inlet and outlet can be eliminated by feedback linearization. The Popov criteria from nonlinear system theory was used to prove that systems with load force control with feedback linearization are stable for a range of variations in the fluid elasticity [19].

1.2.3 VR Simulation

A literature review shows that dynamic systems were simulated in VR for various purposes. Most notably aircraft flight simulators were used for training, design review, and games. Also, driving simulators such as the Iowa Driving Simulator were built with realistic graphics and vehicle dynamics [24].

Currently, machine concepts are evaluated in the VR environment before they are realized as actual hardware. This includes viewing and interacting with the static machine geometry. Also, there was some work done to allow a person to operate a type of construction equipment know as a hydraulic excavator in VR using joysticks and other input devices [9][8]. There are even VR simulations of machines which can interact with their environments in terms of digging forces [5]. A virtual prototype machine based on a detailed wheel loader model was developed for evaluating steering performance [22]. Such simulations are extremely useful for developing and testing of machine controls and related systems before a prototype is built.

One of the main barriers to VR simulation in the past was the computational speed requirement for real-time simulation. Some work was done to model a wheel loader chassis and hydraulic system in VR environment using multi-rate integration to speed up the overall model execution [2][1]. Modern desktop computers now allow complex simulations to run in real time.

1.3 Contributions

The contributions of this research span over three different areas: dynamic modeling, control design, and VR interface. The contributions in the modeling primarily relate to the modeling of hydraulic systems. The model used for analysis in this work includes a load sensing pump. Load sensing pumps are rarely considered in the research which focuses on advanced robust control design techniques such as mixed sensitivity H_∞ design. It is often reasonable to eliminate pump dynamics from models by assuming that the pump is an ideal pressure source. This is a common practice for much of the research focused on hydraulic servo systems which are designed to have a constant supply pressure. In the model presented in this work, the

pump pressure varies greatly while the pump control system attempts to maintain a constant pressure drop across a particular metering orifice associated with the highest pressure load.

In this work a new analysis of how feedback linearization effects the robustness of a hydraulic system is presented. This analysis is based on linear robust control theory. It is shown that feedback linearization reduces the effects of the dynamics which are most related to the robustness issues.

A new virtual reality-based assessment of a wheel loader control system is presented in this work. An operator can operate a virtual wheel loader electro-hydraulically actuated linkage system with and without the aid of the control system. Data can be collected during the simulation for later analysis. A simple test is presented that explores the difficulty of operating the wheel loader without the aid of an automatic control system. The feedback controller is shown to make a great improvement in the control of the bucket position.

1.4 Organization of this Dissertation

In Chapter, 2 the system model is presented which mainly focuses on the hydraulic system. Chapter 3 contains analysis of the model pertaining to controller design and real time simulation. Chapter 4 presents controller designs, robustness analysis, and simulations for each control system. VR implementation and simulation results are given in Chapter 5. Finally, in Chapter 6 conclusions and future work are discussed.

CHAPTER 2. SYSTEM MODEL

The wheel loader system was modeled in two parts - the loader hydraulics and the linkage model. The main objective of the modeling effort was to obtain a fairly accurate model for control design and simulation while maintaining its simplicity for efficient execution in real time simulation in the VR environment. The model needs to be of high fidelity with the important dynamics included so that the control system design is effective and the VR simulation is realistic.

2.1 Nomenclature

The nomenclature in table 2.1 is used throughout the paper. The variables such as pressures and volumes for the tilt and lift functions are differentiated from each other by labelling the tilt variables with a "1" and the lift variables with a "2". Also, the head end and rod end volumes of cylinders are denoted as A and B respectively.

Table 2.1 Nomenclature

Symbol	Description	Symbol	Description
D_p	Pump displacement	$A_{cyA,n}$	Cylinder n area on side A
P_p	Pump pressure	$V_{A,n}$	Volume of cylinder n on side A
P_{LS}	Load sense pressure	C_d	Valve discharge coefficient
P_T	Tank pressure	$Q_{AB,n}$	Flow from "A" to "B" for
$P_{A,1}$	Tilt cylinder head end pressure		the n^{th} function
$P_{B,1}$	Tilt cylinder rod end pressure	M	Inertia matrix for linkage
$P_{A,2}$	Lift cylinder head end pressure	G_p	Pump displacement control gain
$P_{B,2}$	Lift cylinder rod end pressure	G_v	Valve actuator gain
i_1	Tilt valve solenoid current	r	Ref. input for tracking control
i_2	Lift valve solenoid current	b	Viscous friction coefficient
s_1	Tilt valve spool displacement	β	Fluid bulk modulus
s_2	Lift valve spool displacement	ρ	Fluid density
x_1	Cylinder 1 displacement	C_d	Orifice discharge coefficient
x_2	Cylinder 2 displacement	K_{LP}	Leakage factor for pump
x	State vector	ω_p	Pump speed
$A(s_n)_{PA,n}$	Orifice area funct. of s, valve	θ_1	Boom angle w.r.t. chassis
	n, vol. P (pump out.) to A	θ_{21}	Bucket angle w.r.t. boom
Q_v	Sum of flows from pump to valves	P_{margin}	Pump margin pressure setting

2.2 Loader Model

The complete dynamic model of the loader system includes electro-hydraulics and boom and bucket mechanism linkage. The boom and bucket mechanism is attached to the front of an articulated wheel loader (Figs. 2.1 and 5.6). The plant has two control inputs corresponding to the two current inputs to the hydraulic valves 1 and 2. These inputs are intended to control the tilt and lift functions of the loader, respectively. The outputs are the tilt cylinder position and the lift cylinder position. The tilt and lift functions refer to the tilting of the bucket and lifting of the boom.

2.2.1 Hydraulics

The hydraulics portion of the model includes valves, cylinders, and a pump. Each of these components is modeled using Simulink. The entire hydraulic model is a result of converting the governing equations to Simulink block diagram form. The governing equations are derived

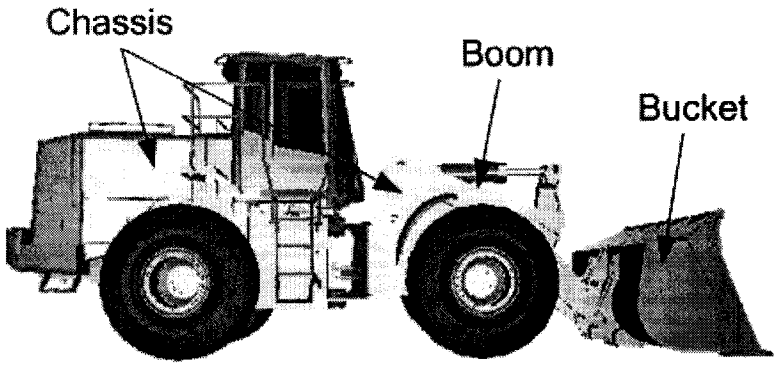

Figure 2.1 Side view of wheel loader

for the main components of the hydraulic system. They are given for the tilt valve, lift valve, and load sensing pump in the following sections.

Several assumptions have been made in developing the hydraulic model:

1. Constant tank pressure
2. Turbulent flow through orifices
3. Constant pump drive speed
4. Laminar pump leakage
5. Viscous friction on the cylinders
6. Negligible pipe, hose, and other chamber dynamics
7. First order valve actuator dynamics

The justification for assumptions 1, 2, 4, 5, 6 are standard and are also given in reference [18]. Assumption 3 is made because of two reasons: the pump speed only effects the maximum flow of the system when the pump displacement is saturated, and the engine is designed to provide good speed control before its maximum torque is reached (torque saturation). Assumption 7 is justified in [10] and references therein.

2.2.1.1 Tilt Valve

The valve cylinder combination for lift function model includes orifices, fluid volumes, and pressure areas. The tilt valve (valve 1) schematic is given in Fig. 2.2. This schematic shows several orifices, some of which are varied by the valve spool position. Other orifices are fixed. Hydraulic fluid flows from the pump and through inlet restriction area, A_0, and then through variable orifice areas, $A_{SA,1}$ and $A_{SB,1}$, leading to the cylinder. Flow from the pump can also go through restriction, A_1, and priority orifice, A_2, to the lift function (valve 2). Hydraulic fluid can flow out of the cylinder through variable orifices, $A_{TA,1}$ and $A_{TB,1}$, and in to the reservoir tank. The variable orifices are linked together and varied mechanically as a function of s_1. The sign convention for the flows is given according to the order of the letters of the subscript in the symbol that identifies each flow and by arrows on the hydraulic diagrams. For example, $Q_{AB,1}$, is the symbol for positive flow leading from volume A to volume B for cylinder 1. For each end (A or B) of cylinder 1, there is a mass balance equation [14] that can be written in terms of flows across orifices as

$$\dot{m}_A = \rho(Q_{SA,1} - Q_{AB,1} + Q_{TA,1}) \tag{2.1}$$

and

$$\dot{m}_B = \rho(Q_{SB,1} + Q_{AB,1} + Q_{TB,1}). \tag{2.2}$$

The expressions for the mass of the fluid in volume A and B are

$$m_{A,1} = \rho V_{A,1} \tag{2.3}$$

and

$$m_{B,1} = \rho V_{B,1}. \tag{2.4}$$

Taking the derivative, the following are obtained:

$$\dot{m}_{A,1} = \dot{\rho} V_{A,1} + \rho \dot{V}_{A,1} \tag{2.5}$$

$$\dot{m}_{B,1} = \dot{\rho} V_{A,1} + \rho \dot{V}_{B,1} \tag{2.6}$$

Using $\beta\rho\dot{P} = \dot{\rho}$ from the definition of bulk modulus, equation 2.1, 2.2, 2.5, and 2.6 can be combined to form the following:

$$\dot{P}_{A,1} = \frac{\beta}{V_{A,1}}(-\dot{V}_{A,1} + Q_{SA,1} + Q_{TA,1} - Q_{AB,1}) \tag{2.7}$$

$$\dot{P}_{B,1} = \frac{\beta}{V_{B,1}}(-\dot{V}_{B,1} + Q_{SB,1} + Q_{TB,1} + Q_{AB,1}) \tag{2.8}$$

Equation 2.7 has been converted into block diagram form in Fig. 2.3 for use in simulation software. The volumes denoted as A and B which are the volumes between the valve and of each side of the cylinder piston including the hoses are given as

$$V_{A,1} = A_{cyA,1}x_1 + V_{0A,1} \tag{2.9}$$

and

$$V_{B,1} = A_{cyB,1}(x_{m,1} - x_1) + V_{0B,1}. \tag{2.10}$$

The rate of change of volumes A and B for the tilt function are given as

$$\dot{V}_{A,1} = A_{cyA,1}\dot{x}_1 \tag{2.11}$$

and

$$\dot{V}_{B,1} = A_{cyB,1}\dot{x}_1. \tag{2.12}$$

The force on the cylinder is

$$F = F_L - \dot{x}_1 b, \tag{2.13}$$

which includes the viscous friction factor, b. In general, the flow across each orifice in the hydraulic valve is given by

$$Q = AC_d\sqrt{\frac{2(P_{in} - P_{out})}{\rho}}sign(P_{in} - P_{out}). \tag{2.14}$$

The block diagram for an orifice is given in Fig. 2.4. The flows across each orifice in the lift valve are given by

$$Q_{PS,1} = A_o C_d\sqrt{\frac{2(P_P - P_S)}{\rho}}sign(P_P - P_S) \tag{2.15}$$

$$Q_{SA,1} = A_{SA}(s_1)C_d\sqrt{\frac{2(P_S - P_A)}{\rho}}sign(P_S - P_A) \tag{2.16}$$

$$Q_{SB,1} = A_{SB}(s_1)C_d\sqrt{\frac{2(P_S - P_B)}{\rho}}sign(P_S - P_B) \tag{2.17}$$

$$Q_2 = A_2C_d\sqrt{\frac{2(P_2 - P_{S,2})}{\rho}}sign(P_2 - P_{S,2}) \tag{2.18}$$

$$Q_1 = A_1C_d\sqrt{\frac{2(P_P - P_1)}{\rho}}sign(P_P - P_1) \tag{2.19}$$

$$Q_{TA,1} = A_{TA}(s_1)C_d\sqrt{\frac{2(P_T - P_A)}{\rho}}sign(P_T - P_A) \tag{2.20}$$

$$Q_{TB} = A_{TB}(s)C_d\sqrt{\frac{2(P_T - P_B)}{\rho}}sign(P_T - P_B) \tag{2.21}$$

$$\tag{2.22}$$

Due to the geometry of the valve, either A_{SB} and A_{TA} or A_{SA} and A_{TB} are zero. Therefore, the flow from the supply (point S) is

$$Q_{PS} = Q_{SA} = Q_{PA} \tag{2.23}$$

or

$$Q_{PS} = Q_{SB} = Q_{PB}. \tag{2.24}$$

Since there is no volume of fluid modeled between point S and point A, the pressure at point S can be eliminated from the dynamic equations by equating 2.15 and 2.16 to solve for P_S in terms of A_0, $A_{SA}(s)$, P_P, and P_A. A flow equation,

$$Q_{PA,1} = A'_A(s_1)C_d\sqrt{\frac{2(P_P - P_A)}{\rho}}sign(P_P - P_A), \tag{2.25}$$

can be formed by using the new expression for P_S in equation 2.16 where $A'_A(s)$ is given by

$$A'_A(s_1) = \frac{A_{SA}(s_1)A_0}{\sqrt{A_{SA}(s_1)^2 + A_0^2}}. \tag{2.26}$$

Similarly, an expression for P to B flow can be formed as

$$Q_{PB,1} = A'_B(s_1)_AC_d\sqrt{\frac{2(P_P - P_B)}{\rho}}sign(P_P - P_B), \tag{2.27}$$

where $A'_B(s)$ is given by

$$A'_B(s_1) = \frac{A_{SB}(s_1)A_0}{\sqrt{A_{SB}(s_1)^2 + A_0^2}}. \tag{2.28}$$

Also, the flow from point P to point 2 which leads to the secondary valve (controlling the lift function) can be expressed as

$$Q_2 = A'_2(s_1)C_d\sqrt{\frac{2(P_P - P_2)}{\rho}}sign(P_P - P_2), \tag{2.29}$$

where

$$A'_2(s_1) = \frac{A_2(s_1)A_1}{\sqrt{A_2(s_1)^2 + A_1^2}}. \tag{2.30}$$

The displacement of the spool valve, s_1 is given as a first order lag as indicated in the assumptions. The valve actuators in this machine model have a break frequency, ω_v. Therefore the valve displacement rate is given as

$$\dot{s_1} = (-s_1 + G_v u_1)\omega_v. \tag{2.31}$$

2.2.1.2 Lift Valve

The derivations for the second valve which controls the lift function is similar to that of the tilt function except there is no priority flow path leading to another valve (see Fig. 2.5). The time derivatives of $P_{A,2}$ and $P_{B,2}$ are

$$\dot{P}_{A,2} = \frac{\beta}{V_A}(-\dot{V}_{A,2} + Q_{PA,2} + Q_{TA,2} - Q_{BA,2}) \tag{2.32}$$

and

$$\dot{P}_{B,2} = \frac{\beta}{V_B}(-\dot{V}_{B,2} + Q_{PB,2} + Q_{TB,2} + Q_{BA,2}). \tag{2.33}$$

The volumes A and B are

$$V_{A,2} = A_{cyA,2}(x_2) + V_{0A,2} \tag{2.34}$$

and

$$V_B, 2 = A_{cyB,2}(x_{m,2} - x_2) + V_{0B,2}. \tag{2.35}$$

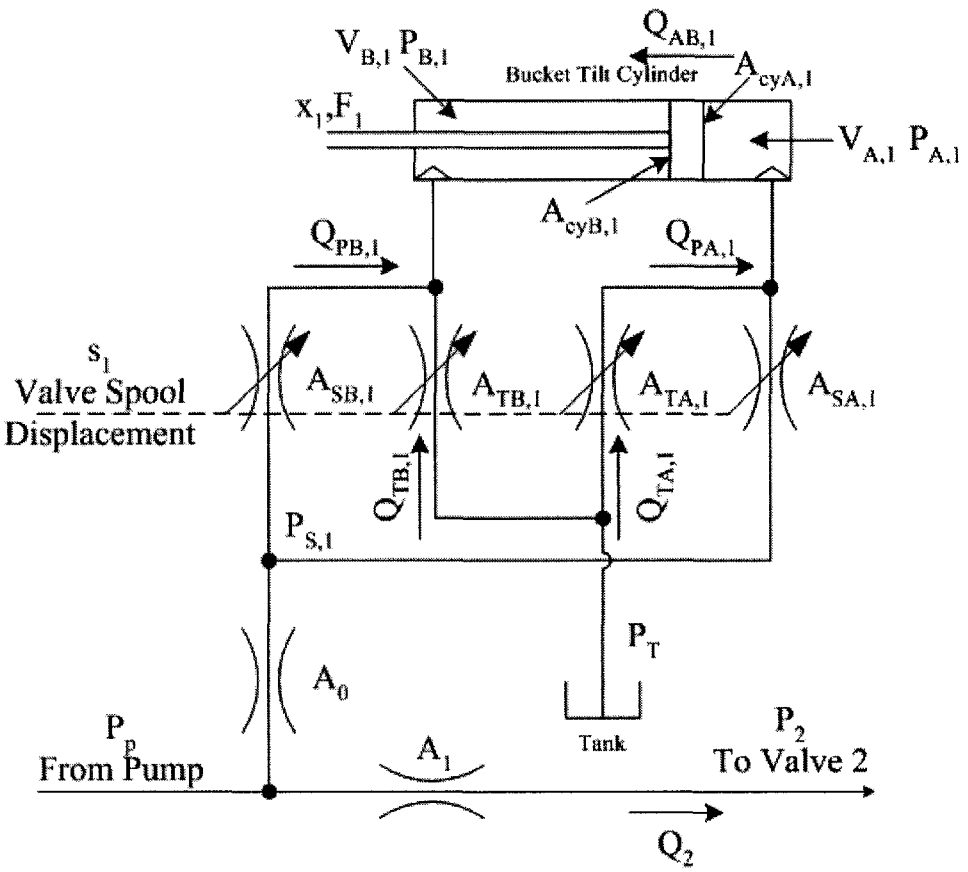

Figure 2.2 Tilt valve section schematic

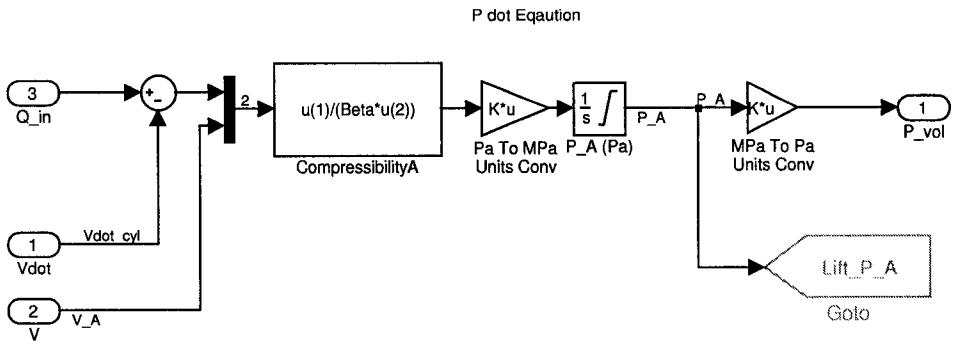

Figure 2.3 Pressure dynamics for a volume of fluid

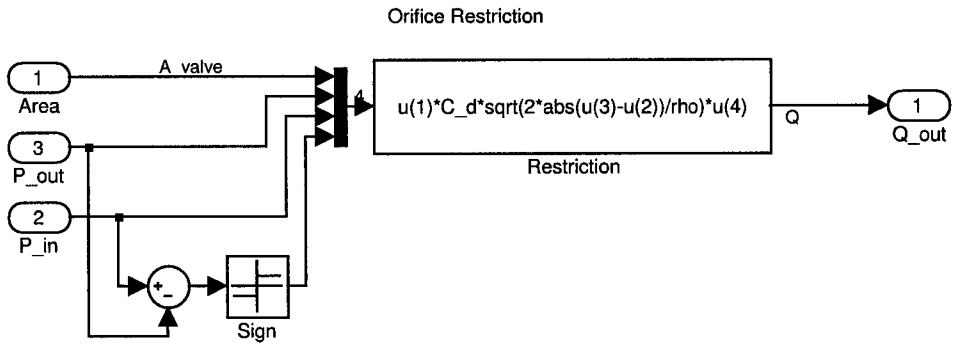

Figure 2.4 Valve orifice diagram

The rate of change of volumes A and B are given as

$$\dot{V}_{A,2} = A_{cyA,2}\dot{x}_2 \tag{2.36}$$

and

$$\dot{V}_{B,2} = A_{cyB,2}\dot{x}_2. \tag{2.37}$$

The flows in valve two are

$$Q_{PA,2} = A'_{PA,2}(s_2)C_d\sqrt{\frac{2(P_P - P_{A,2})}{\rho}}sign(P_P - P_{A,2}), \tag{2.38}$$

$$Q_{PB,2} = A'_{PB,2}(s_2)C_d\sqrt{\frac{2(P_P - P_{B,2})}{\rho}}sign(P_P - P_{B,2}), \tag{2.39}$$

$$Q_{TA,2} = A_{TA,2}(s_2)C_d\sqrt{\frac{2(P_T - P_{A,2})}{\rho}}sign(P_T - P_{A,2}), \tag{2.40}$$

and

$$Q_{TB,2} = A_{TB,2}(s_2)C_d\sqrt{\frac{2(P_T - P_{B,2})}{\rho}}sign(P_T - P_{B,2}) \tag{2.41}$$

where

$$A'_{PA,2}(s_2) = \frac{A'_2 A'_{2A,2}(s_2)}{\sqrt{{A'_2}^2 + A'_{2A,2}(s_2)^2}}. \tag{2.42}$$

and

$$A'_{PA,2}(s_2) = \frac{A'_2 A'_{2B,2}(s_2)}{\sqrt{{A'_2}^2 + A'_{2B,2}(s_2)^2}}. \tag{2.43}$$

Similar to valve one, the valve spool displacement rate for valve two is given as

$$\dot{s}_2 = (-s_2 + G_v u_2)\omega_v. \tag{2.44}$$

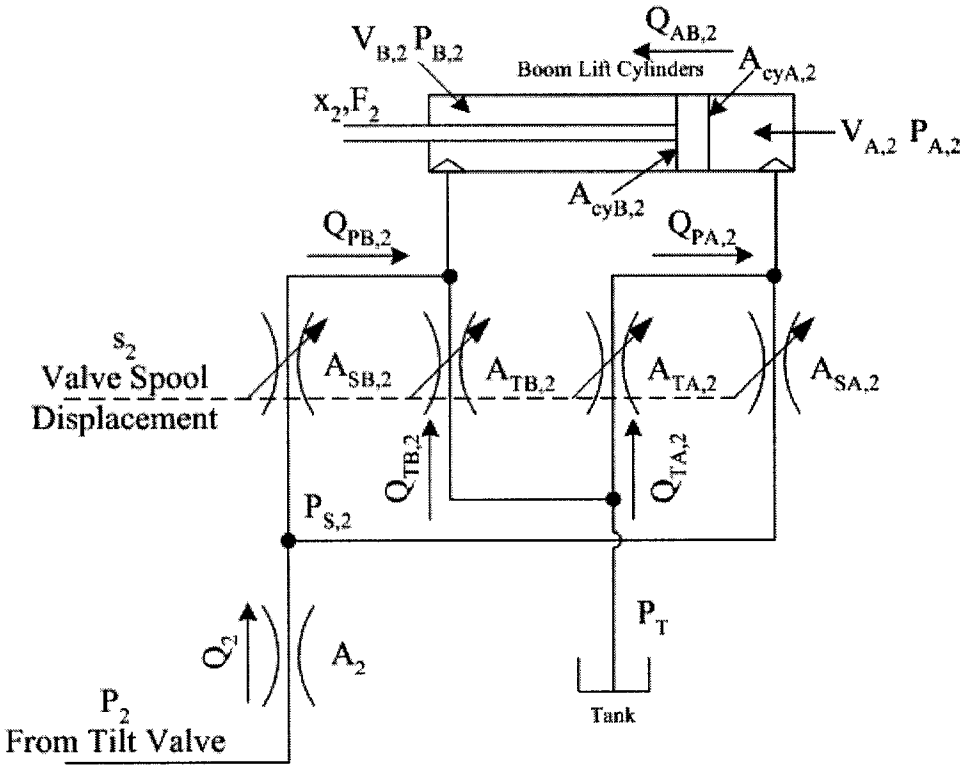

Figure 2.5 Lift valve section schematic

2.2.1.3 Load Sensing Pump

The load sense pump is modeled using a variable flow source with displacement input, a volume, and a leakage (Fig. 2.6). Taking the difference between desired margin pressure and the load sense signal gives the margin pressure error. The integral of the margin pressure error signal, $(P_P - P_{LS}) - P_{margin}$, controls the pump displacement. This is because the pump displacement servo is designed to increase the displacement of the pump at a rate proportional to the margin pressure error. Therefore, the load sense displacement servo dynamics are described by

$$\dot{D}_p = ((P_P - P_{LS}) - P_{margin})G_p. \tag{2.45}$$

To give a realistic lag between the pressure signal and the response of the displacement servo, the load sense pressure rate of change at the displacement servo is approximated by

$$\dot{P}'_{LS} = (P_{LS} - P'_{LS})120. \tag{2.46}$$

$P'_{LS} = \max(P_{A,1}, P_{B,1}, P_{A,2}, P_{B,2})$ is the load sense signal as it occurs at the valve with the highest load while P_LS is the load sense signal after the lag. The rate of change in mass of the pump outlet volume fluid is

$$\dot{m}_p = \rho_p(Q_p - Q_v - Q_L) \tag{2.47}$$

in terms of fluid flow. The flows from the pump and leakage are

$$Q_p = \omega_p D_p / 2\pi \tag{2.48}$$

and

$$Q_L = P_p K_{Lp}. \tag{2.49}$$

Since $m_p = \rho V_p$, the rate of change in mass of the pump outlet volume fluid is also given by

$$\dot{m}_p = \dot{\rho} V_p + \rho \dot{V}_p \tag{2.50}$$

The bulk modulus of the fluid, pressure rate of change, and density rate of change can be related by $\frac{1}{\beta} = \frac{1}{\rho}\frac{\partial \rho}{\partial P_p}$ with temperature held constant in the partial derivative. Therefore,

$$\dot{\rho} = \frac{\dot{P}_p \rho}{\beta} \tag{2.51}$$

can be substituted into equation 2.50 in combination with equations 2.48 and 2.49 to get

$$\dot{P}_p = (\omega_p D_p/2\pi - Q_v - P_p K_{LP})\frac{\beta}{V_p} \tag{2.52}$$

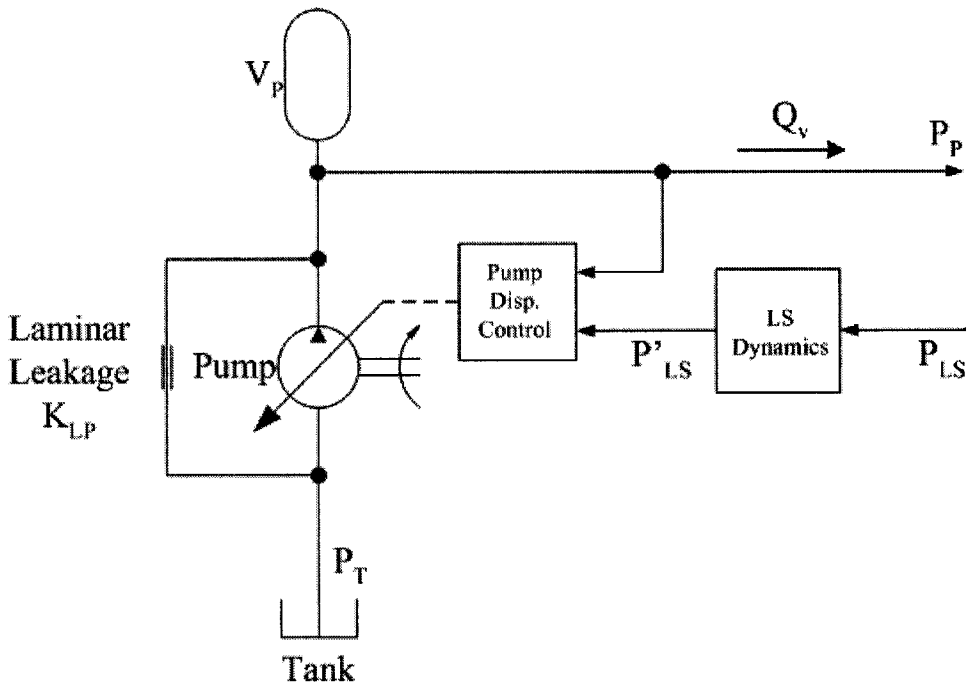

Figure 2.6 Load sensing pump schematic

2.2.2 Linkage

The loader linkage may be described as a collection of 8 bodies subject to a set of constraints including 3 kinematic loops leaving a total of 2 overall degrees-of-freedom (Fig. 2.7. The linkage is a typical mechanical system in that the number of bodies significantly outnumber the number of generalized coordinates. A multibody formulation taking advantage of this difference would be ideal. For this reason, a reduced coordinate formulation equipped with a numerical rank test for determination of a suitable set of generalized coordinates was used [7]. The equations of motion may be expressed in the form,

$$\tau = M\ddot{q} + h(q, \dot{q})$$

where τ represents the external forces, M is the inertia matrix, q denotes the generalized position coordinates, and $h(q, \dot{q})$ describes the centrifugal, Coriolis, and potential forces. Notice that solving for the generalized accelerations requires the the inversion of a 2×2 matrix.

Since linear models are critical to the project including control design, a general numerical algorithm for finding exact linear models of rigid multibody systems containing holonomic constraints was used. The derivation follows closely with [7] and is similar in approach to [3].

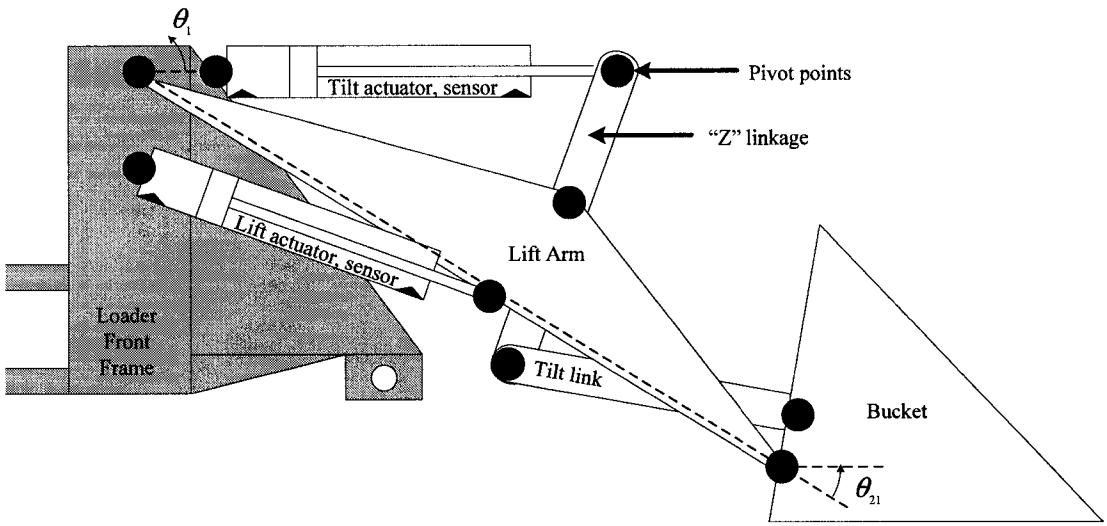

Figure 2.7 Loader Diagram

2.2.3 Combined Linkage and Hydraulics Model

The dynamic equations for the linkage and hydraulic system can be combined to form a MIMO state space system. The input, u, and state vector, x, are defined as follows:

$$u = [i_1, i_2]^T$$

$$x = [x_1, x_2, \dot{x}_1, \dot{x}_2, P_p, D_p, P'_{LS}, s_1, P_{A,1}, P_{B,1}, s_2, P_{A,2}, P_{B,2}]^T$$

The output is given as,

$$y = [\theta_1, \theta_{21}],$$

where θ_1 and θ_{21} are the angular positions of the boom and bucket with respect to the boom which can be determined from the cylinder positions.

The states of the model are summarized in table 2.2. The dynamic equations for the linkage and electrohydraulic system in terms of state variables can be written as follows:

$$
\begin{aligned}
\dot{x}_1 &= x_3 \\
\dot{x}_2 &= x_4 \\
\begin{bmatrix} \dot{x}_3 \\ \dot{x}_4 \end{bmatrix} &= M^{-1}(\tau(x_9, x_{10}, x_{12}, x_{13}) - h(x_1, x_2, x_3, x_4)) \\
\dot{x}_5 &= \frac{\beta}{V_p}(\omega_p x_6/2\pi - x_5 K_{Lp} - (Q_{PA,1}(x_5, x_8, x_9) + \\
&\quad Q_{PB,1}(x_8, x_{10}) + Q_{PA,2}(x_5, x_{11}, x_{12}) + \\
&\quad Q_{PB,2}(x_5, x_{11}, x_{13}))) \\
\dot{x}_6 &= [x_7 - x_5 + P_{margin}]G_p \\
\dot{x}_7 &= (max(x_9, x_{10}, x_{12}, x_{13}) - x_7)120 \\
\dot{x}_8 &= (-x_8 + G_v u_1)\omega_v \\
\dot{x}_9 &= \frac{\beta}{V_{A,1}(x_1)}(Q_{PA,1}(x_5, x_8, x_9) + \\
&\quad Q_{TA,1}(x_8, x_9) - \dot{V}_{A,1}(x_3)) \\
\dot{x}_{10} &= \frac{\beta}{V_{B,1}(x_1)}(Q_{PB,1}(x_8, x_{10}) + \\
&\quad Q_{TB,1}(x_8, x_{10}) - \dot{V}_{B,1}(x_3)) \\
\dot{x}_{11} &= (-x_{11} + G_v u_2)\omega_v \\
\dot{x}_{12} &= \frac{\beta}{V_{A,2}(x_2)}(Q_{PA,2}(x_5, x_{11}, x_{12}) + \\
&\quad Q_{TA,2}(x_{11}, x_{12}) - \dot{V}_{A,2}(x_4)) \\
\dot{x}_{13} &= \frac{\beta}{V_{B,2}(x_2)}(Q_{PB,2}(x_5, x_{11}, x_{13}) + \\
&\quad Q_{TB,2}(x_{11}, x_{13}) - \dot{V}_{B,2}(x_4))
\end{aligned}
\tag{2.53}
$$

Table 2.2 Plant states

State	Symbol	Description
1	x_1	Tilt cylinder position
2	x_2	Lift cylinder position
3	$\dot{x}_1$	Tilt cylinder velocity
4	$\dot{x}_2$	Lift cylinder velocity
5	P_p	Pump pressure
6	D_p	Pump displacement
7	P'_{LS}	Load sense pressure
8	s_1	Tilt function spool valve position
9	$P_{A,1}$	Tilt cylinder cap end pressure
10	$P_{B,1}$	Tilt cylinder rod end pressure
11	s_2	Lift function spool valve position
12	$P_{A,2}$	Lift cylinder cap end pressure
13	$P_{B,2}$	Lift cylinder rod end pressure

2.2.4 Linearization

The control system, given in Chapter 4, is designed using a linearized model of the loader. A numerical technique is used to determine the model linearization. The resulting linearized model has 13 states. The operating point about which the plant was linearized is given by

$$x_0 = [4.7916, 2.8968, 0.9884, 0.5877, 1.8119, 8.2571, 10.3600,$$

$$-0.0460, 5.7652, 9.6282, -0.0322, 8.2573, 9.7195]^T.$$

This operating point was selected as a typical level lift condition, with both valves open, causing the boom to lift upward slowly and the bucket to tilt upward slowly. The resulting linearized plant is of the form

$$\dot{x} = Ax + B_u u$$

$$y = C_y x$$

where x is the state vector of the model, u is the input, and y is the output. The model is the perturbation model about the operating point.

CHAPTER 3. OPEN-LOOP ANALYSIS AND UNCERTAINTY CHARACTERIZATION

In this chapter, the dynamic model of the wheel loader is analyzed with several goals in mind. One of the important reasons to analyze the model is to determine what challenges will be faced in the control system design process including performance limitations and uncertainty assessment. Also, it is desired to use the model in a real time VR simulation which can be used to assess the performance of the wheel loader system. Therefore, it is essential to evaluate whether the model can run at the real time speeds so that a human-in-the-loop simulation is possible.

3.1 Open-Loop Characteristics

The open-loop characteristics were examined to determine if there are any performance limitations in terms of the linear model. Before any analysis the linear plant model was scaled on both the input and the output. The input and output scalings, D_u, and D_y, respectively, were selected such that the expected input and output magnitudes were less than or equal to unity for the scaled plant:

$$G = D_y^{-1} G_{unscaled} D_u$$

The maximum and minimum singular values for the plant were plotted over a large frequency range as shown in Fig. 3.1. The plot shows that the system has a high gain at low frequencies indicating that low steady state error should be achieved with a closed-loop control system. Considering that this is a MIMO system, the observation that the system has a -20 dB per decade slope starting at low frequencies would suggest that the system would be able to

track step commands with less error. Another observation is that the system appears to have resonant peaks at approximately 10 Hz and 20 Hz.

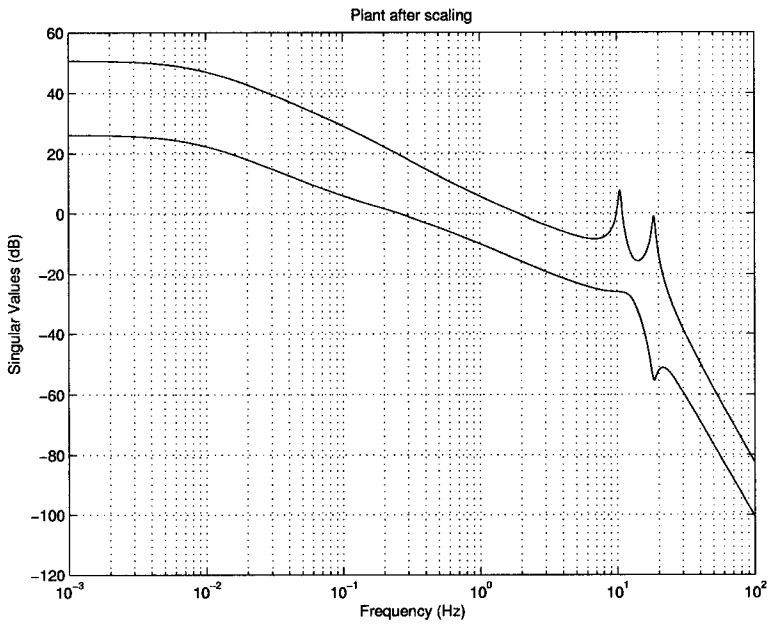

Figure 3.1 Singular value plot of the plant after scaling

The open-loop poles and zeros of the system are given in Table 3.1 and in Fig. 3.2. There are no right half plane poles which indicates that there are no apparent bandwidth limitations for the linear model[15]. Therefore the saturations limits of the input and internal states of the model are the limiting factor on performance.

3.2 Uncertainty

An effort has been made to formulate a model which accurately represents the dynamics of the wheel loader system. Typically, hydraulic systems have complex dynamics. The complexity requires that simplifications to the model be made in the interest of making the control design and analysis process more manageable. In some cases dynamics were eliminated and parameters were estimated. For example, the valve actuator dynamics were reduced to a first order systems and the discharge coefficient was estimated without verification with test

Table 3.1 Plant poles and zeros

Poles
-123.09
$-2.76 + 116.20i$
$-2.76 - 116.20i$
$-28.07 + 113.69i$
$-28.07 - 113.69i$
$-1.42 + 66.17i$
$-1.42 - 66.17i$
$-1.50 + 0.05i$
$-1.50 - 0.05i$
0.05
0.05
-107.00
-107.00

Zeros
$-512 + 115.43i$
$-5.12 - 115.43i$
-119.94
-2.41
-0.79

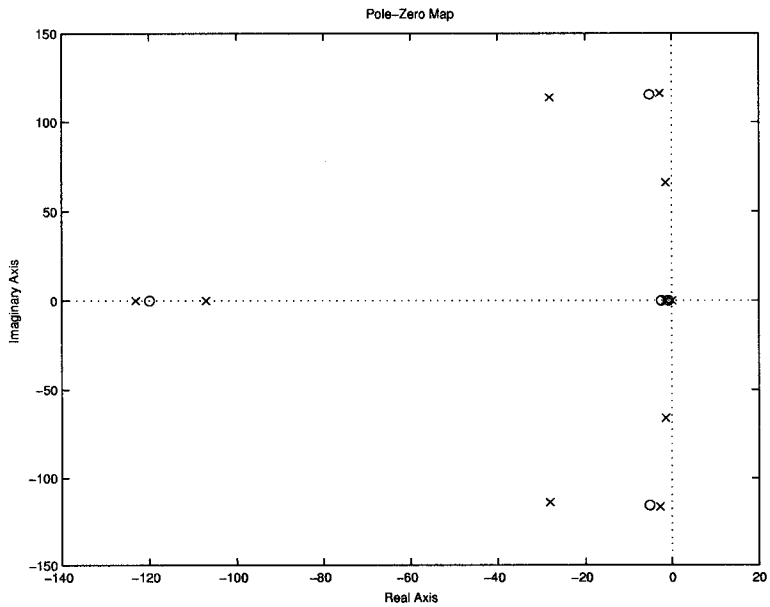

Figure 3.2 Plot of poles and zeros for the model

data. The linear control designs given in Chapter 4 are based on a linearization of the model. Therefore any inaccuracy in the model will have an effect on the control design. An attempt to quantify the uncertainty in the model using linear analysis is given in the following sections. The uncertainties considered are due to uncertain parameters, un-modeled dynamics, and nonlinearities.

3.2.1 Parametric Uncertainty

The effective bulk modulus of the system can be difficult to determine whether by measurement or analytically. This is because many complicated factors are involved such as the compliance of the structure which contains the fluid volume and entrained air in the fluid [14]. The effective bulk modulus is a parameter which can vary by as much as 50 percent [18]. The discharge coefficient can vary depending on the geometry within the metering orifices. Uncertainty in the valve area geometry due to manufacturing variations can be captured as variations of the discharge coefficient by considering discharge coefficient as a gain on the pressure flow relationship or the valve area. A family of linearizations of the system model, G, was created with each having the same operating point but different randomly selected values within an interval of $\pm 50\%$ of nominal bulk modulus and discharge coefficient (Fig. 3.3). The nominal values of the parameters are $C_d = .62$ and $\beta = 1.7 \times 10^9$ Pa. The plant description including uncertainty can be given as

$$G = G_{nom}(I + \mathbf{\Delta}), \tag{3.1}$$

where $\mathbf{\Delta}$ represents the uncertainty in the model. Let $\mathbf{\Delta} = \Delta W_i$ where Δ is the set of all model perturbations which are transfer matrices with the infinity norm less than or equal to one. The term, W_i becomes a weight in the form of transfer function matrix which bounds all of the possible perturbations of the plant model. The weight is plotted in Fig. 3.4 along with the family of plant perturbations.

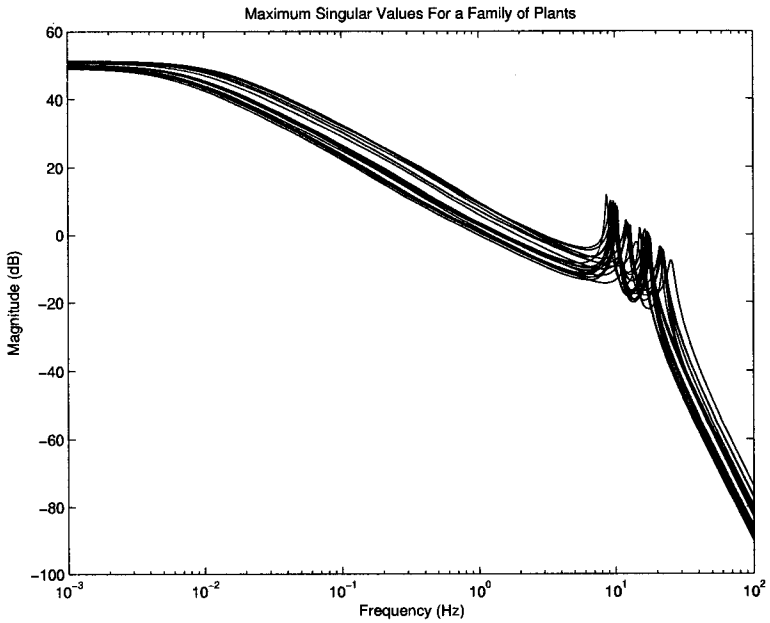

Figure 3.3 Singular value plot of plants with varying parameters

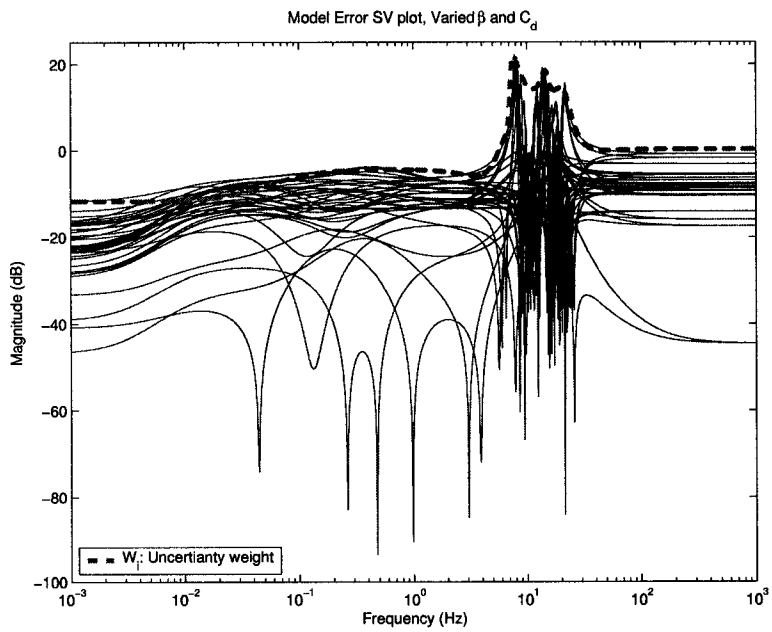

Figure 3.4 Singular value plot of plant uncertainty and bounding weight for varied parameters, β and C_d

3.2.2 Nonlinearities

Due to the nonlinear nature of the machine's dynamics, the linearization of the plant model depends on the operating point about which the linearization is computed. One way to study this effect is to create a family of plants similar to those in the previous section to study the effects of varying operating points. A number of operating points were selected from a simulation of the system operating in level lift control mode (see the control designs presented in Chapter 4). A linearization was computed at each of these operating points for a total of 20 linearized plant models. Similar to the previous section a set of perturbations were created and are plotted in Fig. 3.5.

The main source of nonlinear behavior in the system model is the pressure dynamics for both the tilt and lift functions. The inputs to the pressure subsystem corresponding to states 9, 10, 12, and 13 are the valve positions, states 8 and 11. The outputs are the cylinder pressures which are directly related to the force of the hydraulic cylinders on the linkage by the cylinder piston areas. The nonlinearities are due to the square root relationship in the orifice flows and the varying cylinder volumes.

3.2.3 Un-modeled Dynamics

The dynamics in the actual system are simplified in the wheel loader model presented in this work. Since there is no data from actual machinery tests in this work, there is no method to verify the accuracy of the model. There is no quantification of the degree to which the un-modeled dynamics effects the modeling accuracy. Since the uncertainty analysis of the input and parameter variations are conservative, it is likely that the unmodeled dynamics uncertainty would be less significant. Model identification tests could be designed to characterize the uncertainty due to un-modeled dynamics

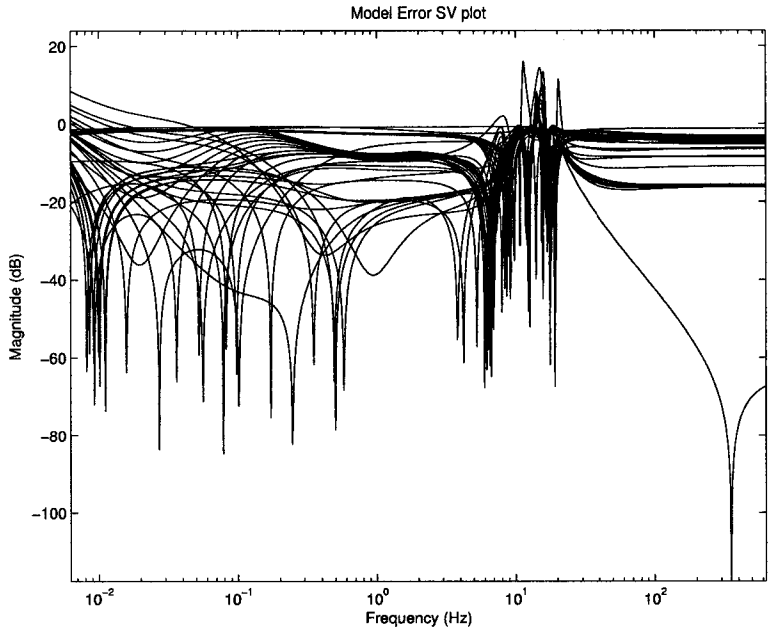

Figure 3.5 Singular value plot of plant uncertainty for various operating points

3.3 Analysis of Model Execution Speed

The wheel loader model is simulated by computing numerical solutions to the differential equations. A fixed time step fourth order Runge-Kutta method is used for the numerical integration. The model simulation must compute simulated time outputs at a rate faster than time passes on the real time clock. That is, simulated time must pass faster than real time.

The first step in analyzing the model execution speed is to select a simulation time step. In this project, a fixed step ODE solver was selected to guarantee a certain reasonably constant amount of CPU activity per unit of simulation time. A rule of thumb for simulations is to choose a time step which corresponds to a frequency which is ten times the value of the fastest eigenfrequency of the system under consideration. In the case of the wheel loader model the highest eigenfrequency is approximately $20Hz$ which corresponds to a period of 0.05 seconds. If the thumb rule of using factor of 10 was applied, the time step would be 0.005 seconds. For the simulations, the period was divided by 100 (rather than 10) resulting in a very conservative

time step of 0.0005 seconds. Note that this small time step is partly justified since the control designs given later yield systems with a slightly higher maximum eigenfrequency. Also, the eigenfrequencies change when parameters change and when the system moves away from its operating point.

The next step in analyzing the model execution speed is to preform a timed test where the simulation computes a predetermined amount of simulation time outputs. A simple test was set up where the model was allowed to simulate 10 seconds of operation. This test was done using the PC's real time clock to determine the time it took for the simulation to complete. The time interval between the start and the end of the simulation was less than 0.72 seconds. This indicates that the model is certainly capable of running at real time speed if properly controlled by a timing scheme. Also, the test result indicates that adequate time is available for other real time process execution tasks.

CHAPTER 4. CONTROL DESIGN

This chapter presents controller designs and simulation results including analysis of control design requirements, robustness, analysis, and performance requirements. The controller designs presented include PI, LQG, H_∞ and nonlinear controllers along with explanations of how each design methodology is applicable to the wheel loader problem. The linear controllers were designed using the linearized model given in Chapter 2 while the nonlinear controllers do not rely on the linearized model. Each controller design was simulated on the nonlinear plant model under realistic conditions to determine if these requirements are adequately met. At the end of the chapter, conclusions are made about the applicability of each controller design.

4.1 Design Requirements

The goal of the controller design is to be able to lift the boom (or lift arm) at a desired rate while maintaining the bucket in a levelled position. This is a challenge for open-loop operation since the boom and bucket are coupled both in terms of the kinematics of the linkage and in terms of having a common hydraulic system power source. When the boom is raised to an angular position, θ_1, the relative angle of the bucket with respect to the boom must be,

$$\theta_{21} = -\theta_1 \tag{4.1}$$

for the bucket to be levelled.

Ramp inputs are found to be reasonable approximations of the level lift reference inputs. Therefore, a control requirement is to track ramp inputs for the tilt and lift functions with low tracking error. The tracking errors for the bucket and boom angular positions in this control system are defined as the desired positions minus the actual positions.

Another requirement is to have reasonably fast response. This allows the machine to be acceptably productive as it is used for material handling and earthmoving in commercial applications where time is critical. A bandwidth of 1.0 Hz is desired to meet the targeted speed of response.

The final requirement is robust stability. Any controller design should remain stable for all known plant perturbations. Perturbations in the plant are discussed in Chapter 3. Uncertainty in the plant is modeled as an input multiplicative (see Fig. 4.1) uncertainty. Two different uncertainty models are considered for this work. One is a diagonal uncertainty block which accounts for for variations in the current amplifier and valve actuator combination. The weight used for this uncertainty model is given by

$$W_i = \begin{bmatrix} .5 & 0 \\ 0 & .5 \end{bmatrix},$$

which represents 50% uncertainty in the input. This range of input error is possible due to uncertainties in the current amplifier used in control implementation and variations in the actuator hardware such as the valve solenoids. The other uncertainty model was given in Chapter 3 as a part of the analysis of uncertainty due to variations in parameters β and C_d.

The controller (LQG, H_∞, etc.), the plant, and the uncertainty model can be transformed into a standard form (Fig. 4.2) by manipulating the block diagram of Fig. 4.1 and by applying a linear fractional transformation (LFT). The robust stability conditions for this configuration are that the nominal plant is stable and the following inequality given in terms of the maximum singular value is satisfied.

$$\bar{\sigma}(N_{11}) < 1. \tag{4.2}$$

4.2 PI Control

Proportional plus integral (PI) control design is generally considered for SISO systems. It is considered here for the purpose of comparison. PI controllers are commonly used by industry

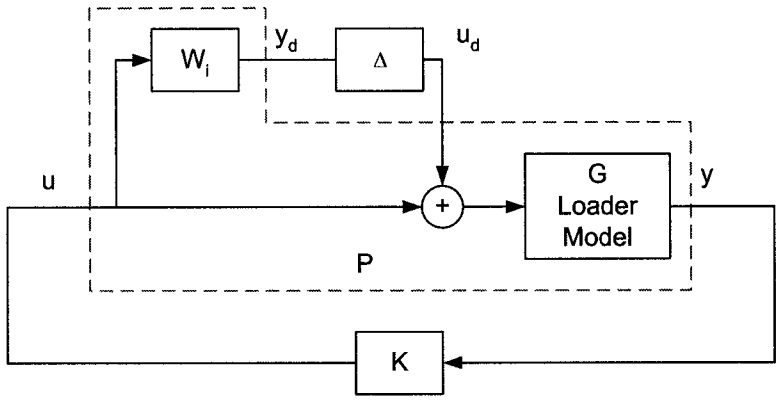

Figure 4.1 Controller and plant including uncertainty

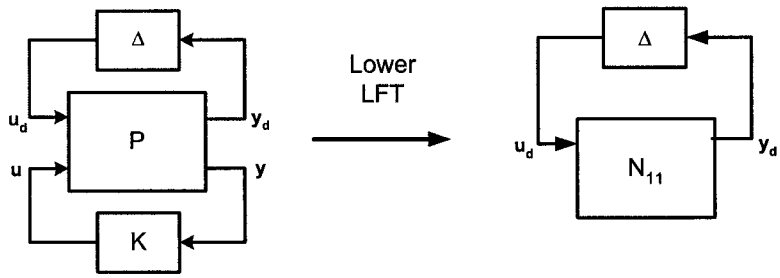

Figure 4.2 Transformed plant

in mobile hydraulic applications. Derivative control is often avoided because of the difficulty in obtaining useable velocity signals due to noise. The integral portion of the controller provides additional gain for the system at low frequencies to provide better tracking performance. For this work, a PI controller was designed for the tilt and lift systems separately using a root locus synthesis to determine the controller gain.

To do this the transfer functions for the SISO tilt and lift functions were approximated as the diagonal elements of the 2- input-2-output plant, G. These diagonal elements will be referred to as G_1 for the tilt transfer function and G_2 for the lift transfer function. Speed of response, steady state error, and robustness are be achieved by tuning the gains on the controller.

Eliminating the off diagonal elements of the G is not necessarily justified since there are physical interactions between the tilt and lift systems which correspond to the off diagonal elements. Therefore some measure is needed of how much interaction there is between the diagonal input output pairs. The relative gain array (RGA) of the plant at low frequencies is often used for this purpose [15]. The value of the RGA of G is given below:

$$\wedge(G(0)) = \begin{bmatrix} 0.9934 & 0.0066 \\ 0.0066 & 0.9934 \end{bmatrix}$$

The RGA has many interpretations. One of which is a measure of the interactions of input output pairs. Since in this case the RGA is nearly the identity matrix, it is reasonable to assume that there is little interaction between the input output pairs corresponding to the off diagonal elements of G. Thus, the common industry practice of considering hydraulic subsystems as separate SISO systems has some merit.

The structure of the PI controller is simple. The input vector to the plant, u, is related to the position tracking error vector, $y - y_{ref}$, by the following equation:

$$u = K_{PI}(y - y_{ref}).$$

K_{PI} is a diagonal matrix containing the controller transfer functions.

The proposed PI compensators are given as follows for the tilt and lift functions:

$$\begin{aligned} C_{PI1} &= 0.5 + \frac{1.3}{s} \\ C_{PI2} &= 2.0 + \frac{3.0}{s} \end{aligned} \tag{4.3}$$

The desired speed of response and steady state error have been tuned by adjusting the proportional and integral parameters, respectively. Root locus plots are given for each open-loop compensated plant in Fig. 4.3. The PI parameters were designed with the constraint that the root locus paths were such that a stabilizing root locus gain could be selected.

The next step is to choose a root locus gain for each compensator, K_1 and K_2, to complete the controller design. The limitation on the maximum of each controller gain is due to the two complex conjugate pairs of poles near the jw axis. The range of gains in which the root

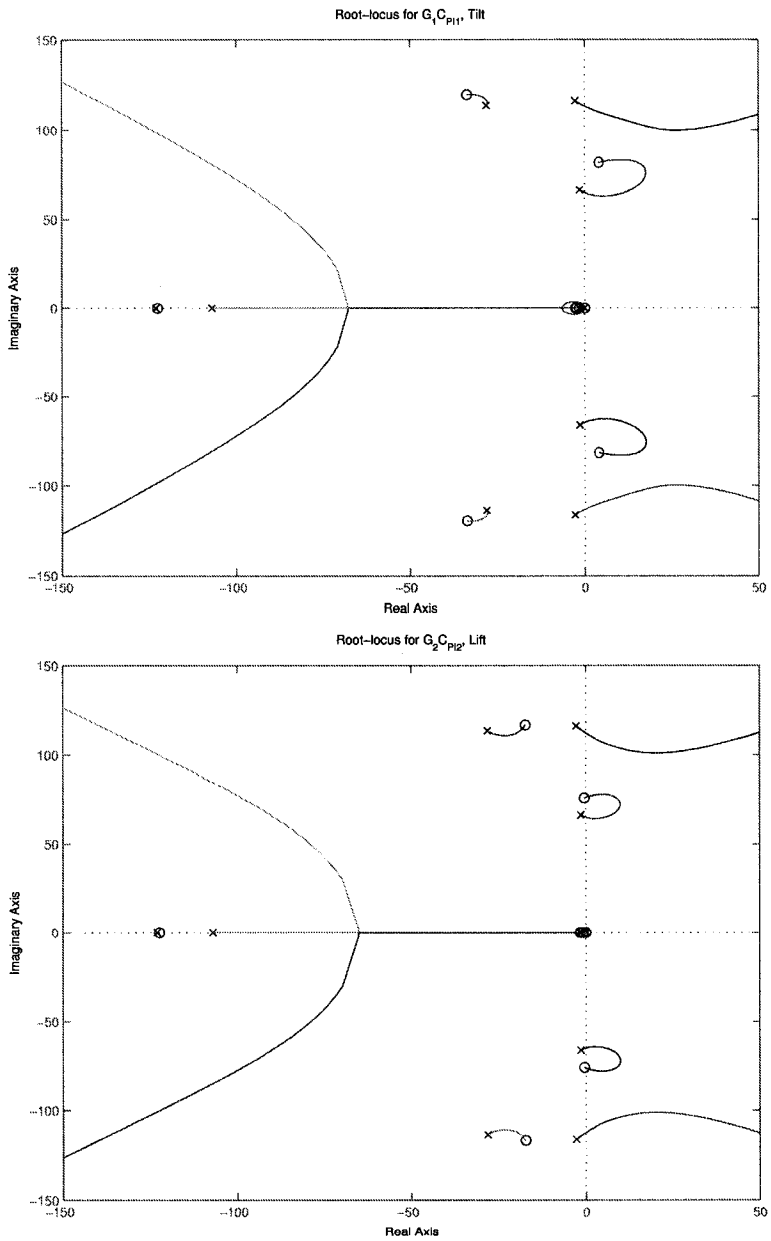

Figure 4.3 Root loci for the compensated plants

locus of the compensated lift system is contained in the left half plane is approximately 0.01 to 1.38. The gains that stabilize the lift system lie approximately in the range 0.01 to 2.9. The controller gains, for the tilt and lift systems were each selected to be one in the interest of robust stability. The high frequency poles near the jw axis indicate that the system has an under-damped oscillations near 10 Hz and 20 Hz. A higher order compensator is needed to control the under-damped oscillations.

The two controllers can be combined together to form one controller with a diagonal form:

$$K_{PI} = \begin{bmatrix} K_1 C_{PI1} & 0 \\ 0 & K_2 C_{PI2} \end{bmatrix} = \begin{bmatrix} 0.5 + \frac{1.3}{s} & 0 \\ 0 & 2.0 + \frac{3.0}{s} \end{bmatrix}$$

An obvious drawback of this controller design is that it does not take into account any of the coupling between the two input output pairs of the plant.

The sensitivity and complementary sensitivity transfer function matrices are given as

$$\begin{aligned} S_{PI} &= (I + GK_{PI})^{-1} \\ T_{PI} &= GK_{PI}(I + GK_{PI})^{-1}. \end{aligned} \tag{4.4}$$

The sensitivity transfer function matrix can be interpreted as the dynamics between a disturbance on the system's output and the actual output. It is therefore desired that S_{PI} be small at low frequencies so that the disturbance response is kept small. Another reason to keep the sensitivity small at low frequencies is for good tracking. It can be shown that the sensitivity represents the dynamics between the reference input and the tracking error [15]. The complementary sensitivity transfer function matrix can be thought of as the dynamics between the reference input and the output. Therefore, T_{PI} should be near unity at low frequencies since it is desired to track low frequency signals. Also, T_{PI} defines the dynamic relationship between input noise and the output. The noise has high frequency content generally and therefore T_{PI} should be small at high frequencies to attenuate it. For robust stability, the peak of the infinity norm of the sensitivity transfer function should be low. The rule of thumb often applied is that the sensitivity transfer function should have a peak of less than 2 (6 dB). The preceding discussion on the sensitivities generally applies to feedback control systems [15].

The frequency response of the sensitivity and complementary sensitivity transfer function matrices for the PI control systems can be seen in Fig. 4.4. It can be seen from the plot that the magnitude of sensitivity is low at low frequencies indicating good rejection of low frequency disturbances. Also the complementary sensitivity is low at high frequencies indicating good rejection of high frequency noise low tracking error. Since the peak of the sensitivity is not over 6 dB (though it is close), a reasonable level of robust stability can be expected.

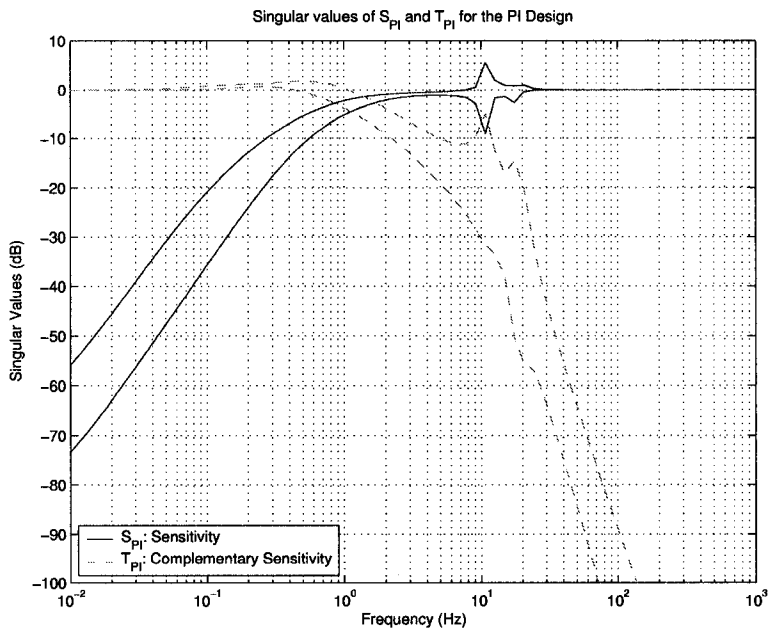

Figure 4.4 Frequency resposne of sensitivity and complementary sensitivity transfer function matrices for the PI system

4.2.1 Robustness Analysis

In this section, the robust stability is analyzed using the robustness norm condition in equation 4.2. Two separate analysis are given, one for 50% input uncertainty and another for uncertainty due to varying parameters β and C_d. In Fig. 4.5, the singular values of N_{11} are plotted for 50% input uncertainty. Any singular value above 1 indicates that the system is not robustly stable since it would violate the robust stability condition of equation 4.2. The

system has clearly failed the robustness test. This means that while the nominal system is stable, instability is possible in the uncertain system. Note that the robustness condition is violated in a very narrow band around 10 Hz where the lightly damped oscillations that are predicted from the root locus plots.

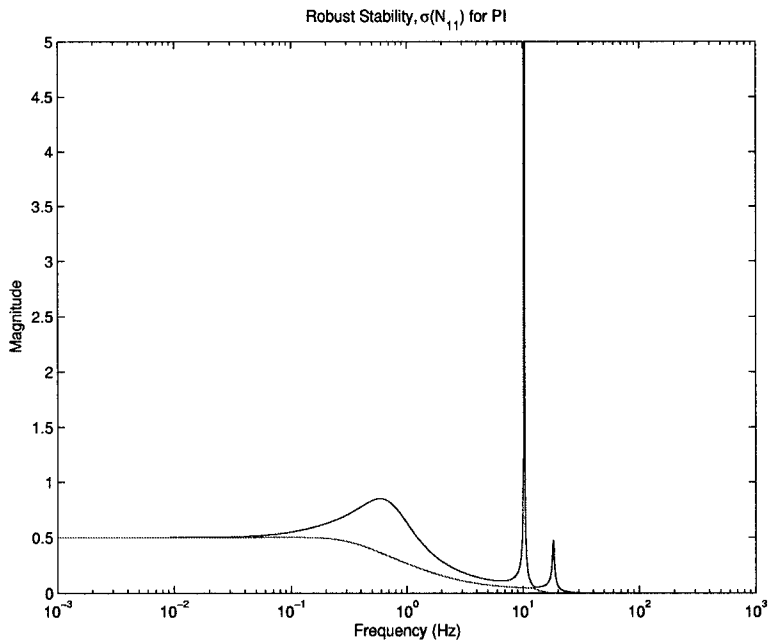

Figure 4.5 Singular value plot for the robust stability of the PI controlled system

In Fig. 4.6 a plot of the maximum singular values of N_{11} is given for the system with varying parameters, fluid bulk modulus, β, and valve discharge coefficient, C_d. This shows a clear violation of the robust stability condition near 8 and 25 Hz. Also there is a violation of the condition below 1 Hz. This shows that the system may become unstable given the variation in parameters considered in the plant uncertainty description.

4.2.2 Simulations

In this section the simulation results for the PI control design are given for both linear and nonlinear models. Step responses and level lift functionality are demonstrated. In level lift

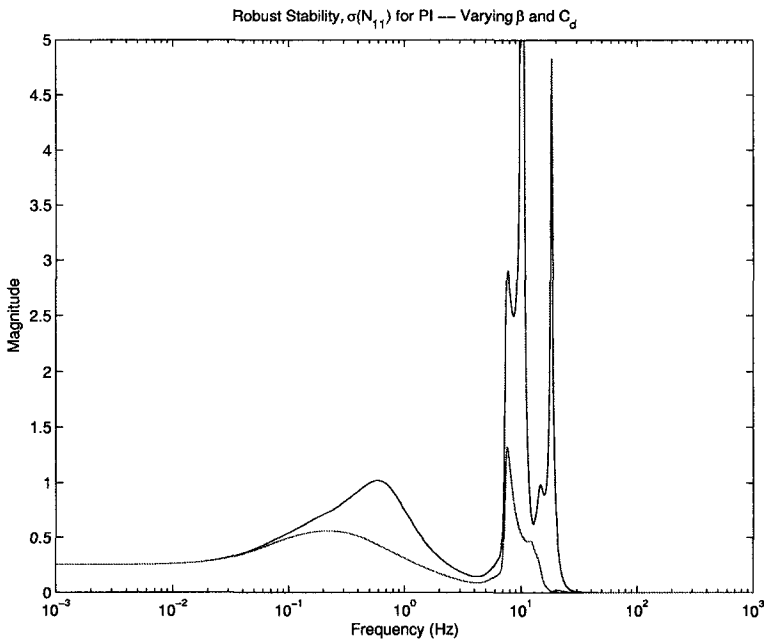

Figure 4.6 Singular value plot for the robust stability of the PI controlled system with varying parameters

mode, the desired bucket cylinder position is a function of the boom lift cylinder position such that the bucket floor remains level as the boom is raised. This represents motion coordinated between two separate actuators.

The PI controlled system was simulated on the linear model to test the ability of the system to track lift and tilt reference inputs simultaneously (Fig. 4.7). Step commands were given for desired tilt cylinder and lift cylinder position. Notice that there are oscillations as expected in the 10 Hz range. In the next simulation (Fig. 4.8), a ramp reference is given which is similar to level lift operation. The steady state error for the tilt position is negligible.

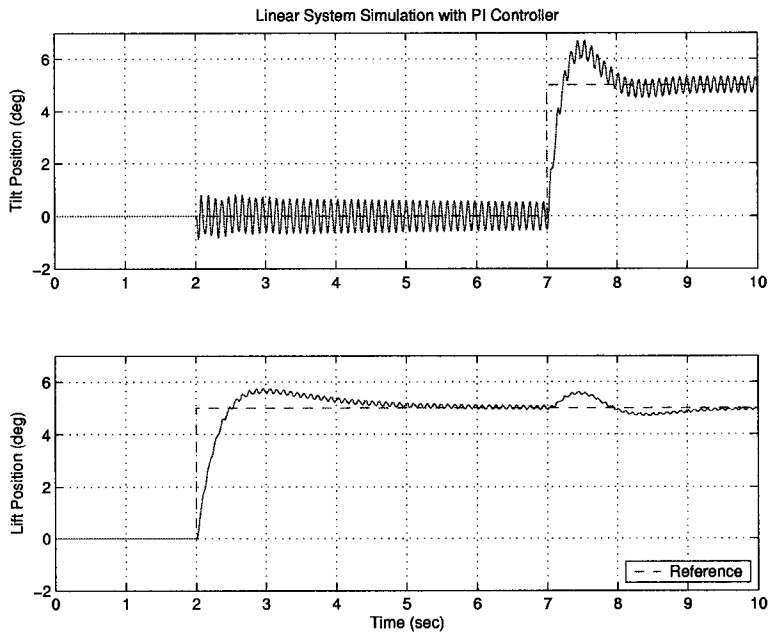

Figure 4.7 Tracking of reference lift position and tilt velocity references simulating the linear model with the PI controller

Nonlinear simulations of the PI controlled system reveal additional information about the closed-loop behavior of the system. Simulation results of the PI control system with the nonlinear model are given in Figs. 4.9 through 4.16. Two sets of inputs are given for these simulations: first is a step input on both tilt and lift reference positions and second is a ramp input to the lift function while the tilt tracks the level lift requirement, $\theta_{21} = -\theta_1$. Each set of simulations includes a simulation with the nominal nonlinear model and a simulation with

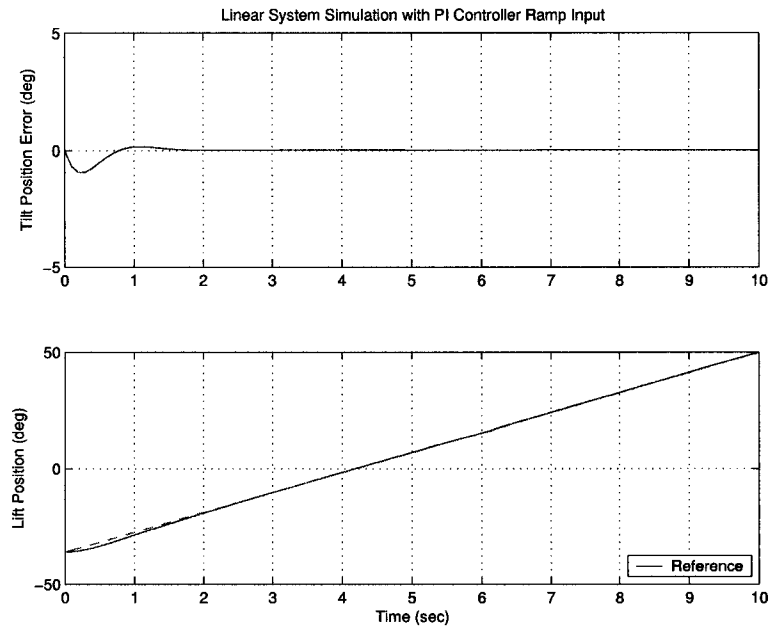

Figure 4.8 Tracking of ramp reference lift and tilt positions with the linear model and PI controller

the nonlinear model having a perturbation in the parameters, C_d and β. These parameters are larger than their nominal values by a factor of 1.5. This serves as a demonstration of the controller's robustness to parameter variation.

Figures 4.9 and 4.10 contain plots of the response to a step input. Similar to the linear case, some oscillations occur. These oscillations show up in the output position of the bucket as well as the margin pressure. Figures 4.11 and 4.12 show the same response but with perturbations in the bulk modulus an discharge coefficient parameters. The oscillations occur at a higher frequency and with much less amplitude in the case of the margin pressure.

In the level lift simulations, Figs. 4.13 and 4.14, the PI controller provides low tilt and lift tracking error, less than 2 degrees for the tilt function. Some oscillation is evident in the margin pressure. The simulations with perturbed parameters show that level lift performance has changed little other than an increase in the amplitude of oscillations of the margin pressure near the end of the simulation.

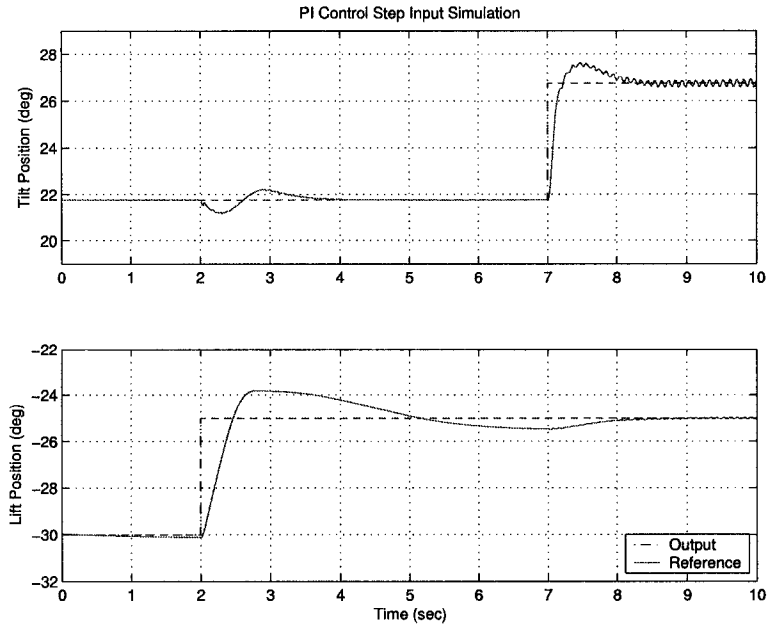

Figure 4.9 Step simulation result using PI and the nonlinear model

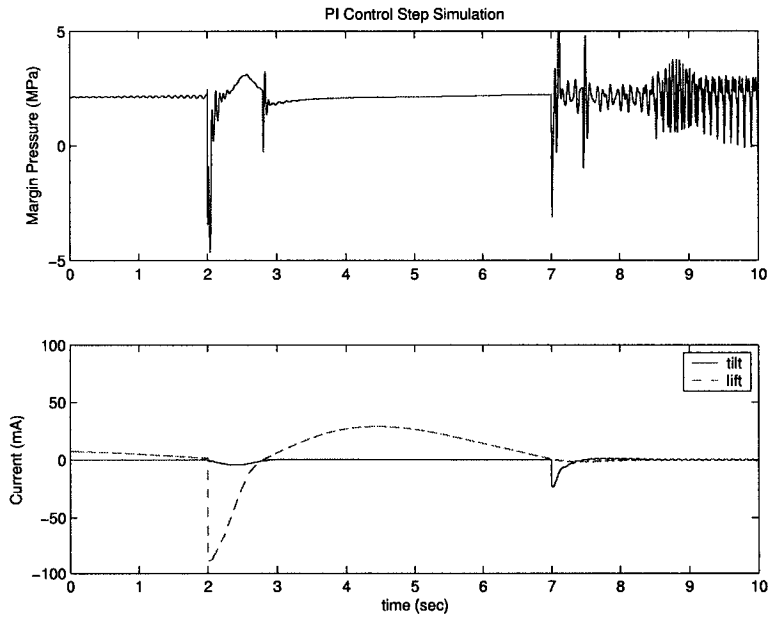

Figure 4.10 Margin pressure and valve inputs, PI step simulation

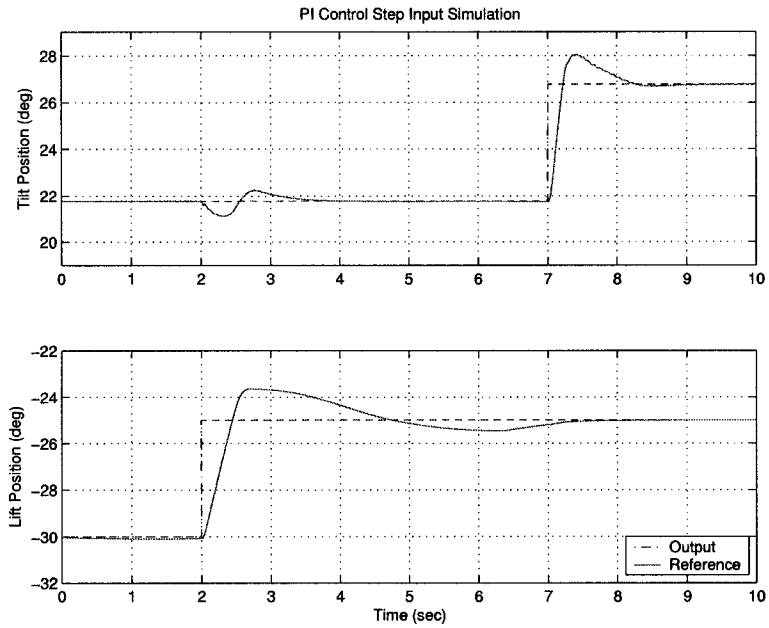

Figure 4.11 Step simulation result using PI and the nonlinear model with perturbation

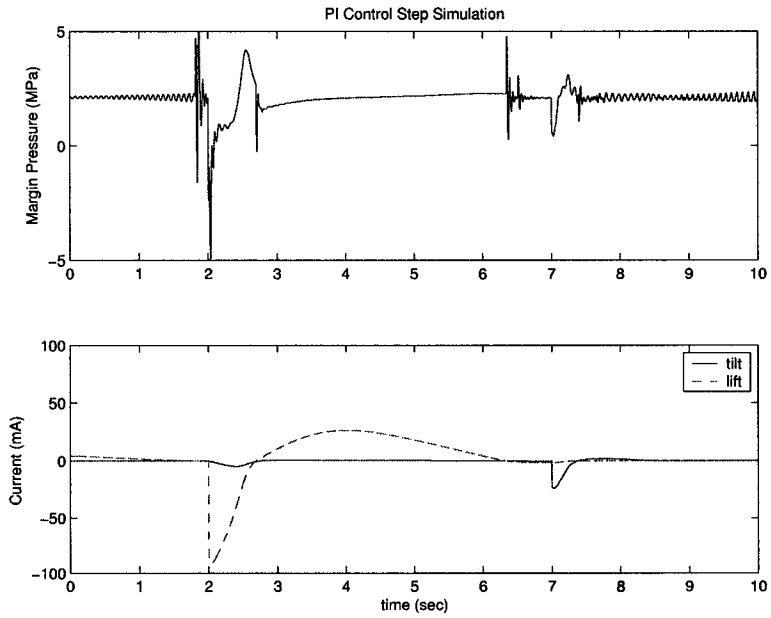

Figure 4.12 Margin pressure and valve inputs, PI step simulation with perturbation

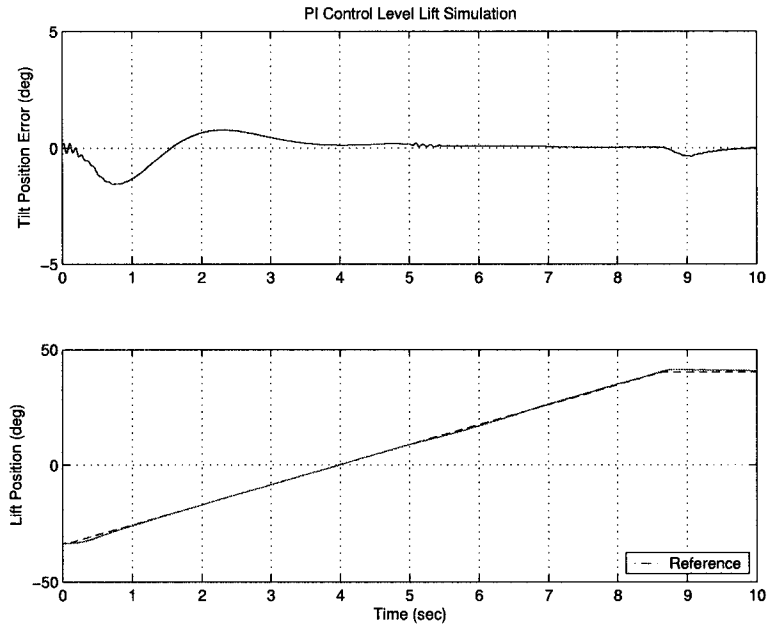

Figure 4.13 Level lift simulation result using PI and the nonlinear model

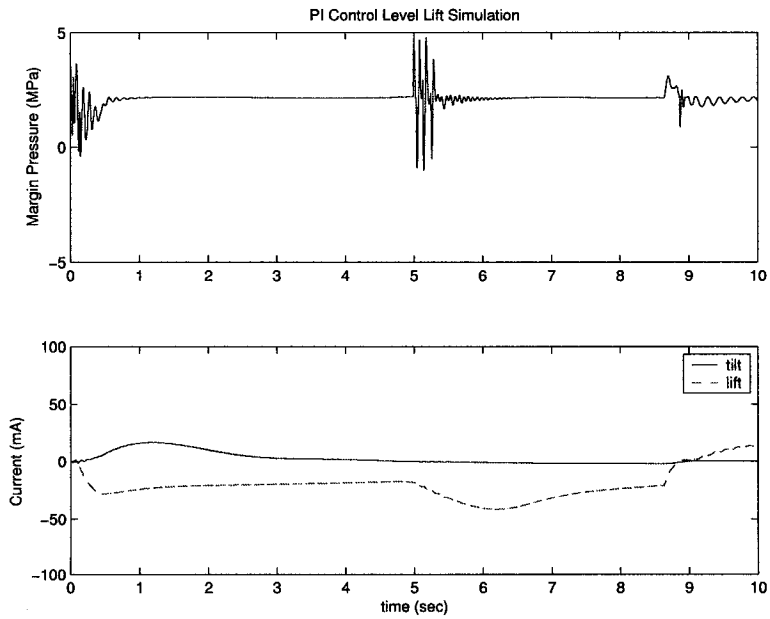

Figure 4.14 Margin pressure and valve inputs, PI level lift simulation

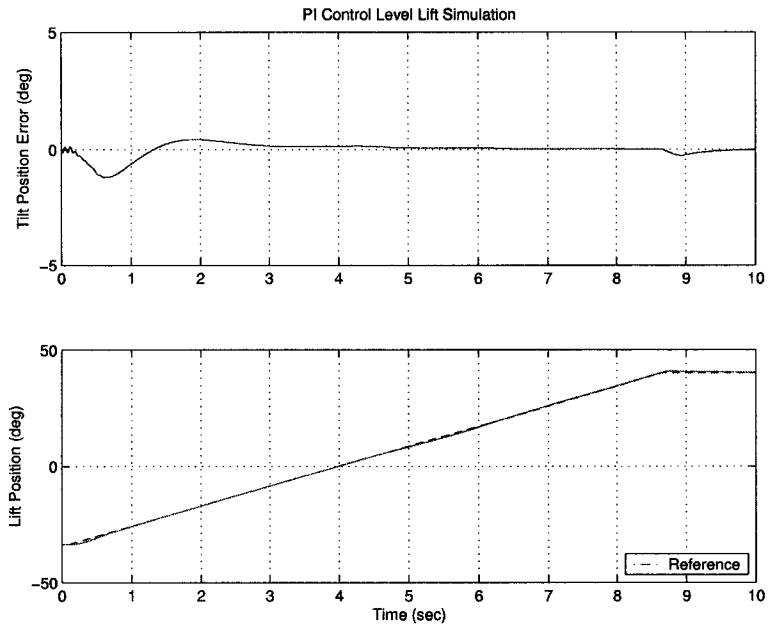

Figure 4.15 Level lift simulation result using PI and the nonlinear model with perturbation

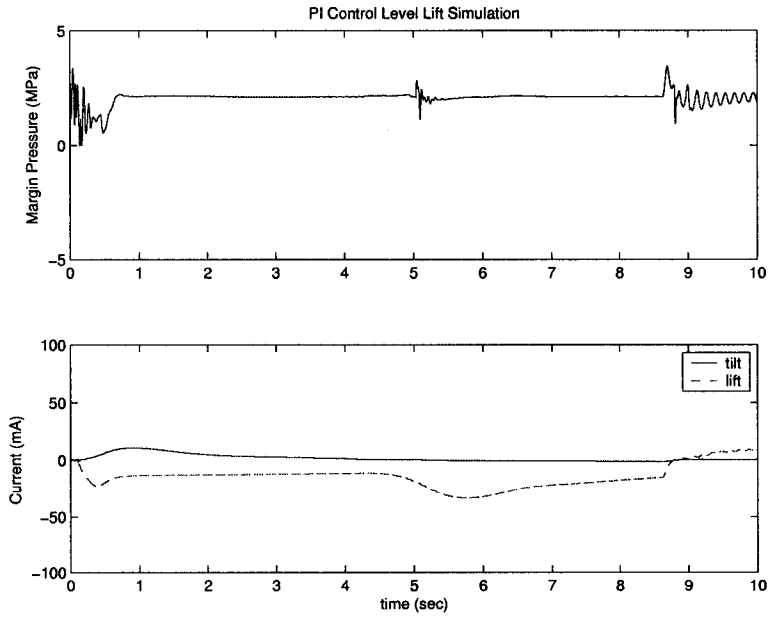

Figure 4.16 Margin pressure and valve inputs, PI level lift simulation with perturbation

4.3 LQG Control

The LQG design presented here is a MIMO state feedback design based on a similar work done previously by the author [17]. The standard LQG design procedure is used for the regulator problems; however, in this case, tracking is the required performance measure which requires augmenting the LQG design procedure to accommodate this modified performance objective. This is accomplished by augmenting the plant model by four new states corresponding to the second integral of both the bucket and boom angle tracking error [4]. The additional integrators allow tracking of step and ramp signals as a consequence of the internal model principle [4]. The equation for the filter dynamics which computes the integrals is given below:

$$\dot{e}_I = A_I e_I + B_I(r - y) \tag{4.5}$$

$$A_I = \begin{bmatrix} 0 & 0 & 0 & 0 \\ 2 & 0 & 0 & 0 \\ 0 & 0 & 0 & 0 \\ 0 & 0 & 2 & 0 \end{bmatrix} \qquad B_I = \begin{bmatrix} 2 & 0 \\ 0 & 0 \\ 0 & 2 \\ 0 & 0 \end{bmatrix}$$

The term, e_I is a vector of the first and second integrals of the tracking error. A diagram of the augmented plant model is given in Figure 4.17. The combined equations for the model and filter become

$$\begin{Bmatrix} \dot{x} \\ \dot{e_I} \end{Bmatrix} = \begin{bmatrix} A & 0 \\ -B_I C_y & A_I \end{bmatrix} \begin{Bmatrix} x \\ e_I \end{Bmatrix} + \begin{bmatrix} B_u \\ 0 \end{bmatrix} (u + w) + \begin{bmatrix} 0 \\ B_I \end{bmatrix} r, \tag{4.6}$$

$$y_m = \begin{bmatrix} C_m & 0 \end{bmatrix} \begin{Bmatrix} x \\ e_I \end{Bmatrix} + v,$$

where w and v are actuator noise and sensor noise respectively and r is the reference input. The bucket tilt cylinder position, x_1, and boom lift cylinder position, x_2, are the only two

measurements in the system. The measurement matrix is given as follows:

$$C_m = \begin{bmatrix} 1 & 0 & 0 & 0 & 0 & 0 & 0 & 0 & 0 & 0 & 0 & 0 & 0 \\ 0 & 1 & 0 & 0 & 0 & 0 & 0 & 0 & 0 & 0 & 0 & 0 & 0 \end{bmatrix}$$

We will make the following substitutions when refereing to the augmented system in equation 4.6 in the rest of this work:

$$A_a = \begin{bmatrix} A & 0 \\ -B_I C_y & A_I \end{bmatrix} \quad B_a = \begin{bmatrix} B_u \\ 0 \end{bmatrix} \quad C_a = \begin{bmatrix} C_m & 0 \end{bmatrix}$$

The integral error states, e_I, are added for the purpose of control. The controller uses the error along with other states to determine the appropriate current command for the bucket control valve solenoid. When the position error states approach zero, the bucket tilt cylinder approaches the desired position. Similarly, when the boom position error states approach zero, the boom lift cylinder position approaches the desired position.

4.3.1 Control Design

Let the feedback control gain, K, be broken into a gain on the plant states and a gain on the added integral error states and be given as, $K = [K_x, K_i]$. Then, the controller input, u, to the system in equation 4.6 is given by

$$u = -[K_x, K_i] \begin{Bmatrix} x \\ e_I \end{Bmatrix}. \tag{4.7}$$

The gain matrix K is designed to minimize the performance cost function

$$J = \int_0^\infty ([x^T, e_I^T] Q [x^T, e_I^T]^T + u^T R u) dt.$$

The weighting gains Q and R were selected to be,

$$\begin{aligned} Q &= diag[0, 0, 1, 1, 1, 0, 0, 0, 1, 1, 0, 1, 1, 9e9, 1e0, 9e9, 1] \\ R &= diag[100000, 1000], \end{aligned}$$

such that the tracking error states approach zero and desirable performance is achieved. Note that by making any of the last four elements of Q large, the highest penalty is on the tracking

error. R was tuned to avoid saturation of the valve solenoid current inputs while giving the fastest response possible.

The controller gain, K, is computed using the controller algebraic Riccati equation:

$$\begin{aligned} A_a^T P_c + P_c A_a - P_c B_a R^{-1} B_a^T P_c + Q &= 0 \quad P_c = P_c^T \geq 0 \\ K &= R^{-1} B_a^T P_c \end{aligned} \tag{4.8}$$

A state estimator was employed to compute the states of the non-augmented system from the measurements. Note that the two augmented states are not computed by the estimator. The dynamic system equations for the state estimator and the controller which uses estimated states, $\hat{x}$, rather than the actual states, x, are given as

$$\begin{aligned} \dot{\hat{x}} &= [A - LC_m]\hat{x} + B_u u + L y_m \\ u &= -K_x \hat{x} - K_i e_I, \end{aligned} \tag{4.9}$$

where $y_m = C_m x = [x_1, x_2]^T$. The filter gain L was computed using the filter algebraic Riccati equation:

$$\begin{aligned} P_f A^T + A P_f - P_f C_m^T S_v C_m P_f + S_w &= 0 \quad P_f = P_f^T \geq 0 \\ L &= P_f C_m^T S_v^{-1} \end{aligned} \tag{4.10}$$

S_v and S_w are the spectral densities of v and w. In this work, S_v and S_w are selected to tune the system response and to make the estimator poles sufficiently fast: $S_v = diag[1 \times 10^{-3}, 1 \times 10^{-3}]$ $S_w = diag[1 \times 10^5, 1 \times 10^5]$. The closed-loop linear system is as follows:

$$\begin{Bmatrix} \dot{x} \\ \dot{\hat{x}} \\ \dot{e_I} \end{Bmatrix} = \begin{bmatrix} A & -B_u K_x & -B_u K_I \\ LC_m & A - LC_m - B_u K_x & -B_u K_I \\ 0 & -B_I C_y & A_I \end{bmatrix} \begin{Bmatrix} x \\ \hat{x} \\ e_I \end{Bmatrix} + \begin{bmatrix} B_u w \\ Lv \\ 0 \end{bmatrix} + \begin{bmatrix} 0 \\ 0 \\ B_I \end{bmatrix} r, \quad \hat{y} = \begin{bmatrix} 0 & C_y & 0 \end{bmatrix} \begin{Bmatrix} x \\ \hat{x} \\ e_I \end{Bmatrix} + v \tag{4.11}$$

A diagram of the closed-loop linear system neglecting the noise inputs is given in Figure 4.18. The control design was also combined with the nonlinear plant model to create a nonlinear closed-loop system.

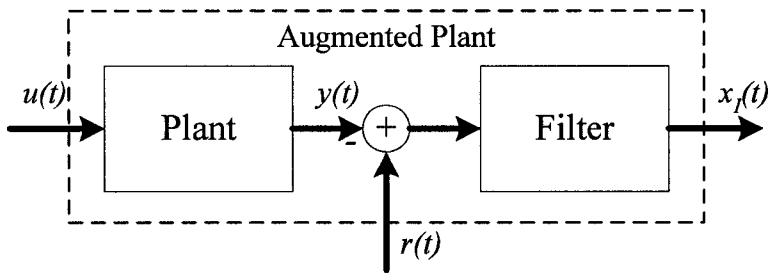

Figure 4.17 Augmented plant

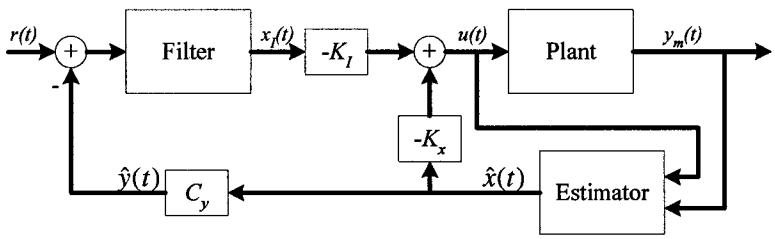

Figure 4.18 Closed-loop system with LQG controller/estimator

Singular value plots of the complementary transfer function matrix, S, and the complementary sensitivity matrix, T, show that some of the control system design requirements are likely to be met (see Fig. 4.19). The gain of S is small at low frequencies which suggests that good tracking will be achieved. The peaks of S and T are reasonably low indicating that the the system is robustly stable. The bandwidth is at least 1 Hz which will provide acceptably fast response times.

4.3.2 Robustness

Robust stability analysis was performed for the controller to determine weather the robust stability condition in equation 4.2 was violated. The singular values of N_{11} with 50% input

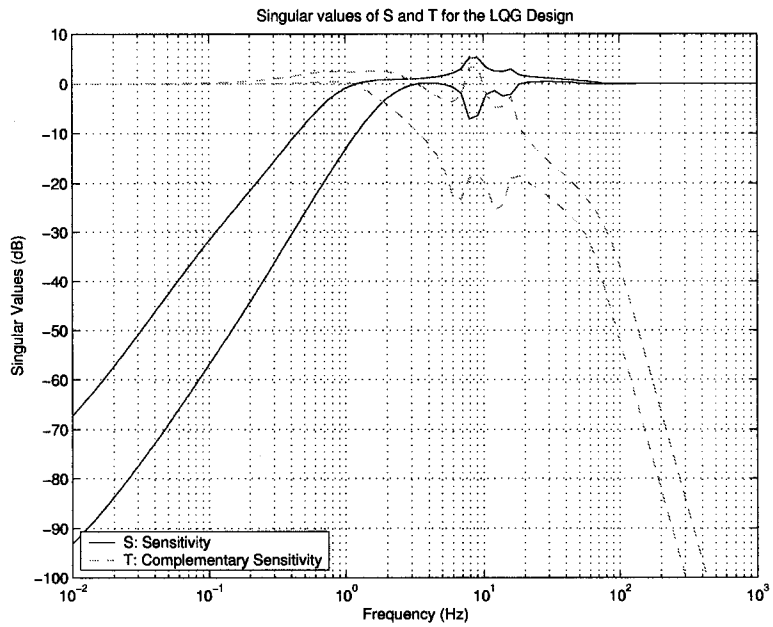

Figure 4.19 Frequency response of sensitivities, S and T, for LQG control

uncertainty are plotted for the LQG case in Fig. 4.20. Since the peak is less than 0.57, the system is robust to the uncertainty in the input.

A plot of the singular values of the N_{11} for the LQG system with the uncertainty model due to varying plant parameters is given in Fig. 4.21. The robust stability condition is violated in the frequency range from 7 Hz and higher frequencies.

4.4 Simulations

A set of simulation results are presented in this section. The presentation is similar to that of the PI control design simulation results.

The LQG controlled system was simulated on the linear model to test the ability of the system to track lift and tilt reference inputs simultaneously (Fig. 4.22). Step commands were given for desired tilt cylinder and lift cylinder position. The steady state error is zero and the percent overshoot is 0.3 degrees or approximately 6 % for both lift and tilt functions. In the next simulation (Fig. 4.23, a ramp reference is given which is similar to level lift operation.

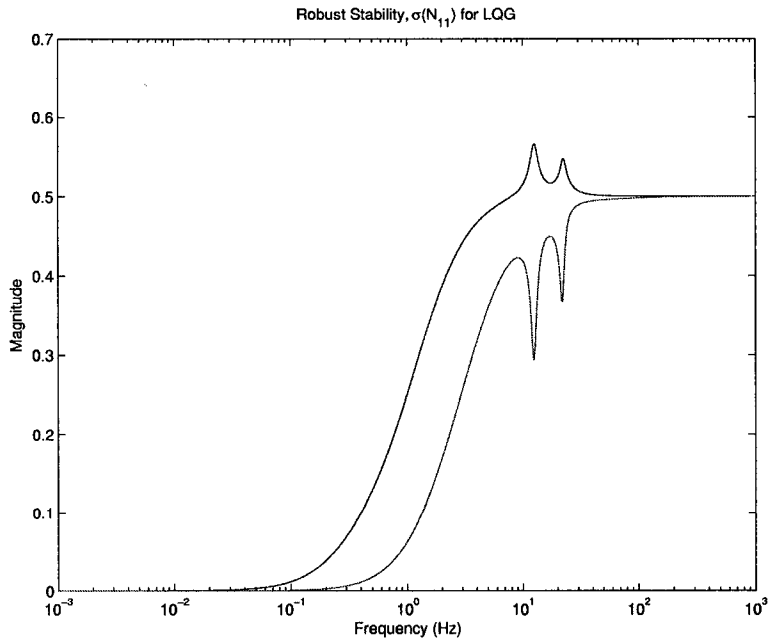

Figure 4.20 Singular value plot for the robust stability of the LQG controlled system with 50% input uncertainty

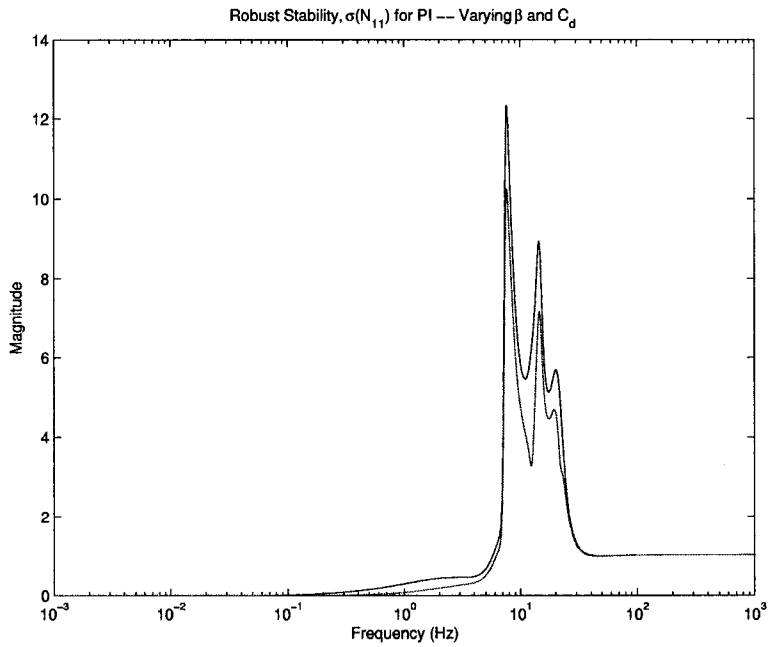

Figure 4.21 Singular value plot for the robust stability of the LQG controlled system with varying parameters

The steady state errors for the tilt and lift positions are negligible.

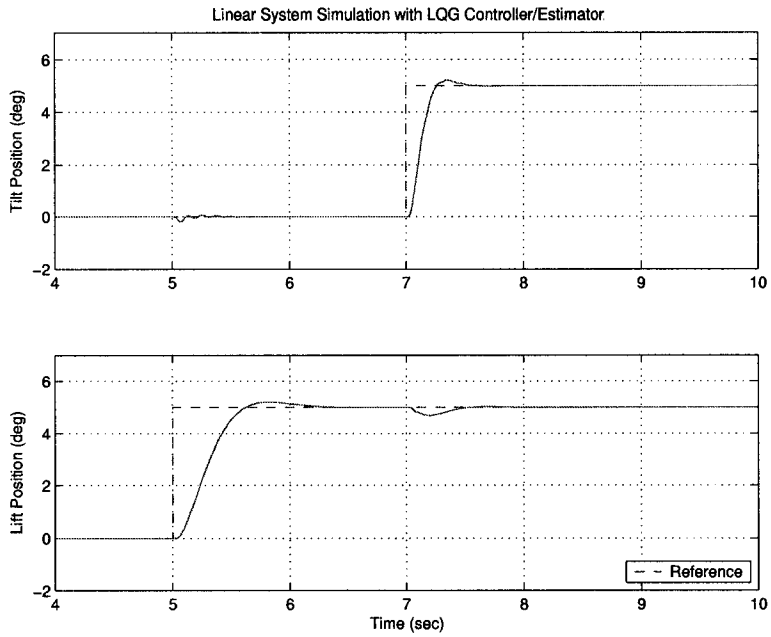

Figure 4.22 Tracking of reference lift position and tilt velocity references simulating the linear model with the LQG controller

The tilt and lift position control functions were simulated on the non-linear model as well. The first simulation is a step response of the closed-loop control system (Figs. 4.24 and 4.25). The steady state error for the lift and tilt functions are zero. The lift position output looks different than the linear simulation. This is likely because of the large excursion of the lift input current from its nominal value. The simulations with perturbed parameters and a step input (Figs. 4.26 and 4.27) show that the lift and tilt performance change little while the margin pressure and input currents oscillate to a great degree.

The next set of simulations is a demonstration of the level lift function. The bucket cylinder position error is plotted (Fig. 4.28). In the same Fig., a plot of the boom lift cylinder position and the desired boom position (determined by a ramp input) are also given. The boom cylinder position plot shows that boom has moved through most of its range. As the simulation progresses, error is reduced to low levels for both the tilt and the lift functions, less than 2 degrees. Again the performance changes little when the parameters β and C_d are altered (Figs.

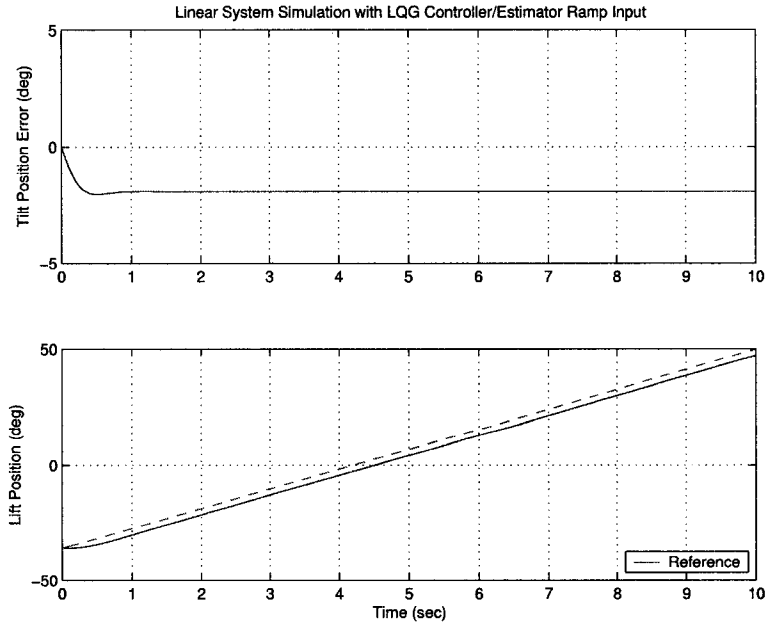

Figure 4.23 Tracking of ramp reference lift and tilt positions with the linear model and LQG controller

4.30 and 4.31) but there is an increased level of oscillation in the inputs and margin pressure.

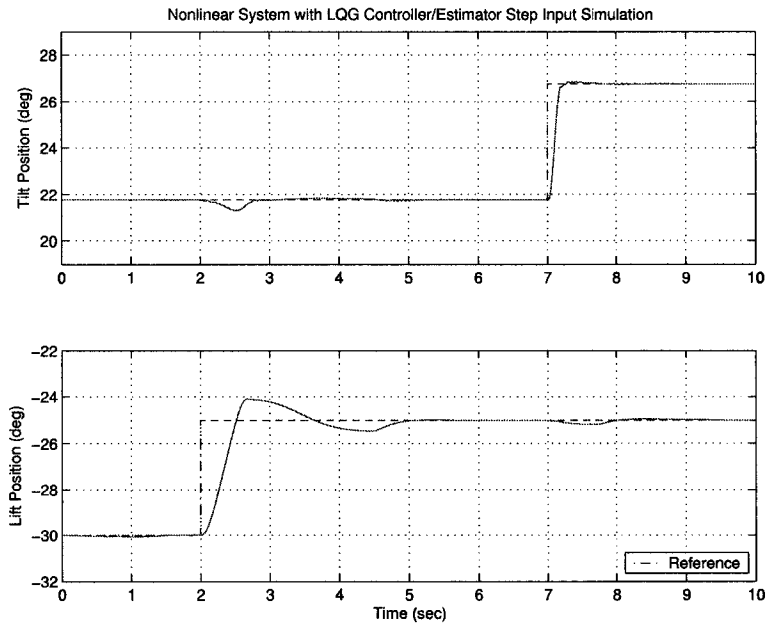

Figure 4.24 Step simulation result using LQG and the nonlinear model

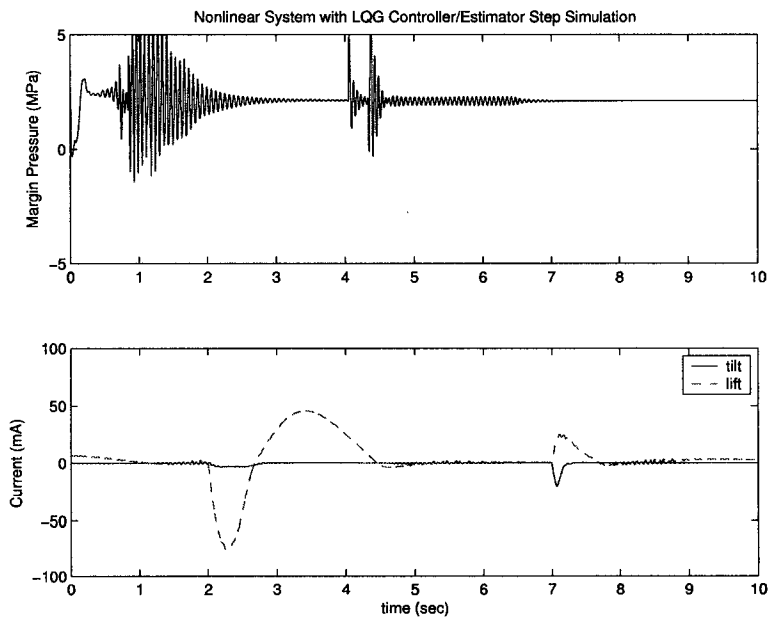

Figure 4.25 Margin pressure and valve inputs, LQG step simulation

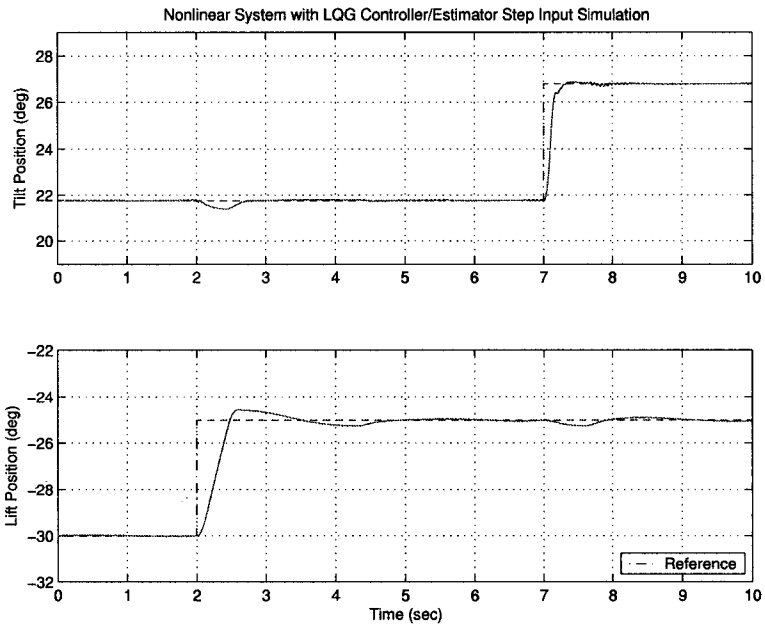

Figure 4.26 Step simulation result using LQG and the nonlinear model with perturbation

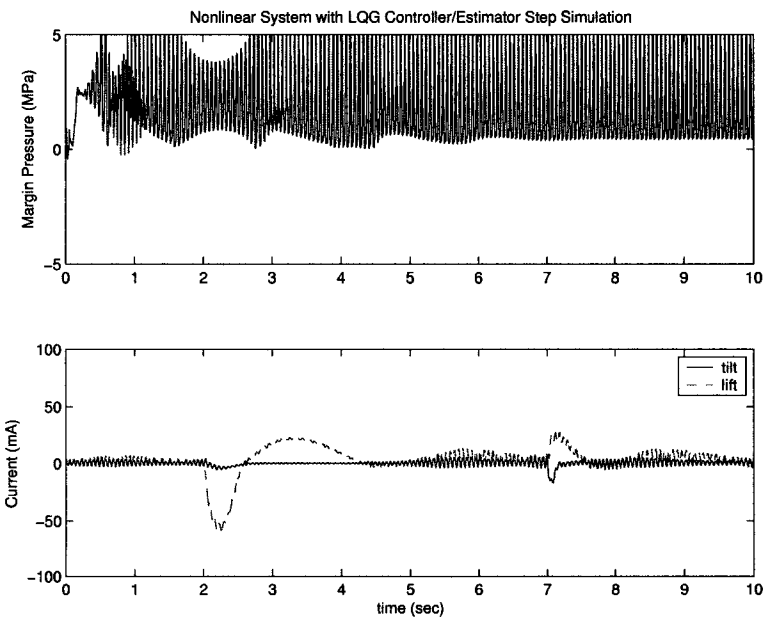

Figure 4.27 Margin pressure and valve inputs, LQG step simulation with perturbation

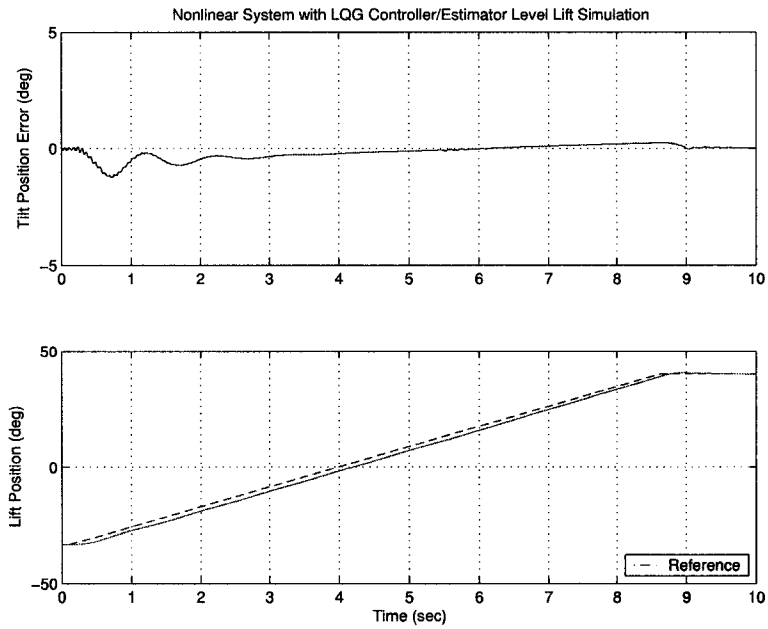

Figure 4.28 Level lift simulation result using LQG and the nonlinear model

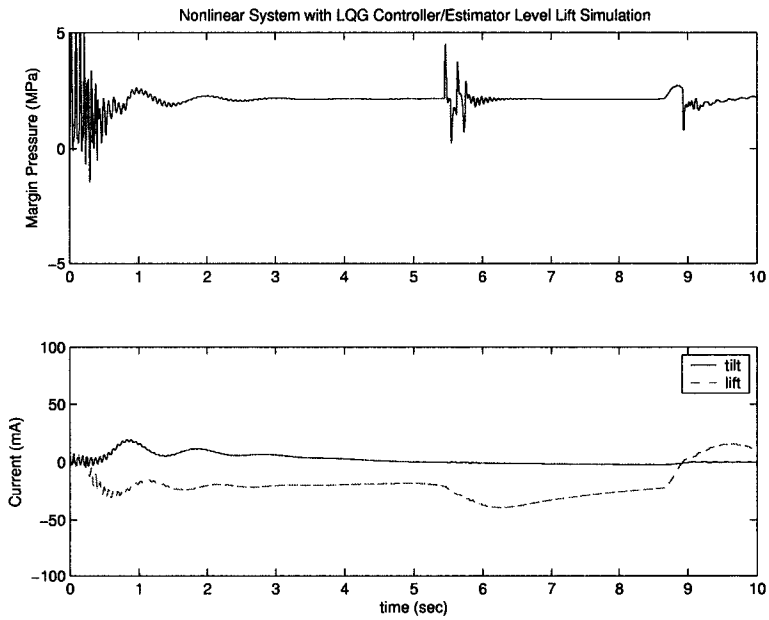

Figure 4.29 Margin pressure and valve inputs, LQG level lift simulation

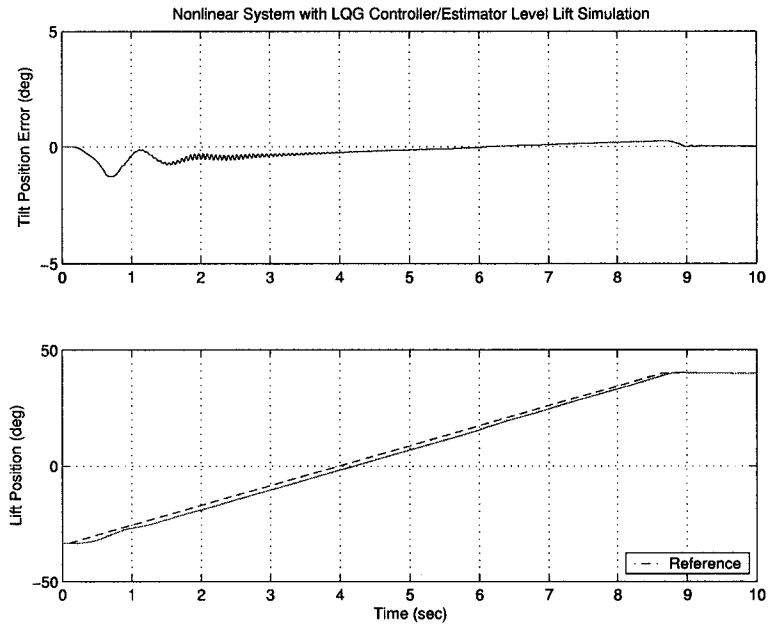

Figure 4.30 Level lift simulation result using LQG and the nonlinear model with perturbation

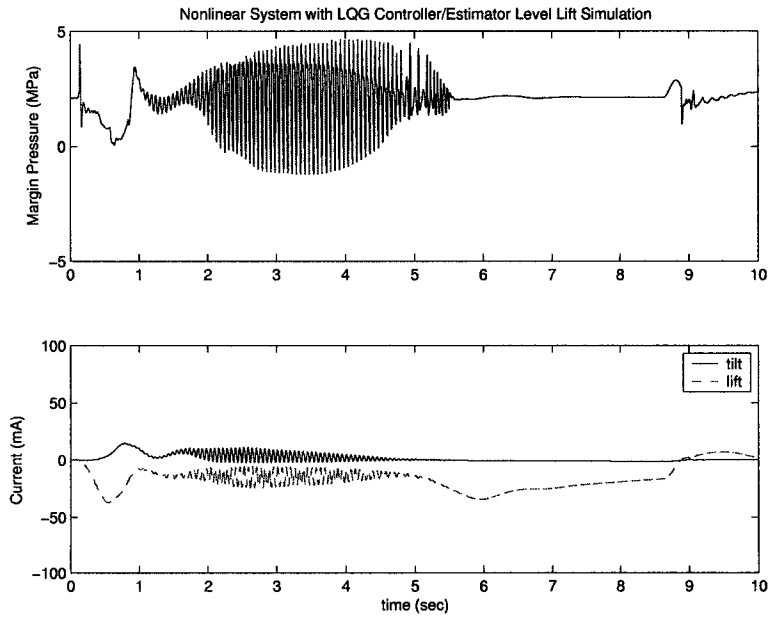

Figure 4.31 Margin pressure and valve inputs, LQG level lift simulation with perturbation

4.5 Mixed Sensitivity H_∞

The mixed sensitivity H_∞ controller design was performed in stages. First, the performance requirements were captured in terms of the weighting functions in the frequency domain. Next, an H_∞ design was synthesized using a standard H_∞ design optimization procedure [16]. The control system was simulated using the nonlinear model. Finally, the performance weights were adjusted and the controller was synthesized with an iterative procedure until the nonlinear simulation gave a satisfactory response. If the closed-loop response with complete nonlinear model was not found to be satisfactory the design process was repeated until a satisfactory design was obtained.

4.5.1 Control Design

The H_∞ design presented here is based on shaping the sensitivity and complementary sensitivity transfer functions which are given as,

$$S = (I + GK)^{-1}$$

and

$$T = GK(I + GK)^{-1},$$

respectively; where, G is the nominal plant model. To reduce the possibility of actuator saturation, the transfer function KS is also considered. Recall that the system has been scaled for the purpose of design such that all input and output signal magnitudes are less than or equal to one. For an H_∞ design, refer to the block diagram which gives the structure of the control system in Fig. 4.32[15]. The closed-loop plant dynamics can be cast into the form,

$$\begin{Bmatrix} z_1 \\ z_2 \\ z_3 \\ v \end{Bmatrix} = \begin{bmatrix} W_p & -W_pG \\ 0 & W_tG \\ 0 & W_u \\ I & -G \end{bmatrix} \begin{Bmatrix} r \\ u \end{Bmatrix}, \tag{4.12}$$

where r is the reference input (desired boom and bucket angles), v is the input to the controller, and $z_{1,2,3}$ are weighted errors. An H_∞ controller is designed to minimize the following cost function,

$$\left\| \begin{array}{c} W_p S \\ W_t T \\ W_u K S \end{array} \right\|_\infty \leq \gamma, \tag{4.13}$$

where K is the resulting controller. The control input to the plant is given by

$$u = K(r - y_m).$$

The weighting matrices, W_p and W_t, are set to

$$W_p = \begin{bmatrix} W_{p1} & 0 \\ 0 & W_{p2} \end{bmatrix}, W_t = \begin{bmatrix} W_{t1} & 0 \\ 0 & W_{t2} \end{bmatrix}, \tag{4.14}$$

$$W_u = \begin{bmatrix} 1 & 0 \\ 0 & 1 \end{bmatrix}$$

with

$$W_{p1} = W_{p2} = \frac{0.667(s + 9.425)^2}{(s + 0.4417)^2}$$

$$W_{t1} = W_{t2} = \frac{31.62(s + 5.027)}{(s + 238.4)}.$$

These weights are designed based on the controller design requirements. It is desired to have good tracking of step and ramp signals therefore a small gain needed on S at low frequencies (unity gain on T at low frequencies, $T = I - S$). A double integrator approximation is used for tilt and lift performance weight, W_p, which is a weight on S (see Fig. 4.33). The slope of W_p is 40 dB/decade at low frequencies and levelling off at very low frequencies. The system should not be effected by high frequency signals either from the reference input or from noise so the weight on T, which is given by W_t, is chosen to have a low gain at high frequencies. Since the reference input for the lift function is from a joystick, the bandwidth on T could be chosen such that operator induced oscillation is attenuated. In this case the weights, W_p and

W_t, have been chosen with a bandwidth of about 1.4 Hz. The H_∞ design process yielded a two input two output controller with $\gamma = 1.77$.

The singular value plots of the resulting sensitivities S and T are given in Fig. 4.34. The bandwidth is greater than desired and the peaks are low indicating good stability robustness since the peaks are less than 1 dB.

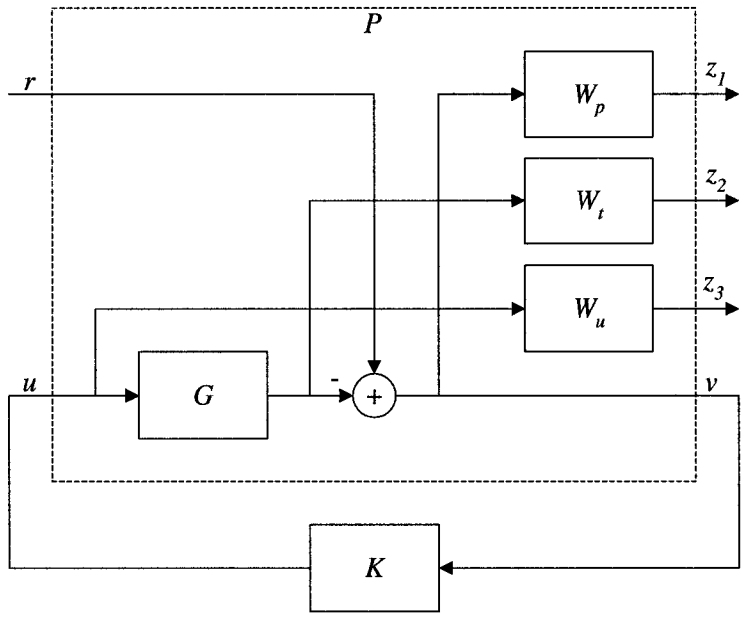

Figure 4.32 Plant with Sensitivity Weights

4.5.2 Robustness Analysis

For the H_∞ case in Fig. 4.35, the magnitude of the maximum singular value of N_{11} is less than one for the entire frequency range. This shows that the robust stability condition is not violated in the presence of the multiplicative input uncertainty considered in this work. The robustness analysis for varying plant parameters, β and C_d, is given in Fig. 4.36 for the H_∞ controlled system. The robust stability condition is violated between about 6 and 25 Hz.

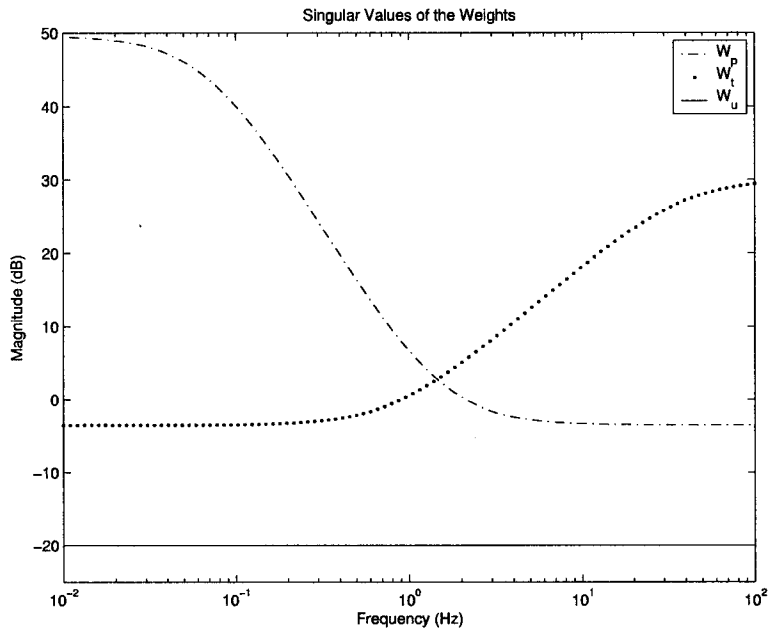

Figure 4.33 Bode diagrams of weights

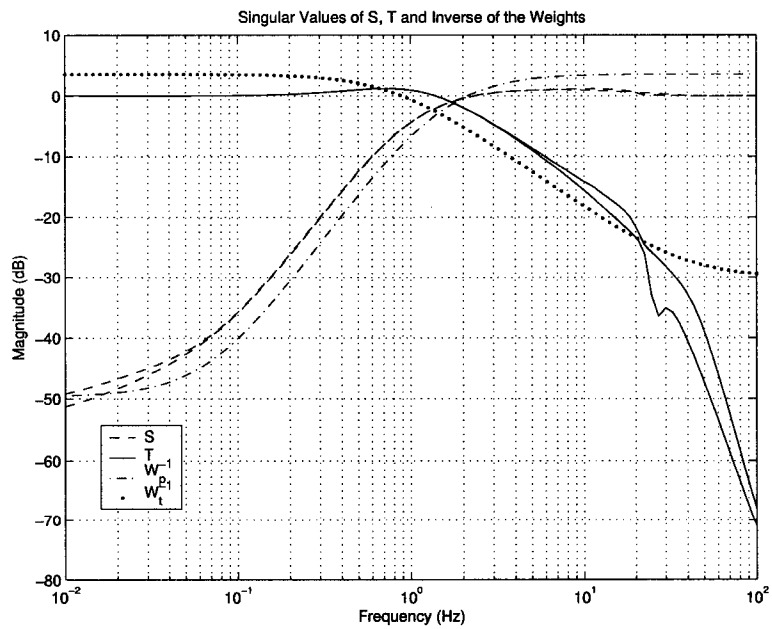

Figure 4.34 Sensitivities S and T for the H_∞ control design

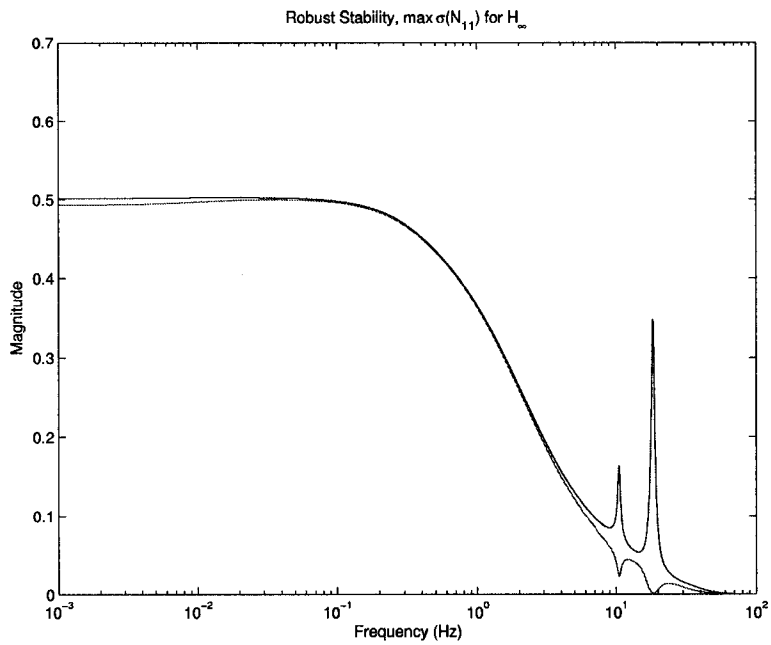

Figure 4.35 Singular value plot for the robust stability of the H_∞ controlled system

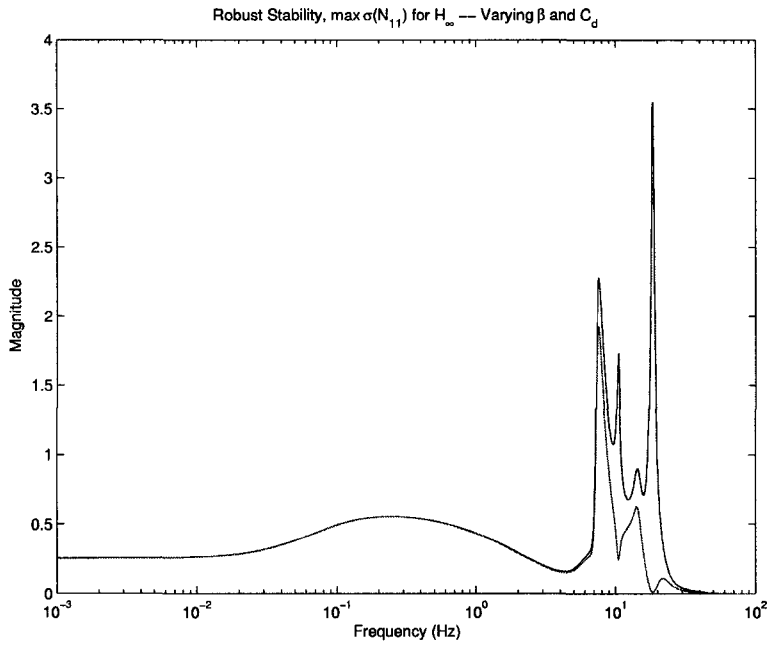

Figure 4.36 Robust stability of the H_∞ controlled system with varying parameters

4.5.3 Simulations

A simulated response of the H_∞ controlled system with step inputs to tilt and lift references is given in Fig. 4.37. The responses to step inputs show that the system is capable of tracking with zero steady state error in the linear case. The percent over shoot and settling time are approximately 13% and 0.85 seconds for both tilt and lift. Notice that the coupling effects between the lift and tilt functions are less than in the LQG case. The responses show that the system is capable of tracking two reference inputs simultaneously.

A ramp input was given to the linear system with the H_∞ control (Fig. 4.38). The steady state tracking error of the tilt angle is very small, 0.25 deg for both. The tracking error for the lift angle is similarly small. The tilt tracking error is very low in comparison to the LQG case. This may be attributed to the selection of the performance weight, W_p.

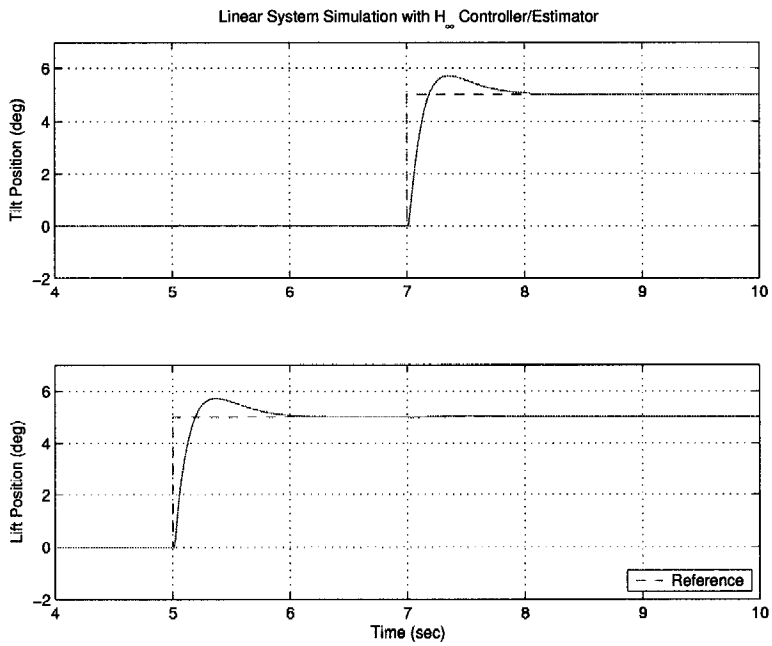

Figure 4.37 Simulation with the H_∞ controller and the linear model with step reference input

Responses for step and level lift reference inputs were generated with the nonlinear model and H_∞ controller. The step response is given in Fig. 4.39 and 4.40. The lift response has

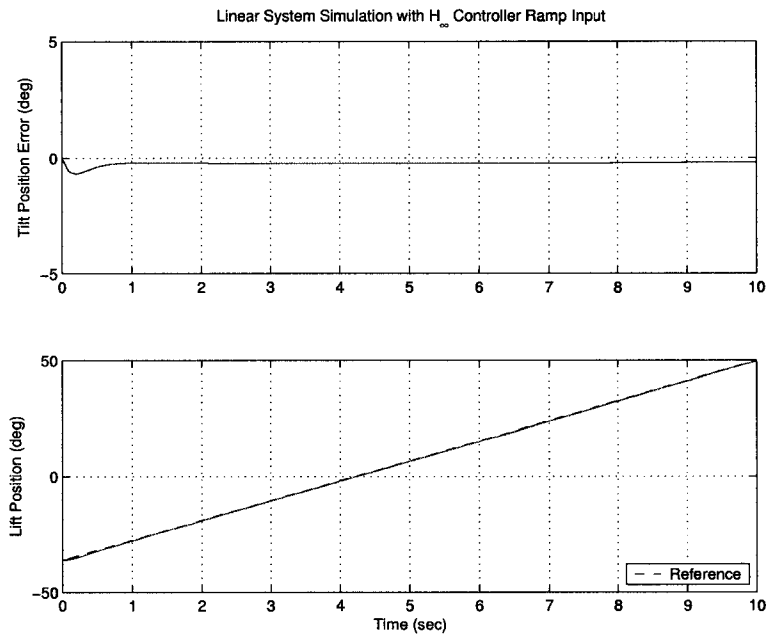

Figure 4.38 Simulation with the H_∞ controller and the linear model with ramp reference input

greater than expected overshoot compared to the linear response. A simulation of the level lift tracking task shows that both functions, lift and tilt, track commanded input well in the H_∞ case (Fig. 4.43 and 4.44).

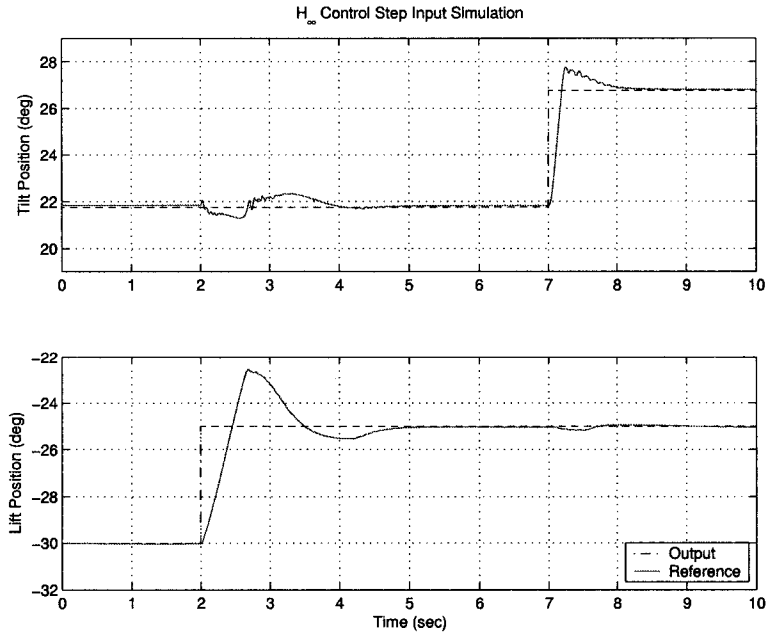

Figure 4.39 Step simulation result using H_∞ and the nonlinear model

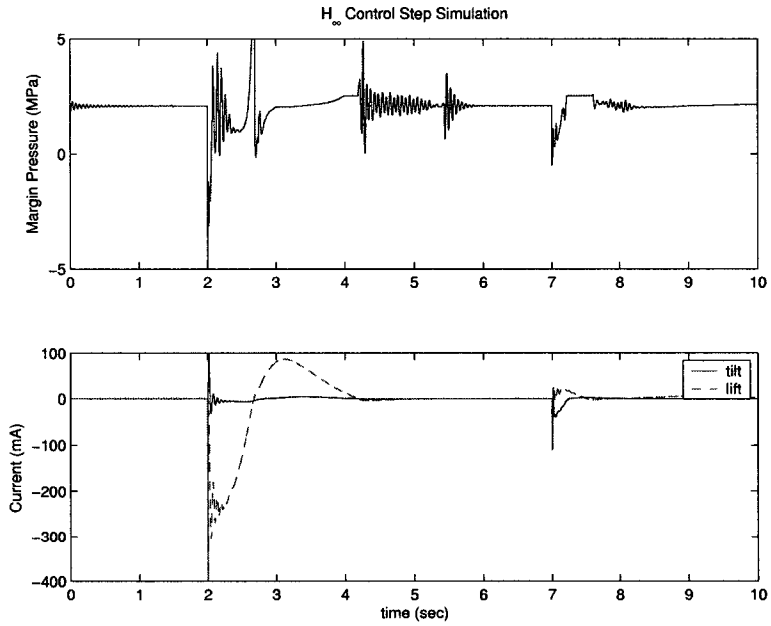

Figure 4.40 Margin pressure and valve inputs, H_∞ step simulation

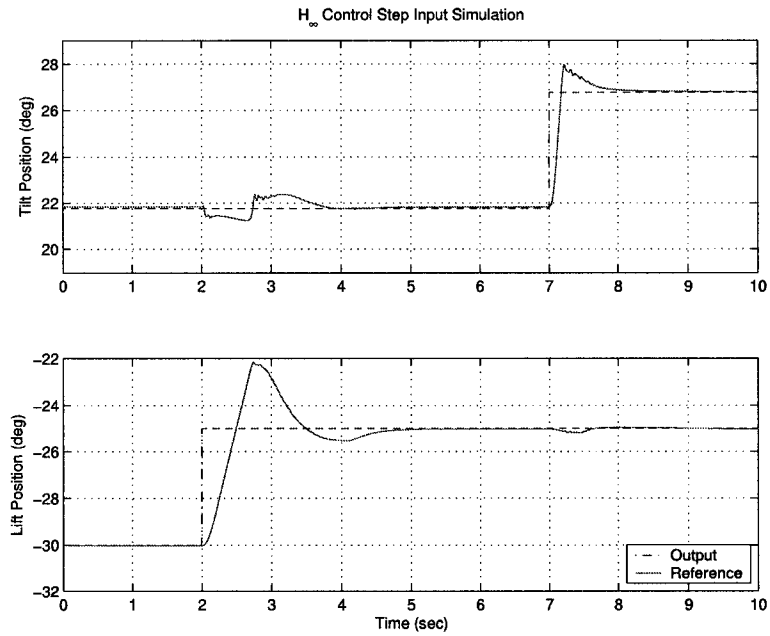

Figure 4.41 Step simulation result using H_∞ and the nonlinear model with perturbation

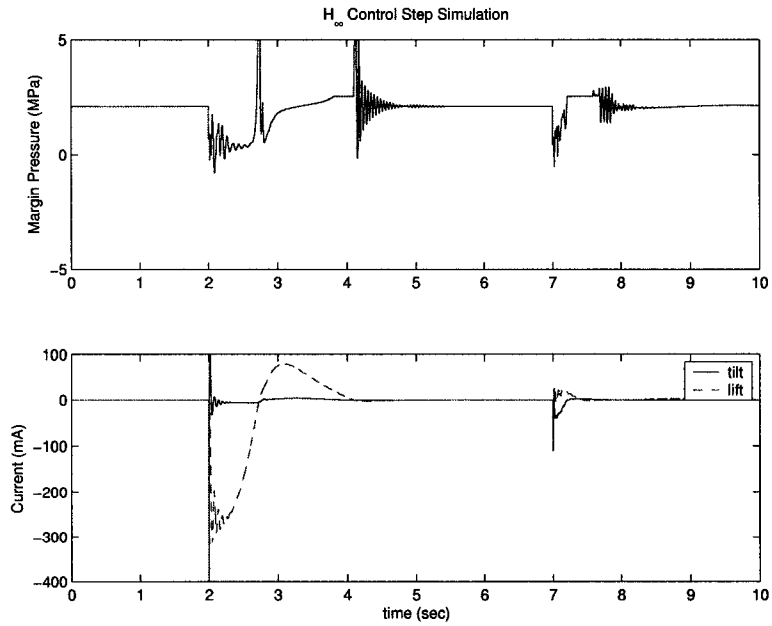

Figure 4.42 Margin pressure and valve inputs, H_∞ step simulation with perturbation

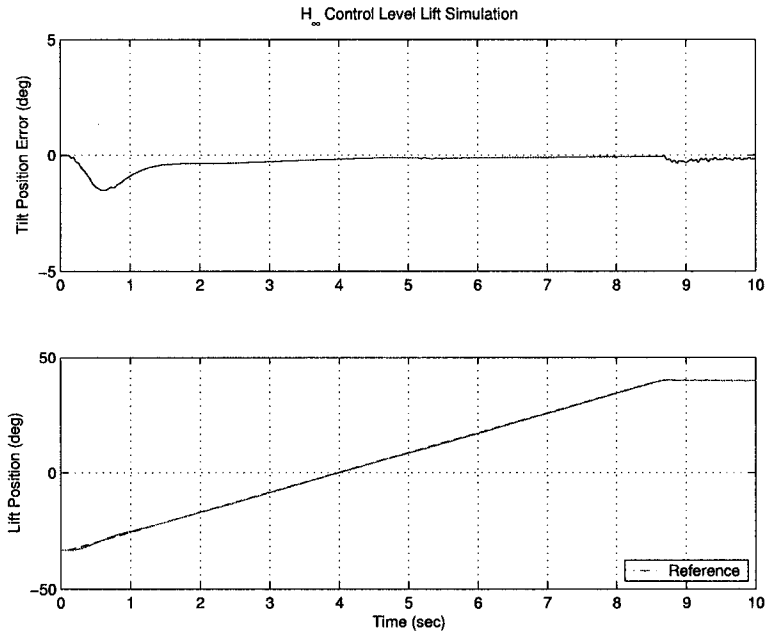

Figure 4.43 Level lift simulation result using H_∞ and the nonlinear model

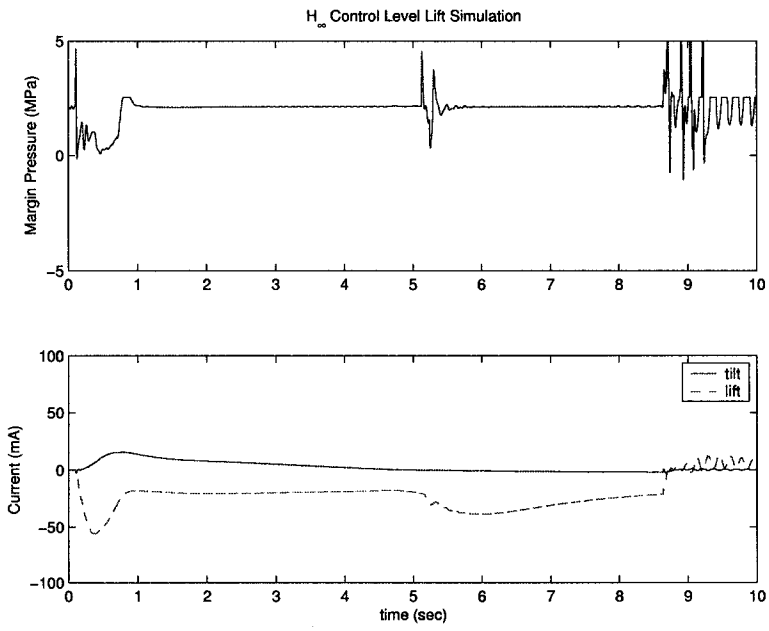

Figure 4.44 Margin pressure and valve inputs, H_∞ level lift simulation

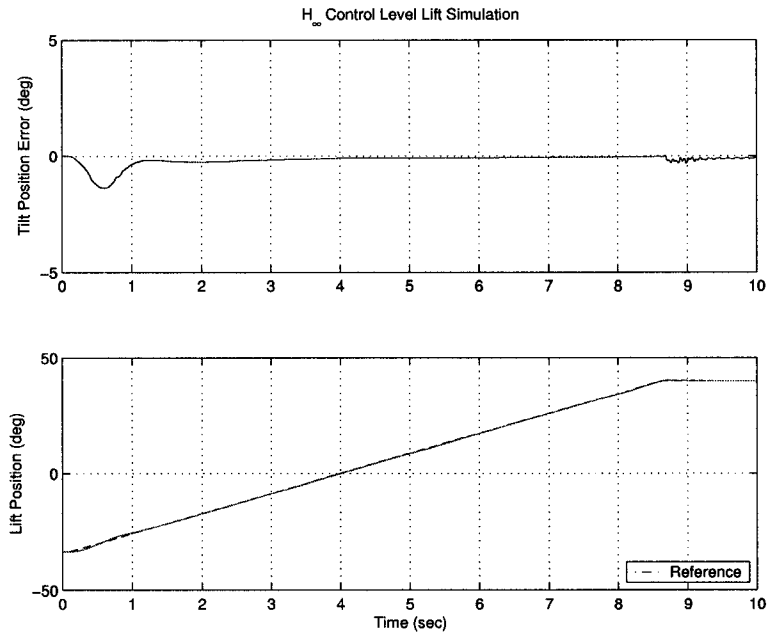

Figure 4.45 Level lift simulation result using H_∞ and the nonlinear model with perturbation

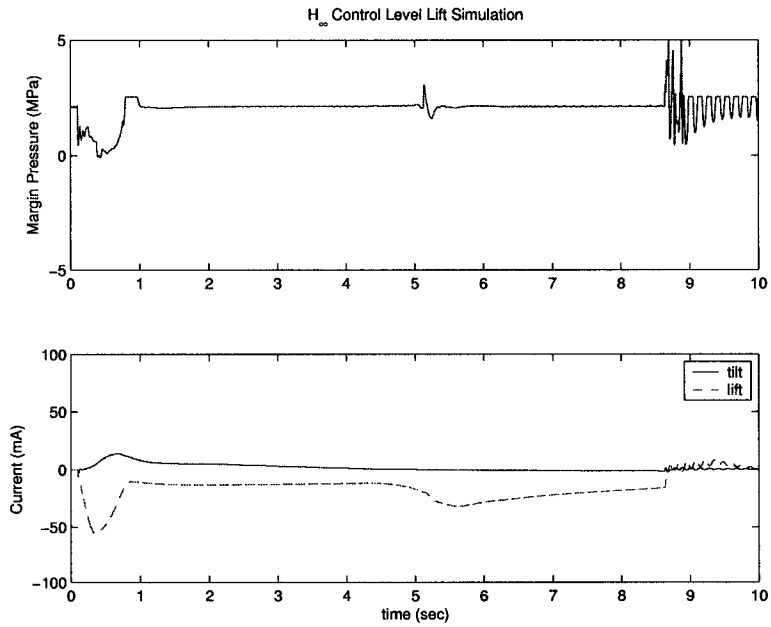

Figure 4.46 Margin pressure and valve inputs, H_∞ level lift simulation with perturbation

4.6 Feedback Linearization

The only nonlinear portion of the dynamics considered in this work is the relationship between the spool valve position and the pressure within the hydraulic cylinders which is highly nonlinear. If this subsystem could be altered to behave more linear in nature, this would make several linear control design methods much more applicable to the entire system. The system could be altered by applying a nonlinear feedback controller which causes the system to appear more linear without modifying the actual physical system. A nonlinear control law that decouples the tilt pressure subsystem from the rest of the system dynamics could be designed.

In this section, the input-output feedback linearization was developed for the tilt and lift pressure dynamics. First, the feedback linearization control law for the tilt pressure system which gives a linear relationship between cylinder force and the input was developed. Also simulations were given for a closed-loop SISO tilt control system. Next, the feedback linearization was extended to provide a linear relationship between two inputs and the force output of both the tilt and lift cylinders. A linearization was given for the plant including the feedback linearization control law. Finally, a tracking control system was developed.

4.6.1 Control Law

To achieve an input-output linearization for the tilt pressure system, the output of load force,

$$y_1 = A_{cy1}(x_9 - \alpha_1 x_{10})$$

is chosen. Recall that states x_9 and x_{10} correspond to the cylinder pressures and α_1 is the ratio of rod and cap end cylinder areas; therefore y_1 is the net force due to the pressure in the cylinder. The input to the system to be made linear is the input valve position. The goal is to obtain a linear relationship between the valve position and the force on the hydraulic cylinder once the control law is applied. To simplify the control law and eliminate the need for velocity

measurements an alternative output is chosen similar to the one given above [19]:

$$y_1 = A_{cy1}(\tilde{x}_9 - \alpha_1 \tilde{x}_{10})$$

The the states denoted by $\tilde{x}_9$ and $\tilde{x}_{10}$ are from the following transformation:

$$\begin{aligned} \tilde{x}_9 &= x_9 + \beta \ln(V_0 + A_{cy1} x_1) \\ \tilde{x}_{10} &= x_{10} + \beta \ln(V_0 + \alpha_1 A_{cy1}(x_{m1} - x_1)) \end{aligned} \tag{4.15}$$

After taking the time derivative of y_1 the valve position, an expression for $\ddot{y}_1$ is obtained and set equal to v_1 which will later become the new control input. The valve position, x_8, can then be solved for. Within the valve actuators bandwidth, the input current, u_1, is approximately equal to the spool position divided by G_v. Therefore, the input-output linearizing control law is given by

$$u_1(t) \approx x_8 \frac{1}{G_v} = \frac{1}{G_v} \frac{v_1(t)}{\sqrt{2}\,\beta\, A_{cy1}\, C_d \left(-\frac{K_{PA1}\sqrt{\frac{x_5(t)-x_9(t)}{\rho}}}{V_0 + A_{cy1}\, x_1(t)} - \frac{K_{TB1}\,\alpha_1 \sqrt{\frac{-P_T + x_{10}(t)}{\rho}}}{V_0 + A_{cy1}\,\alpha_1\,(x_{m1} - x_1(t))} \right)}$$

for $u_1 < 0$ and by

$$u_1(t) \approx x_8 \frac{1}{G_v} = \frac{1}{G_v} \frac{v_1(t)}{\sqrt{2}\,\beta\, A_{cy1}\, C_d \left(-\frac{K_{TA1}\sqrt{\frac{-P_T + x_9(t)}{\rho}}}{V_0 + A_{cy1}\, x_1(t)} - \frac{K_{PB1}\,\alpha_1 \sqrt{\frac{x_5(t)-x_{10}(t)}{\rho}}}{V_0 + A_{cy1}\,\alpha_1\,(x_{m1} - x_1(t))} \right)}$$

for $u_1 > 0$. The new cylinder force dynamics are given by:

$$\dot{y_1} = v_1 \tag{4.16}$$

The force imparted on the linkage due to the hydraulic pressure is

$$F_1 = y_1 + A_{cy1}\beta(\ln(V_0 + A_{cy1} x_1) + \alpha_1 \ln(V_0 + \alpha_1 A_{cy1}(x_{m1} - x_1))). \tag{4.17}$$

The last part of equation 4.19 is nonlinear because of the simplification made in y_1 using equation 4.15.

The control law has no singularities which appear in the normal operating range of the system. The control law accounts for the varying pump pressure which is somewhat unique

to a load sensing system. This feedback linearization eliminates the need for a compensating valve which is a common component in multifunction load sensing systems. The nonlinear volume effect on the hydraulic stiffness has been eliminated. Also significant, the nonlinear pressure flow relationship has been eliminated from the system dynamics.

Two simple controllers were designed for tracking. Each includes a tracking control loop which is simply control input which is proportional to (a single gain on) the tracking error. The first control system is just an implementation of the proportional controller alone. In the second control design, the feedback linearizing control law with force control is used in conjunction with the proportional gain controller. The inner loop force control is given by

$$v_1 = K_{f1}(y_{des} - y_1) = K_{f1}(F_{des} - A_{cy1}(x_9 - \alpha_1 x_{10}))$$

where $F_{des} = y_d$ is the output of the position tracking controller. The new dynamics for the valve input to force output pair are given by

$$\dot{y}_1 = -K_{f1}y_1 + K_{f1}y_d, \tag{4.18}$$

which is a stable force tracking system for $K_{f1} > 0$.

The responses to sinusoidal position tracking references for P controller and the P control with feedback linearization are given in Figs. 4.47 and 4.48 respectively. In the simulations, the controller is switched on at 2 seconds and the reference input was set to zero until 3 seconds. The open-loop lift function was also activated with a sinusoidal input. The output performance is similar for both simulations. Step simulations were also ran (See Figs. 4.49 and 4.50). In this case the nonlinear controller produced fewer oscillations and similar performance.

The force control law can be used as an inner loop while another controller can be designed for the outer loop position tracking control. Since the system is now significantly decoupled and more linear in behavior, the outer loop control can be very simple and still give good results.

A feedback linearization can also be developed for the lift function in a way similar to the tilt function previously given above. The output in this case is

$$y_2 = A_{cy2}(\tilde{x}_{12} - \alpha_2 \tilde{x}_{13}).$$

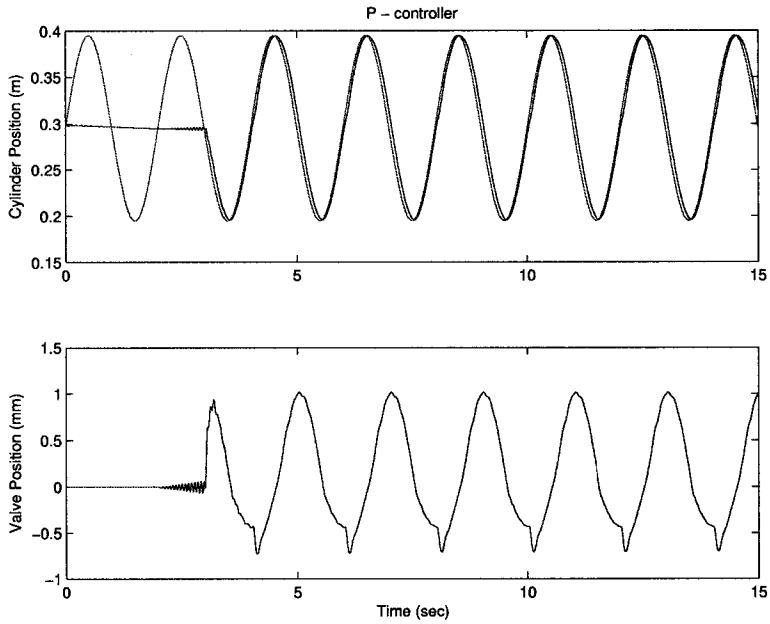

Figure 4.47 Sine tracking - P controller

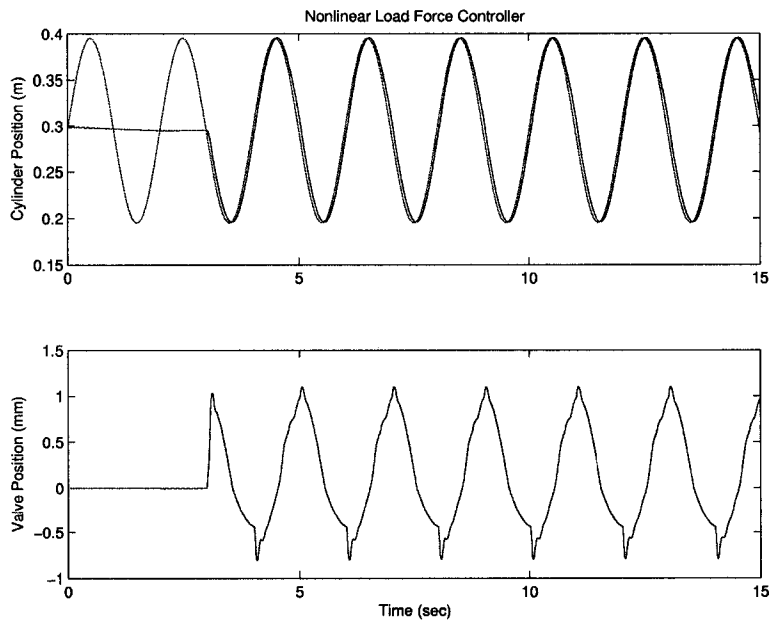

Figure 4.48 Sine tracking - NL force control

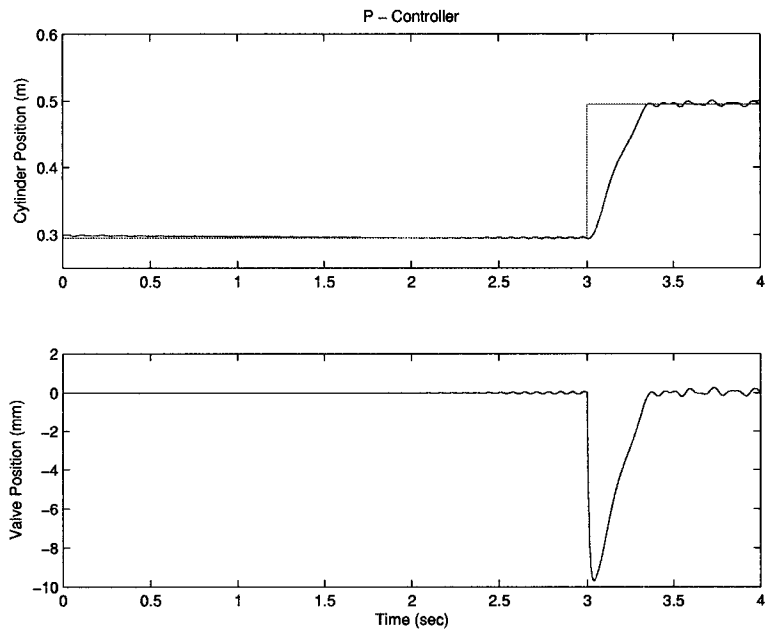

Figure 4.49 Step tracking - P controller

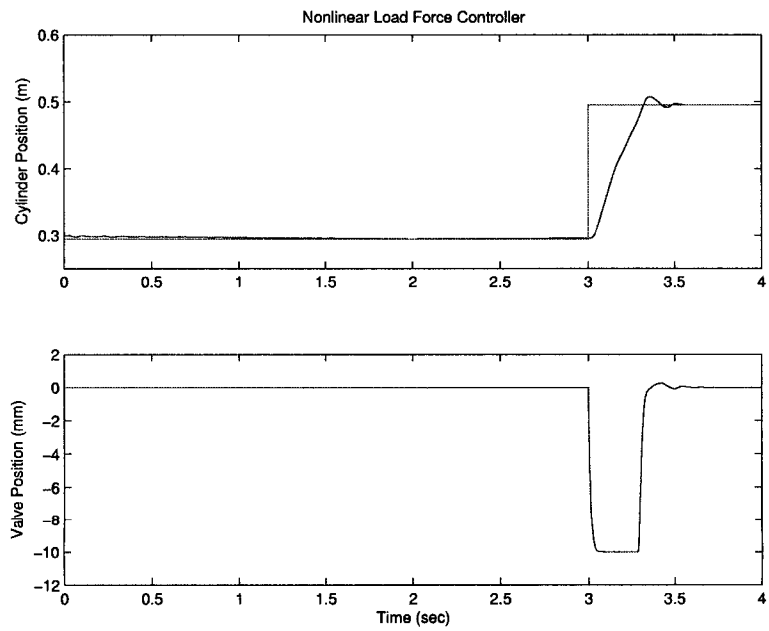

Figure 4.50 Step tracking - NL force control

The input-output linearizing control law for the lift function is given by

$$u_2(t) \approx x_{11}\frac{1}{G_v} = \frac{1}{G_v}\frac{v_2(t)}{\sqrt{2}\,\beta\,A_{cy2}\,C_d\left(-\frac{K_{PA2}\sqrt{\frac{x_5(t)-x_{12}(t)}{\rho}}}{V_0+A_{cy2}\,x_2(t)} - \frac{K_{TB2}\,\alpha_2\sqrt{\frac{-P_T+x_{13}(t)}{\rho}}}{V_0+A_{cy2}\,\alpha_2\,(xm2-x_2(t))}\right)}$$

for $u_2 < 0$ and by

$$u_2(t) \approx x_{11}\frac{1}{G_v} = \frac{1}{G_v}\frac{v_2(t)}{\sqrt{2}\,\beta\,A_{cy2}\,C_d\left(-\frac{K_{TA2}\sqrt{\frac{-P_T+x_{12}(t)}{\rho}}}{V_0+A_{cy2}\,x_2(t)} - \frac{K_{PB2}\,\alpha_2\sqrt{\frac{x_5(t)-x_{13}(t)}{\rho}}}{V_0+A_{cy2}\,\alpha_2\,(xm2-x_2(t))}\right)}$$

for $u_2 > 0$. The force imparted on the linkage due to hydraulic pressure in the lift cylinder is

$$F_2 = y_2 + A_{cy2}\beta(\ln(V_0 + A_{cy2}x_2) + \alpha_2\ln(V_0 + \alpha_2 A_{cy1}(x_{m2} - x_2))). \tag{4.19}$$

With the feedback linearization for the tilt and lift functions, the new system input is

$$\begin{Bmatrix} v_1 \\ v_2 \end{Bmatrix} = \begin{bmatrix} K_{f1}(y_{des1} - y_1) \\ K_{f2}(y_{des2} - y_2) \end{bmatrix} = \begin{bmatrix} K_{f1}(F_{des2} - A_{cy1}(x_9 - \alpha_1 x_{10})) \\ K_{f2}(F_{des2} - A_{cy2}(x_12 - \alpha_2 x_{13})) \end{bmatrix}.$$

An outer loop control used for position tracking which is used to supply the desired force on each cylinder is given as,

$$\begin{Bmatrix} F_{des1} \\ F_{des2} \end{Bmatrix} = K\begin{Bmatrix} e_1 \\ e_2 \end{Bmatrix} + F_{grav},$$

where, K is the outer loop controller gain, F_{grav} is a force vector used to compensate for gravitational forces, and e_1 and e_2 are the position tracking errors for tilt and lift. The structure of the controller can be seen in Fig. 4.51.

4.6.2 Modified Plant Dynamics

It is hoped that the feedback linearization with force control will change the system dynamics in a such a way that the standard linear control methods can be more effective. This means that a new linearization needs to be found which incorporates the feedback linearization and force control. Therefore a new plant on which linear control design can be based has been taken as the "inner loop" system in Fig. 4.51. The new plant will be referred to as G'.

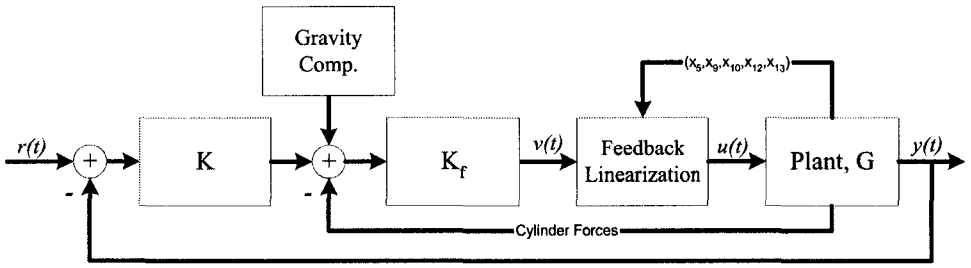

Figure 4.51 Nonlinear force control system structure

The linearization operating point has been selected to be the same as the one used for the linearization presented for the original model. The linearized and scaled plant, G', frequency response in the form of a singular value plot is given in Fig. 4.52. Note that the system no longer has the magnitude peaks near 10 to 20 Hz as the original plant did in Fig. 3.1.

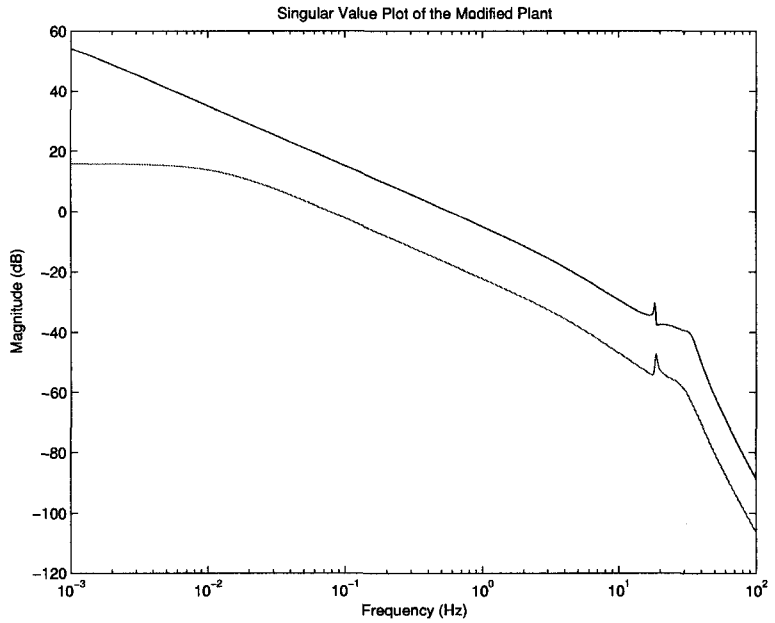

Figure 4.52 Nonlinear force control system frequency response

Since the feedback linearization and force control changes the system dynamics, a new analysis of plant uncertainty is needed. The singular value plot of the modified plant error due

to variations in the bulk modulus and discharge coefficient is given in Fig. 4.53. The error was found in the same way as in Chapter 3. The new function (given on the plot) that bounds the error for use in the robust stability analysis will be referred to as W_i'. A comparison to Fig. 3.4 shows that the peak on the uncertainty is much lower for the system with feedback linearization and force control in comparison to the original plant.

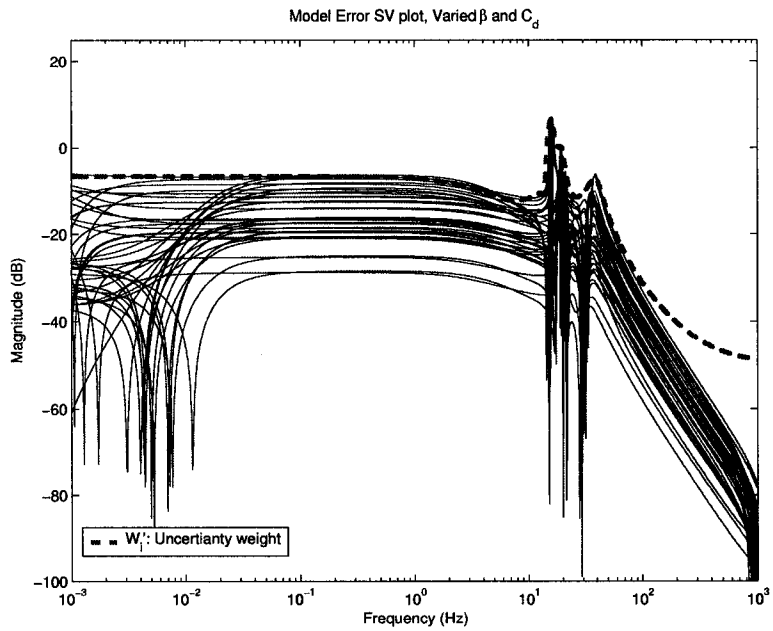

Figure 4.53 Family of input multiplicative errors for the Nonlinear force control system

4.6.3 Proportional and H_∞ Outer Loop Tracking Control Designs

The outer loop controller, K in Fig. 4.51, could be designed in a variety of ways. The linear design techniques presented earlier are good candidates for designing the controller since the model now behaves in a more linear fashion since the feedback linearization control law is being employed. In the following sections, two controllers are presented. One is a simple proportional feedback design. The other is an H_∞ design similar to the H_∞ design for the original unmodified model.

4.6.3.1 Proportional Control Design

The simplest possible control design is a proportional feedback control. In this case the desired force reference input to the nonlinear force control would be the result of multiplying a diagonal gain matrix, K, by the position tracking error vector. The controller gain matrix is $K = diag(3.2398, \quad 17.9987)$ which has been chosen by using a two SISO system approach similar to the PI design which is especially applicable since the feedback linearization decouples the hydraulic portion of the model.

Plots of the frequency response of the sensitivity and complementary sensitivity transfer function matrices are given in Fig. 4.54. Robustness should be adequate since the peak of the sensitivity frequency response is less than 4 dB. The speed of response should be at least what is required since the bandwidth is at least 1 Hz. The system should track step references since the magnitude of the sensitivity is low at low frequencies with a slope of 20 dB per decade. Simulations show how well ramp reference inputs are tracked.

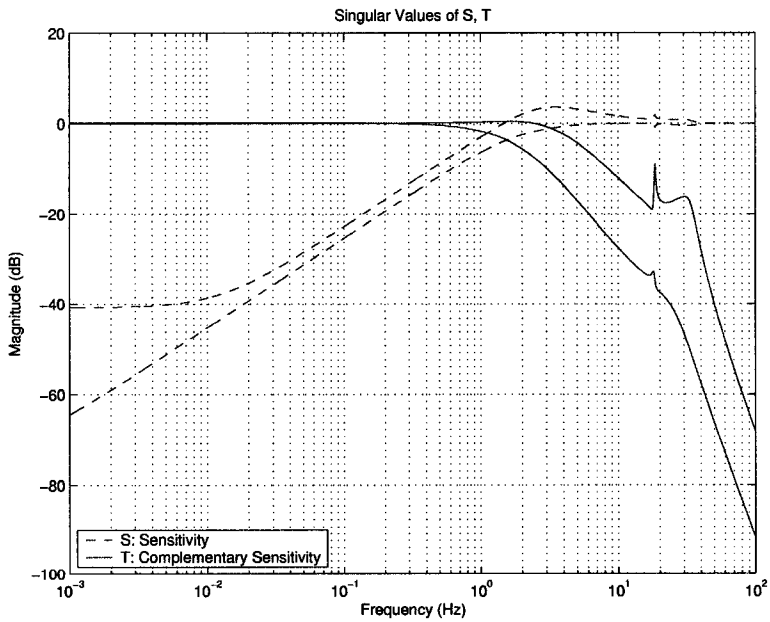

Figure 4.54 Nonlinear force control plus proportional tracking control system sensitivity frequency responses

4.6.3.2 Robustness of the Modified Plant with Proportional Control

The plant modified by the feedback linearization has different dynamics as mentioned before. Therefore, a new description of the model uncertainty, W_i', and the modified plant, G', are used to evaluate the robustness of the controller design based on the modified plant.

The singular values of N_{11} are plotted in Fig. 4.55 for the proportional control system with 50% input multiplicative uncertainty. This shows that proportional control system for the modified plant is robustly stable for 50% input multiplicative uncertainty since the peak value on the plot is 0.5.

For the case when robustness to varying plant parameters is being considered, the description of the model uncertainty, W_i' based on the modified plant, G', is used. The singular values for N_{11} for varying plant parameters, β and C_d, is given in Fig. 4.56. The peak of the maximum singular value plot is 0.47. Therefore, the robust stability condition is not violated which is a significant improvement over all of the previous linear control designs.

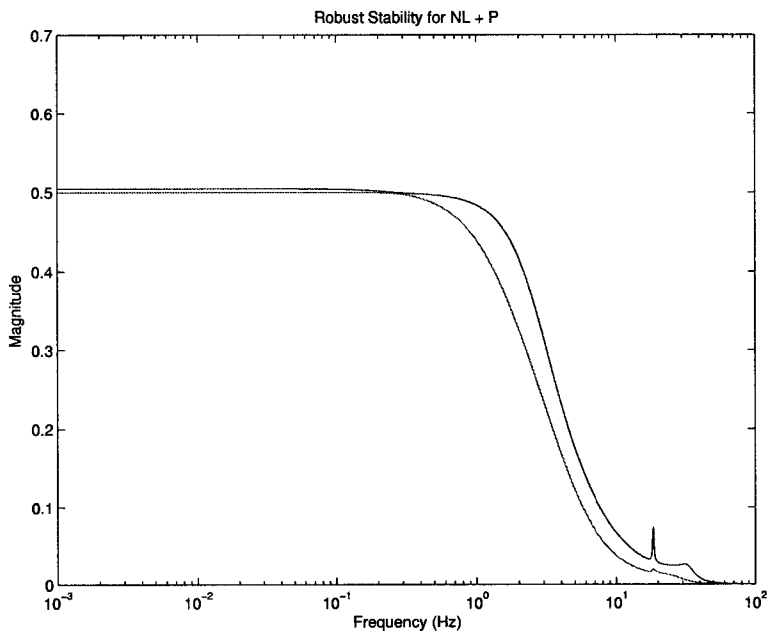

Figure 4.55 Singular value plot for the robust stability of the NL force plus proportional tracking control system

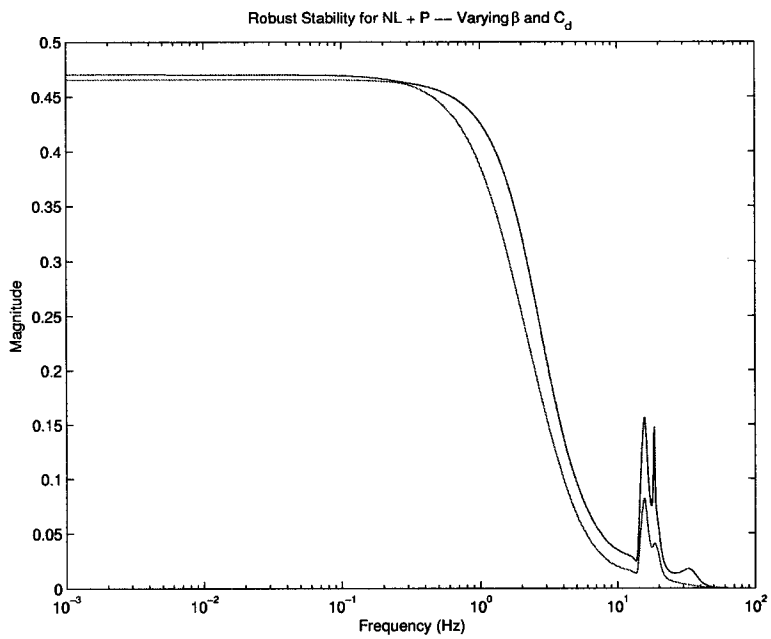

Figure 4.56 Robust stability of the NL force plus proportional tracking control system with varying parameters

4.6.3.3 Simulation Results

A simulated response of the linear plant, G', with the H_∞ controller and step inputs to tilt and lift references is given in Fig. 4.57. The responses to step inputs show that the system is capable of tracking with low steady state error in the linear case. The percent over shoot and settling time are approximately 1% and 0.32 seconds for tilt and lift.

A ramp input was given to the linear system with the proportional control (Fig. 4.58). The steady state tracking errors for both tilt angle and lift angle are very low at 0.75 deg each.

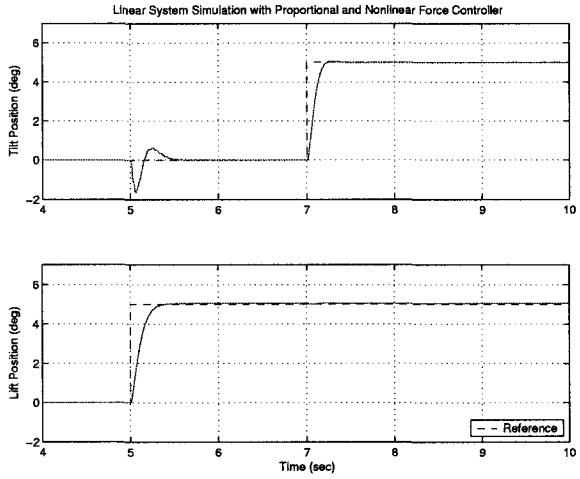

Figure 4.57 Simulation with the proportional controller and the linear model with modified pressure dynamics given a step reference input

The simulation results for the nonlinear proportional force controller with the nonlinear model are in Figs. 4.59 through 4.64.

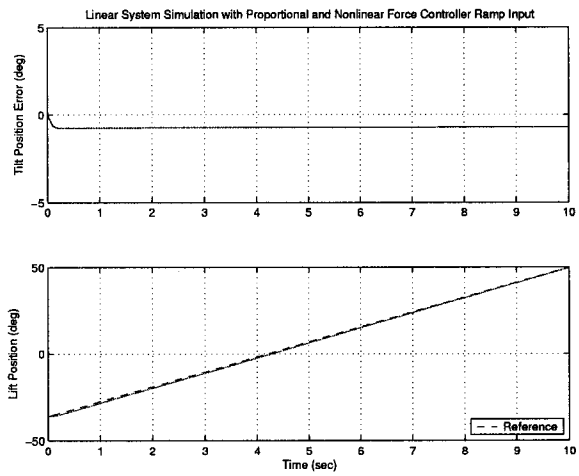

Figure 4.58 Simulation with the proportional controller and the linear model with modified pressure dynamics given a ramp reference input

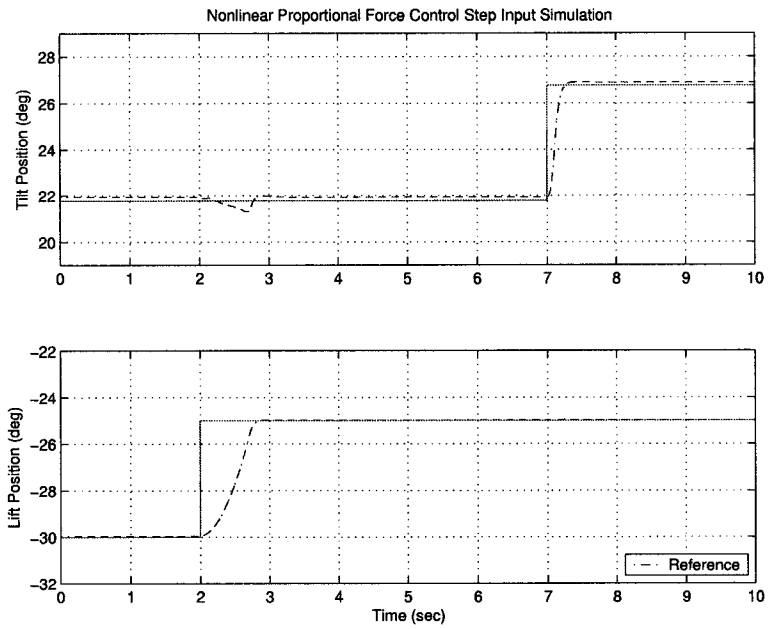

Figure 4.59 Step simulation result using nonlinear force control and the nonlinear model

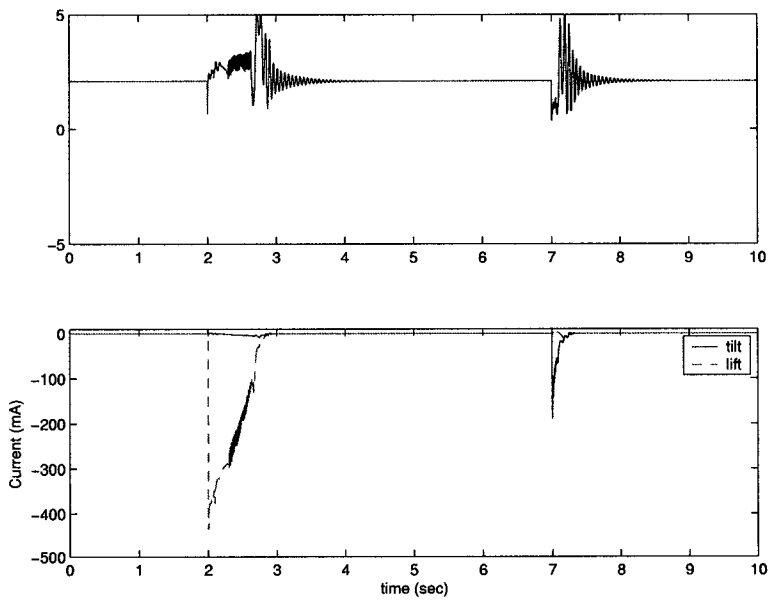

Figure 4.60 Margin pressure and valve inputs, nonlinear force control step simulation

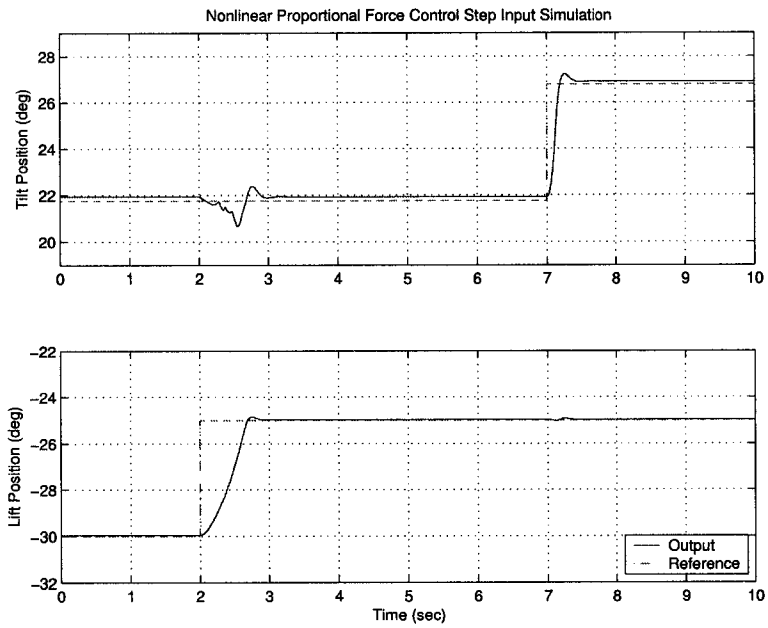

Figure 4.61 Step simulation result using nonlinear force control and the nonlinear model with perturbation

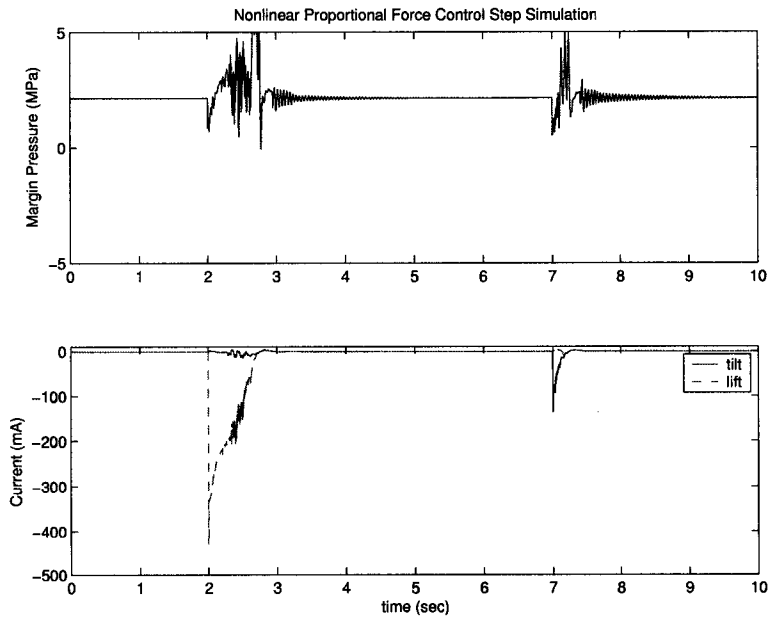

Figure 4.62 Margin pressure and valve inputs, nonlinear force control step simulation with perturbation

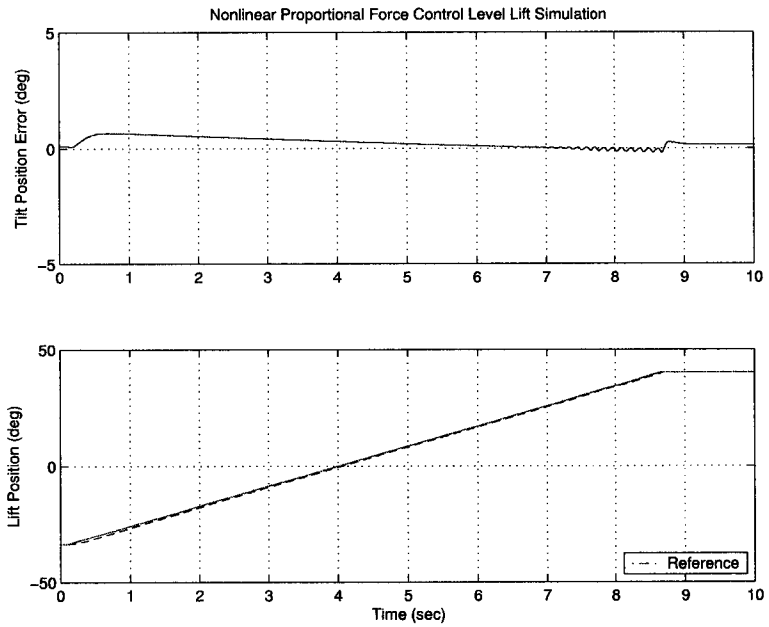

Figure 4.63 Level lift simulation result using the nonlinear control and the nonlinear model

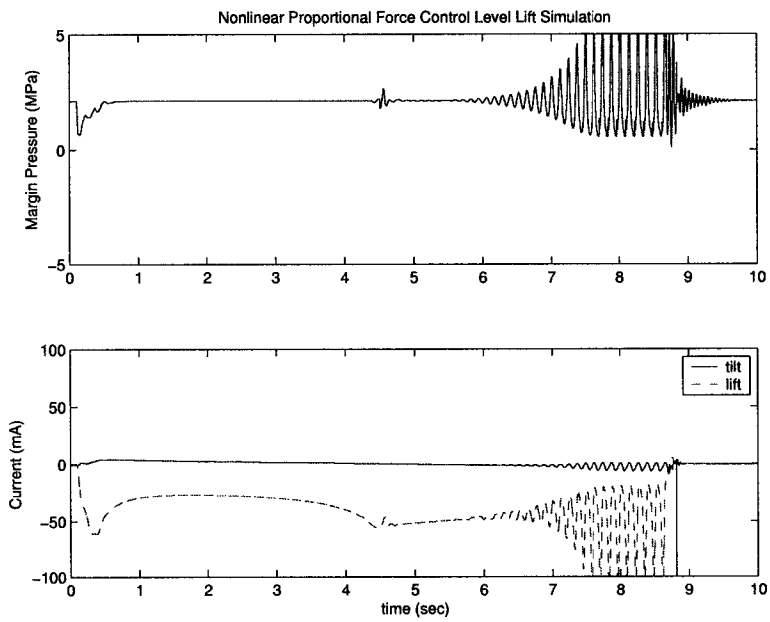

Figure 4.64 Margin pressure and valve inputs, nonlinear control level lift simulation

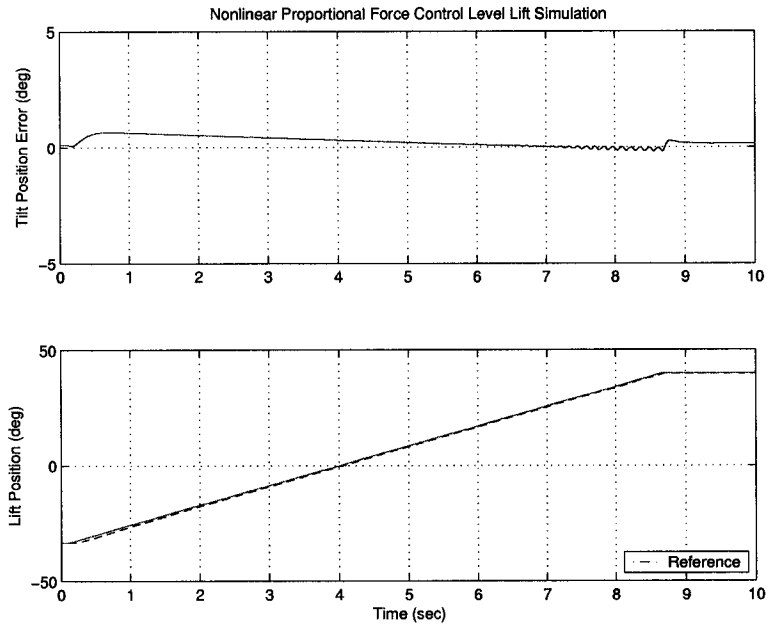

Figure 4.65 Level lift simulation result using the nonlinear control and the nonlinear model with a model parameter perturbation

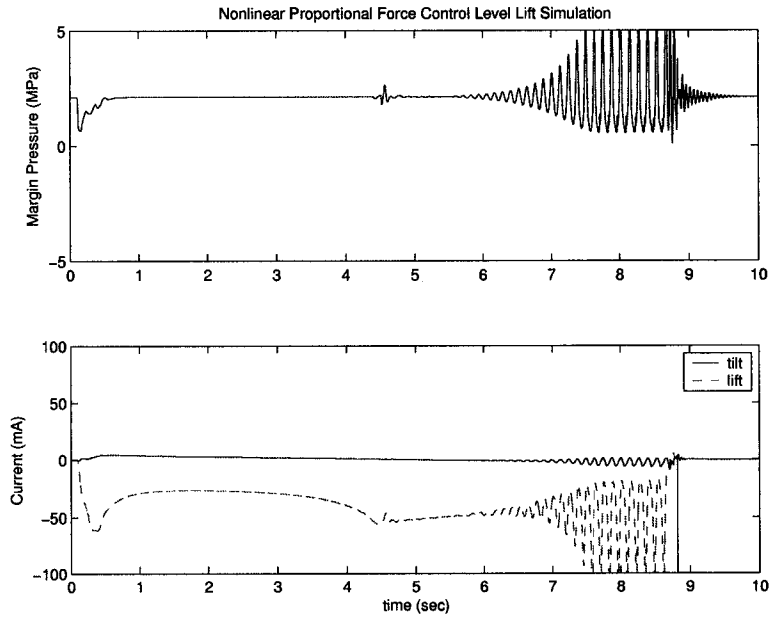

Figure 4.66 Margin pressure and valve inputs, nonlinear control level lift simulation with a model parameter perturbation

4.6.3.4 H_∞ Control Design

The mixed sensitivity H_∞ design procedure given earlier in this work can be used with little modification to design an outer loop control for the plant with the feedback linearization force control. Since all of the design objectives remain the same, the design weights do not need to change. The only difference required is to used the modified plant, G' due to the feedback linearization in the design process.

Applying the previously discussed design weights in the mixed sensitivity H_∞ design process to the new model yielded a new feedback control system. The sensitivity, S, and complementary sensitivity, T, frequency responses are given in Fig. 4.67 along with the design weights. It can be concluded by examining the plots that the desired bandwidth appears to have been met. Also, stability robustness is good because the peaks on the plots of S and T are low.

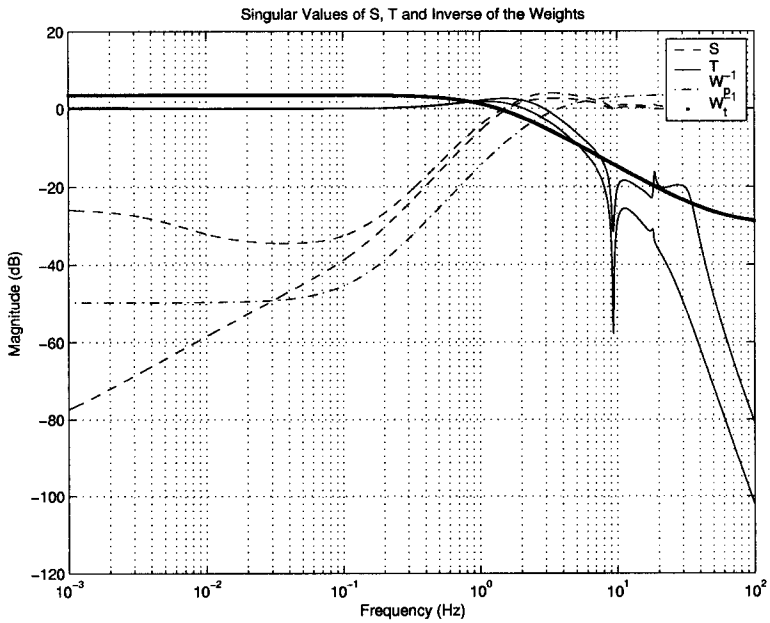

Figure 4.67 Nonlinear/H_∞ force control system sensitivity frequency responses

4.6.3.5 Robustness of the Modified Plant with H_∞ Control

The singular values of N_{11} are plotted in Fig. 4.68 for the system with 50% input multiplicative uncertainty. This shows that H_∞ control system for the modified plant is robustly stable for 50% input multiplicative uncertainty. A comparison with Fig. 4.35 shows that the high frequency peak is reduced by 20% due to the feedback linearization.

For the case when robustness to varying plant parameters is being considered, the description of the model uncertainty, W_i' based on the modified plant, G', is used. The new robustness analysis for varying plant parameters, β and C_d, is given in Fig. 4.69. Clearly the robust stability condition is not violated which is a very significant achievement. Comparing this result to the result for the unmodified plant (see Fig. 4.36) indicates that the robustness problems are much less severe for the modified plant. The feedback linearization reduced the high frequency peak of the robust stability norm by 97% for the parametric uncertainty. The maximum of the robust stability norm has been reduced by 86%.

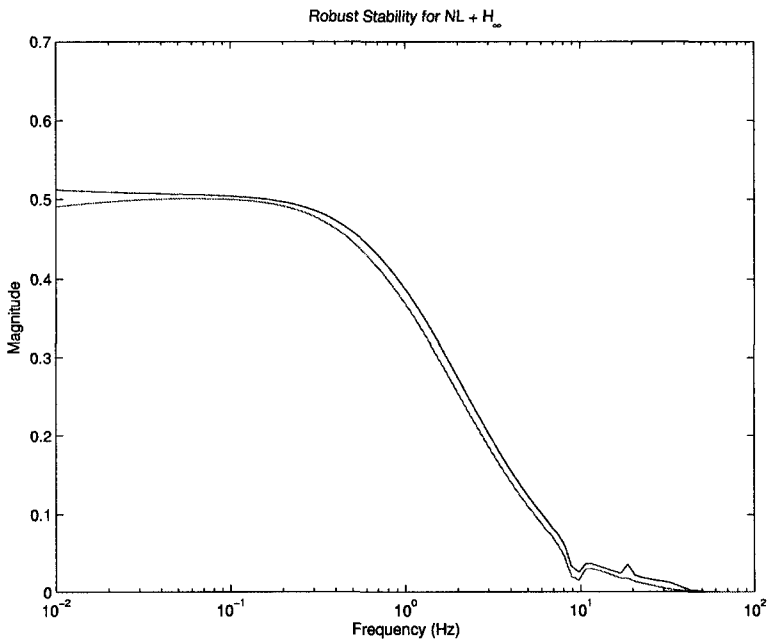

Figure 4.68 Singular value plot for the robust stability of the NL force - H_∞ controlled system

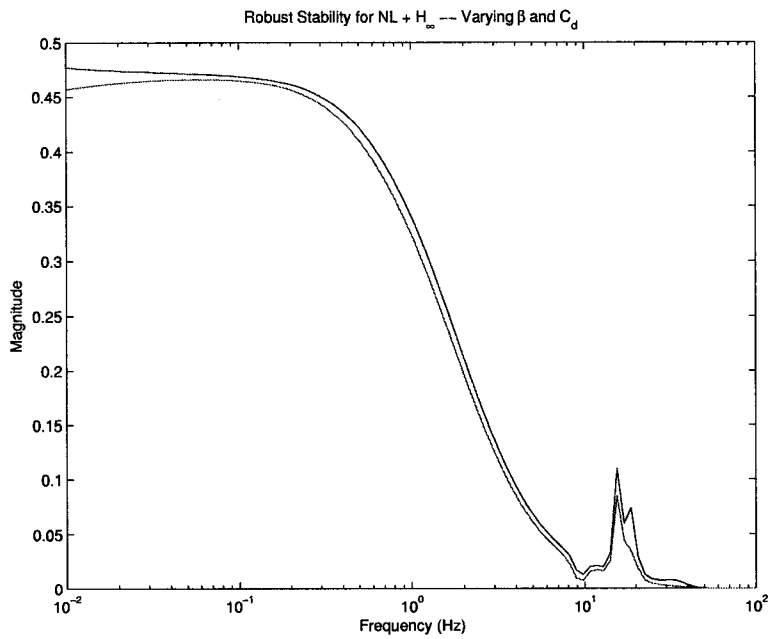

Figure 4.69 Robust stability of the NL force - H_∞ controlled system with varying parameters

4.6.3.6 Simulation Results

A simulated response of the linear plant, G', with the H_∞ controller and step inputs to tilt and lift references is given in Fig. 4.70. The responses to step inputs show that the system is capable of tracking with zero steady state error in the linear case. The percent over shoot and settling time are approximately 27% and 0.508 seconds for tilt and 20% and 0.567 sec for lift. A ramp input was given to the linear system with the H_∞ control (Fig. 4.71). The steady state tracking error of the tilt angle is very small, 0.3 and 0.4 deg for tilt and lift respectively.

Nonlinear simulations of the H_∞ control system with the nonlinear force control show the characteristics of the controller. These simulations are given in Figs. 4.72 through 4.79. The first simulation shows the performance of the control system given a step reference input to both the tilt and lift functions (Fig. 4.72 and 4.73). There is a negligible amount overshoot in the tilt response compared to 27% in the linear simulation. The lift overshoot increased

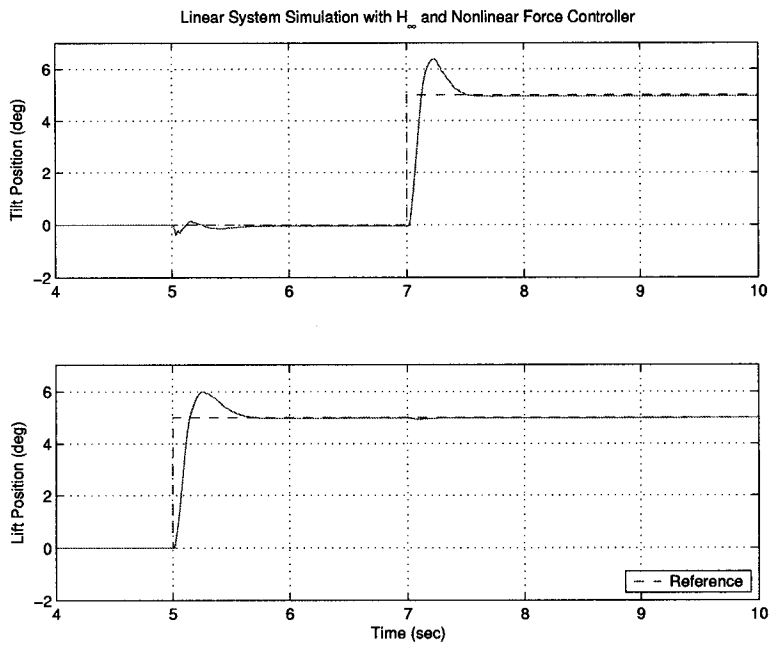

Figure 4.70 Simulation with the H_∞ controller and the linear model with modified pressure dynamics given a step reference input

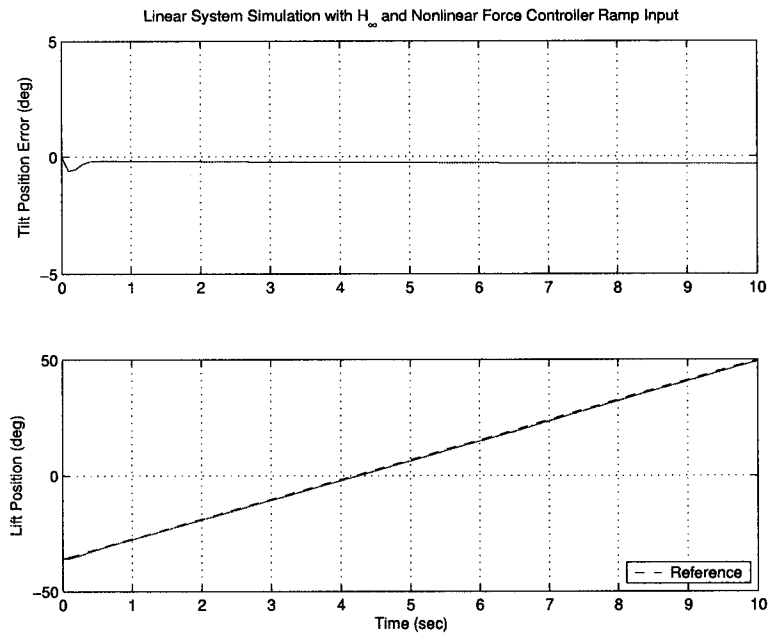

Figure 4.71 Simulation with the H_∞ controller and the linear model with modified pressure dynamics given a ramp reference input

to 27%. In general, the simulation response appears more like the linear response than did the H_∞ design with the unmodified plant. The step reference simulation response with the parameters β and C_d at 1.5 times their nominal values are in Figs. 4.74 and 4.75. The main differences in this response are that the the percent overshoot is increased and there is less oscillation in the margin pressure.

The next set of simulations are responses to the level lift reference input (Figs. 4.76 through 4.79). The first set of plots give the response of the nominal plant. In this case the tracking error is quite small but some oscillation is present in the margin pressure. The next set of plots give the response of the plant with perturbed parameters (Figs. 4.78 and 4.79). The main difference in this simulation is that the oscillations in the margin pressure are of higher amplitude and therefore oscillations begin to show up in the tilt tracking error.

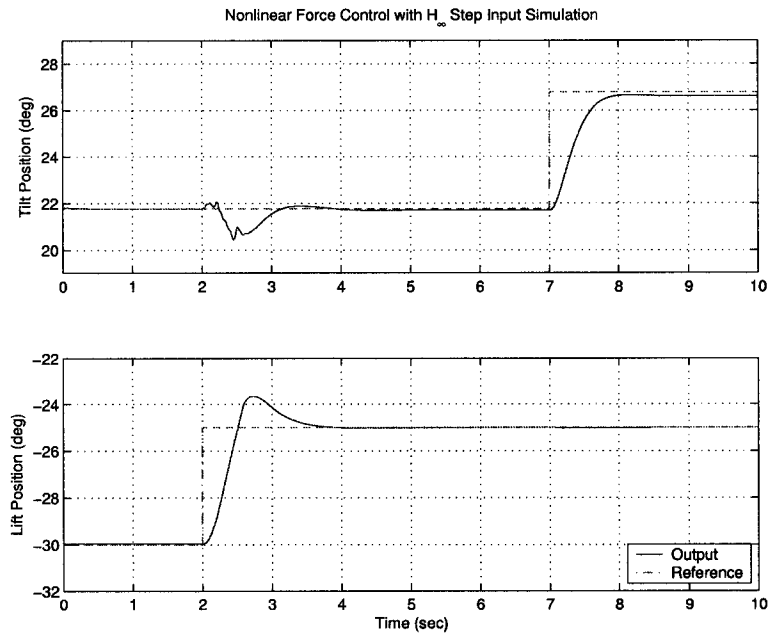

Figure 4.72 Step simulation result using H_∞ nonlinear force control and the nonlinear model

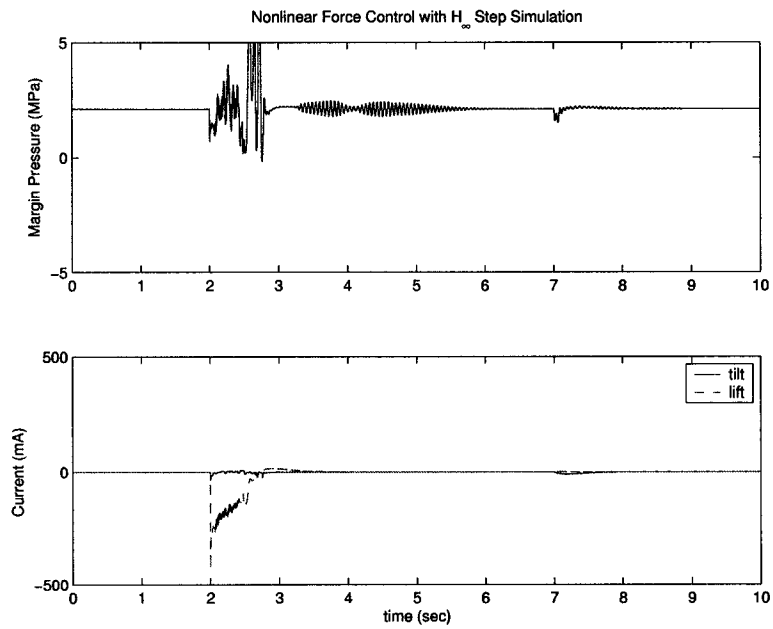

Figure 4.73 Margin pressure and valve inputs, H_∞ nonlinear force control step simulation

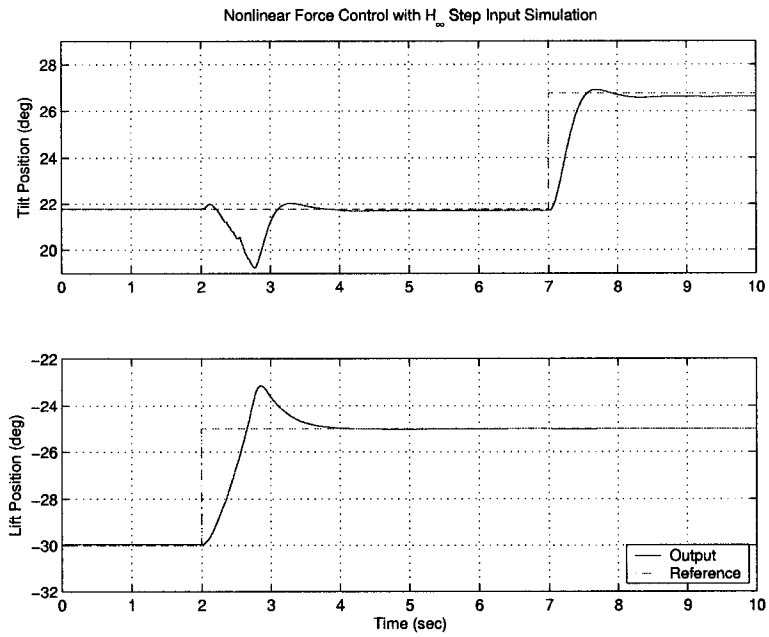

Figure 4.74 Step simulation result using H_∞ nonlinear force control and the nonlinear model with a model perturbation

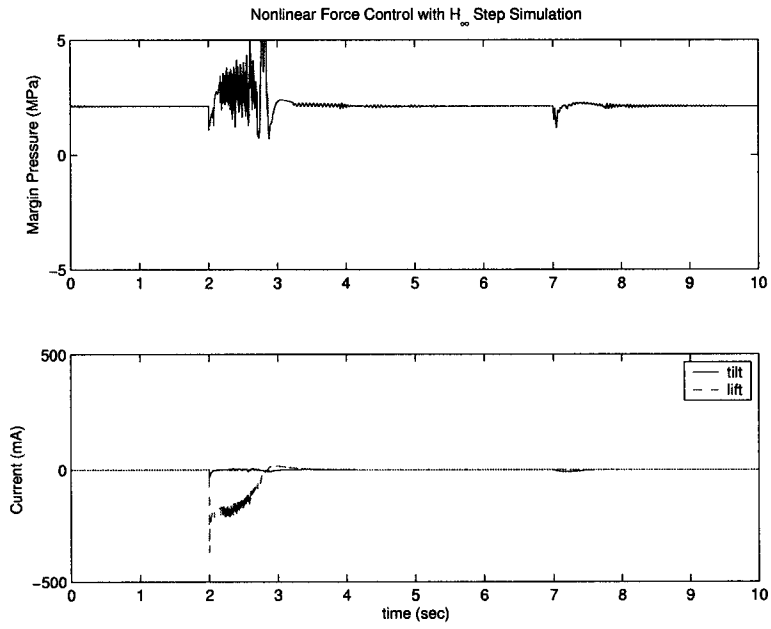

Figure 4.75 Step simulation, Margin pressure and valve inputs, H_∞ nonlinear force control step simulation with a model perturbation

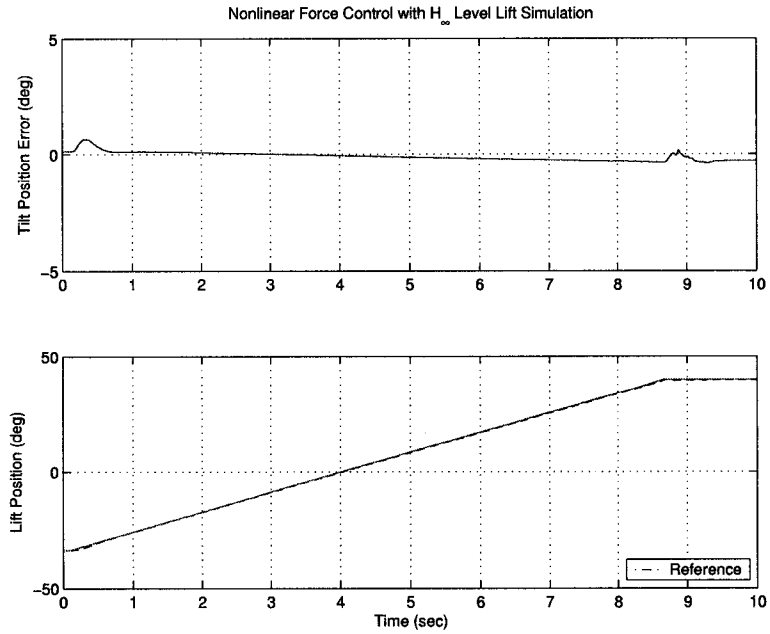

Figure 4.76 Level lift simulation result using the H_∞ and nonlinear force control

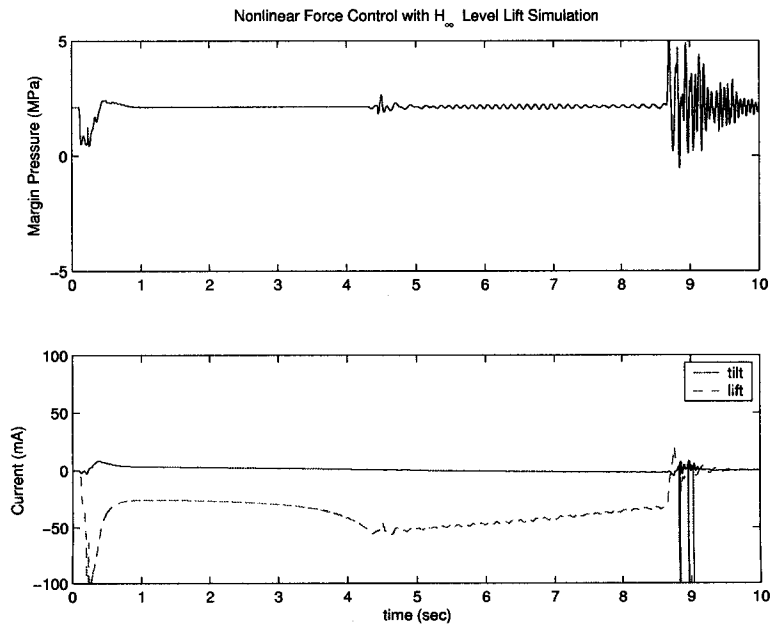

Figure 4.77 Level lift simulation, margin pressure and valve inputs, H_∞ and nonlinear force control

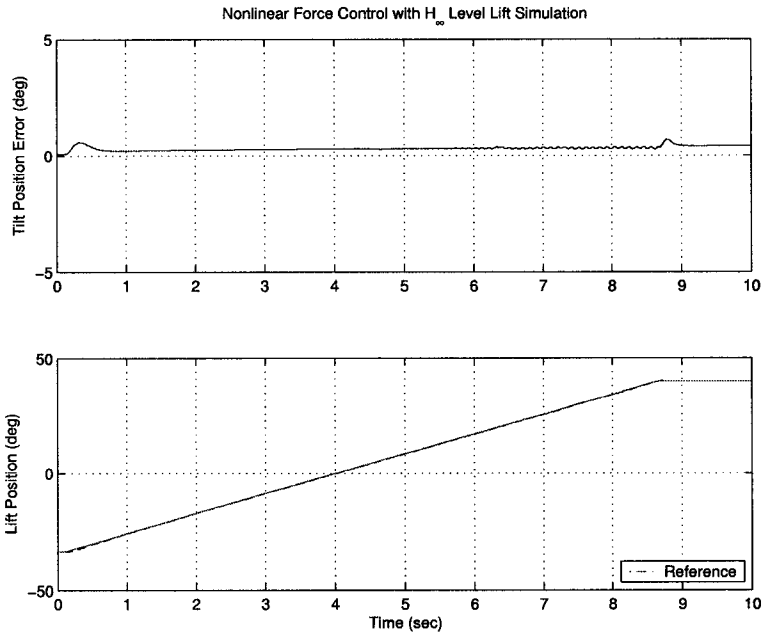

Figure 4.78 Level lift simulation result using the H_∞ and nonlinear force control with a model perturbation

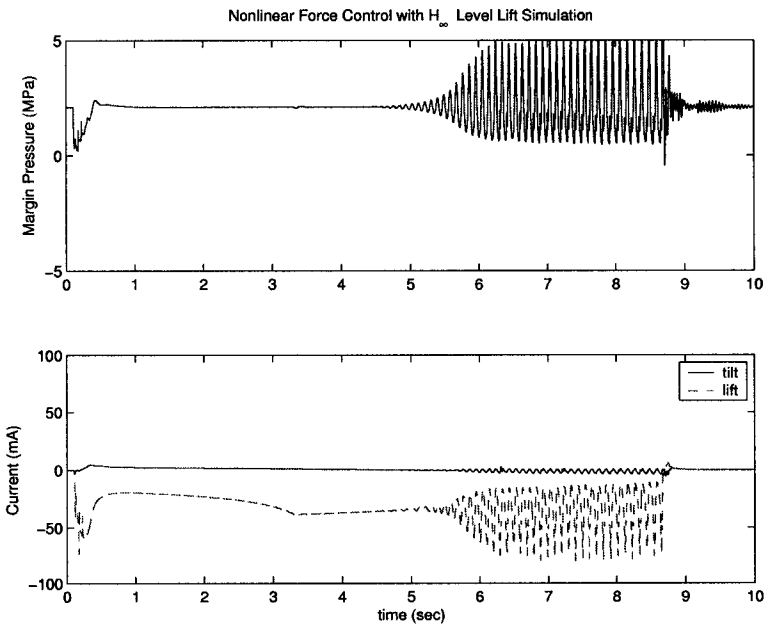

Figure 4.79 Level lift simulation, margin pressure and valve inputs, H_∞ and nonlinear force control with a model perturbation

4.7 Comparison and Summary

In this section, the simulation results were compared for different controller designs. The comparison is based on the performance requirements such as speed of response and steady state error as well as qualitative characteristics such as the tendency toward oscillation. Each controller was able to provide some level of tracking performance and robust stability. Robust controller designs based on LQG and H_∞ methods were presented for automatic bucket levelling of an electro-hydraulically actuated wheel loader. The robustness of controller designs was validated using a complete nonlinear dynamic model of a real-life wheel loader.

In previous sections, linear controller designs - PI, LQG, and H_∞ - were developed, analyzed for robustness, and simulated with both linear and nonlinear plant models. The PI design was prone to oscillate which was demonstrated in the step response outputs. The simulations show that the nonlinear nature of the wheel loader significantly affects the performance. Both the LQG and H_∞ designs provided an acceptable level lift performance with the nominal nonlinear model. In simulations of the nonlinear model, the output had some small oscillations for each controller design. The H_∞ design gave better steady state error performance for the lift function with the nonlinear plant model compared to LQG in the level lift simulations. A singular value analysis of the robustness of the LQG and H_∞ designs showed that both of the systems were robust to 50% input uncertainty. The PI design was the only controller that was not robust to the 50% input uncertainty. However, none of the linear control designs were robust to the uncertainty due to variations in the parameters, C_d and β.

As expected, by accounting for the plant nonlinearities in the control design, the robustness was improved. This is especially evident in the nonlinear simulations with perturbations in the model parameters, though improvements were seen in the 50% input uncertainty which was also considered. The improvement in robustness to the perturbations in the parameters, C_d and β is shown in Fig. 4.80.

The nonlinear controllers, with embedded P and H_∞ designs, showed bad coupling effects in the step response simulations. For example, when a step reference for lift occurred, the

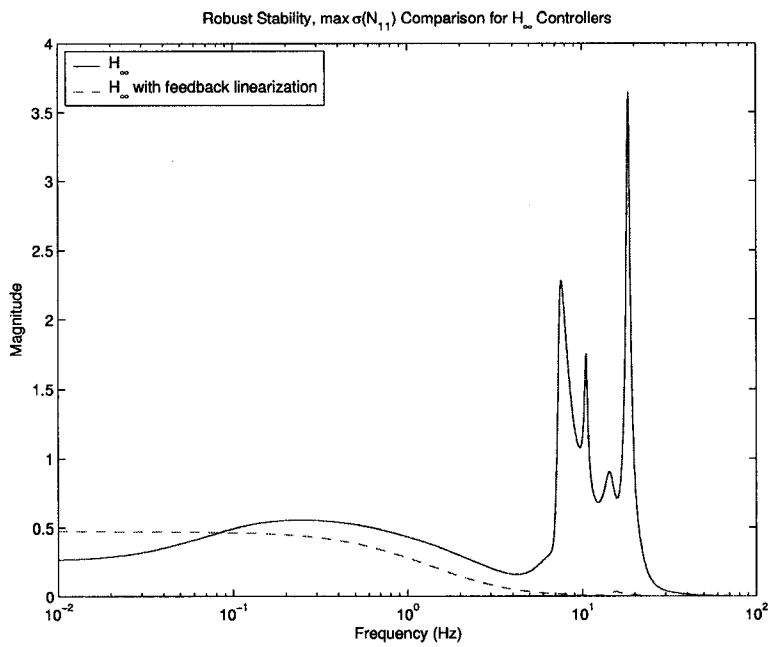

Figure 4.80 Comparison of the robustness to parameter variations for linear and nonlinear control systems

tilt angle was affected greatly. However, this was not seen in the level lift simulations which represent more realistic inputs than step.

The oscillations in the margin pressure were difficult to control in all cases. This is likely because the pump dynamics are difficult to effect by simply controlling the implement valves.

CHAPTER 5. VIRTUAL REALITY INTERFACE

This chapter presents the integration of closed-loop dynamic simulation with a Virtual Reality (VR) interface. The aim is to assess the performance of the control system by evaluating the perception of the operator driving the machine in virtual environment. In VR simulation operator can drive the wheel loader and operate the lift and tilt functions on the loader. This simulation can be used to compare performance with and without a closed-loop control system. In the following sections of this chapter, the VR implementation of the loader control system will be discussed. A test simulation in the VR environment will also be presented.

5.1 Model Interface

The VR interface includes, a joystick interface, a communication interface between the model and the VR display program, and a timing system to control the execution of the model so that it will run in a way that appears to be real time to a human operator (Fig. 5.3). On the model portion of the interface, all interface features are realized using a custom programmed "S-Function" block in Simulink. The simulation diagram setup for creating the real-time simulation with VR interface is given in Fig. 5.1. The block's inputs are the simulation time and the cylinder positions while the outputs are the joystick signals.

Either of two VR programs are used for the VR display, one is called *EDS Jack*, and the other is called *VR Juggler*. On the EDS Jack portion of the interface, the communication is achieved by using code written by others in a scripting language, Python, which runs in conjunction with EDS Jack. A similar setup is used with VR Juggler where similar code was written by others to achieve a communication link with the model.

The entire hardware setup for a VR simulation can be seen in Fig. 5.4. The computer on

the left is the "VR computer" running a VR Juggler application which creates the graphical display on the screen to the left which could be replaced with other display devices such as a large projection screen. The computer on the right is the "model computer" which makes all of the simulation computations and sends information to the VR computer for display. The timing and joystick interface functions are handled by the model computer as well. The two computers are connected to the same network which carries the communication signals.

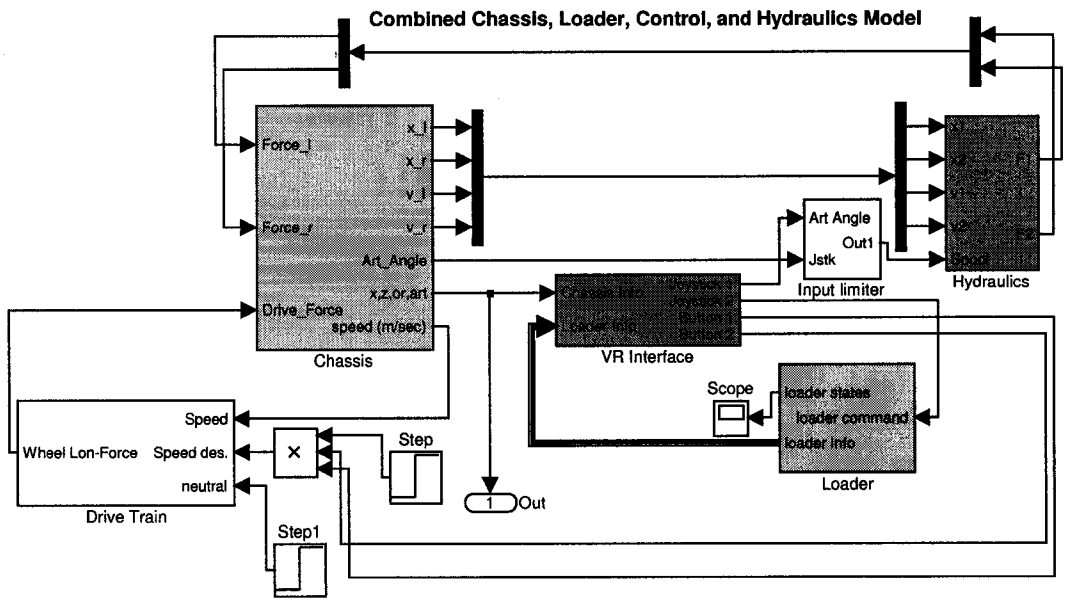

Figure 5.1 VR communication, interface, model, and controls in a simulation block diagram

Real Time Execution

The wheel loader model was combined with the VR interface and the LQG controller to create a complete model for the purpose of the VR simulation. The model was converted into C programming code and compiled to create a stand-alone executable program. The model runs much faster as a stand-alone executable than as a Simulink model making it more likely to keep up with a real time execution requirement.

Necessary approximations were made to ensure that the model would run in real-time.

For example small fluid volumes that have very fast frequencies were eliminated in some cases during the hydraulics modeling process. For example the fluid volumes between the inlet orifices and the variable metering orifices in Fig. 2.2 and 2.5 were not modeled in Chapter 2 because the transients due to these small volumes decay quickly. Also, a linearized version of the linkage model was used for the real time simulations since this is much faster than the nonlinear constrained closed-chain linkage model.

The model equations were integrated using a fixed step Runga-Kutta method. To choose the time step, the pole locations of the model were examined. A time step of 5.0×10^{-4} seconds was chosen corresponding to a frequency which more than satisfies the Nyquist criteria. The Nyquist frequency was determined by examining the maximum eigenfrequency of the linearized system. The chosen time step was more than 16 times smaller than the inverse of the maximum eigenfrequency for any of the closed-loop control systems presented in Chapter 4.

To create a simulation program which executes in real time, a timing scheme was developed which is controlled by a function that is called at each simulation time step. A flow chart is given(Fig. 5.2)for the function that controls the timing and communication between the model and the VR display. The timing scheme is based of the system's PC clock. The simulation is allowed to run 20 ms at a time which is the display real time step, DT. The display time step refers to the target real time interval for updating the VR display. At each 20 ms real time step, the joystick signal is read, cylinder positions are communicated to EDS Jack, and the simulation is allowed to run for 20 ms of simulation time. Once 20 ms of simulation time is completed, the real time from the system's PC clock is poled until the next real time step is reached (i.e. 20 ms of real time has elapsed). The process can repeat forever or for a specified period of time. Note that the 20 ms step time was selected for this research but could be changed for other work.

Communication

The model simulation sends the extension positions of the two cylinder functions, lift and tilt. The VR display receives the information and displays the loader in a configuration dictated

by the two cylinder positions. Communication between the model executable and the VR display is achieved through the use of Windows sockets. In this way, two programs on different computers or the same computer can communicate to one another. The communication code is written into the custom VR interface S-function block along with the joystick interface code.

5.2 Operator Interface

The human interface which the operator interacts with to operate the virtual wheel loader consists of a computer image and a joystick. The joystick is used to operate the functions of the wheel loader as they would in a real machine. The computer image provides a realistic picture of the machine from the operators point of view. As mentioned before the computer images are generated by either *EDS Jack* or a *VR Juggler* application.

The joysticks used have two axes. The left right axis controls the bucket function unless the level lift function is activated. The fore and aft axis controls the lift function. A USB (universal serial bus) connection carries the signal from the joystick to the computer. Computer driver software was written as an interface between the simulation software and the joystick system.

In the case of using *EDS Jack*, the VR display program computes the linkage position given the two cylinder positions from the simulation and allows the operator to see the simulation from any angle using a stereovision head mounted display. The display is updated as fast as once every 20 ms. as new data comes from the model executing simultaneously to the VR display. Figure 5.5 is a picture of the wheel loader geometry in the EDS Jack environment from the point of view looking out of the operator's cabin. Figure 5.6 shows a picture of the VR display looking at the machine from the side. Note that it is difficult to tell whether the bucket is level to the ground by looking at the view from the cabin.

When the *VR Juggler* application is used, the global position of the base body along with the relative position of each other body in the system is sent to the VR computer from the model simulation. The base body of the machine which is the rear part of the chassis is located on a two dimensional plane in terms of translations and rotation, while joint angles are used to describe the relative position of each of the other components. Computer displays of many

types can be used with *VR Juggler*. For this, work, desktop monitors or projection screens were used.

5.3 VR Test Simulation Results

The level lift control system was simulated while running in the real time VR environment and compared with the performance of a novice operator who controlled the VR loader simulation without the aid of automatic controls. In the closed-loop level lift control case, the boom lift reference angular position was proportional to the integral of the joystick position while the bucket angular position reference was determined by the boom position such that the bucket would be levelled. In the open-loop case, the current which controls the hydraulic valves was proportional to the joystick position for each function.

In Figs. 5.7 and 5.8, the bucket tilt angular position with respect to the chassis, θ_2, are plotted (Note that θ_2 is the bucket position error when it is desired for the bucket to be level to the ground $\theta_2 = \theta_{21} + \theta_1$). Also, the lift position, θ_1, is plotted. With and without the level lift controller, the operator controlled the velocity of the lift function using the joystick. The novice operator had difficulty maintaining a level bucket as shown in the Fig. 5.7. Note that the novice operator can tell that the bucket is level only by sight which accounts for much of the inaccuracy. Tracking error was low in the case of the level lift controller (Fig. 5.8). A combination of the plotted output and feedback from the operator's experience in the VR simulation could be used to evaluate the potential usefulness of the level lift controller.

5.4 Conclusions For VR Work

The results of the work done in this research indicate that simulating the physics and controls and displaying the machine geometry in real time is feasible. In this work, a sophisticated simulation of a wheel loader model and control system were able to execute in real time while communicating with a VR display which ran simultaneously. Using the current setup, there was little noticeable lag in the VR display.

The human-in-the-loop VR simulation showed that the level lift algorithm provides significant improvement in the ability of a novice operator to maintain a level bucket. This result gives the designer of the machine the ability to make better decisions about the future development and tuning of the level lift feature. In general VR simulations can be used to reduce the need for testing concepts on prototype machinery.

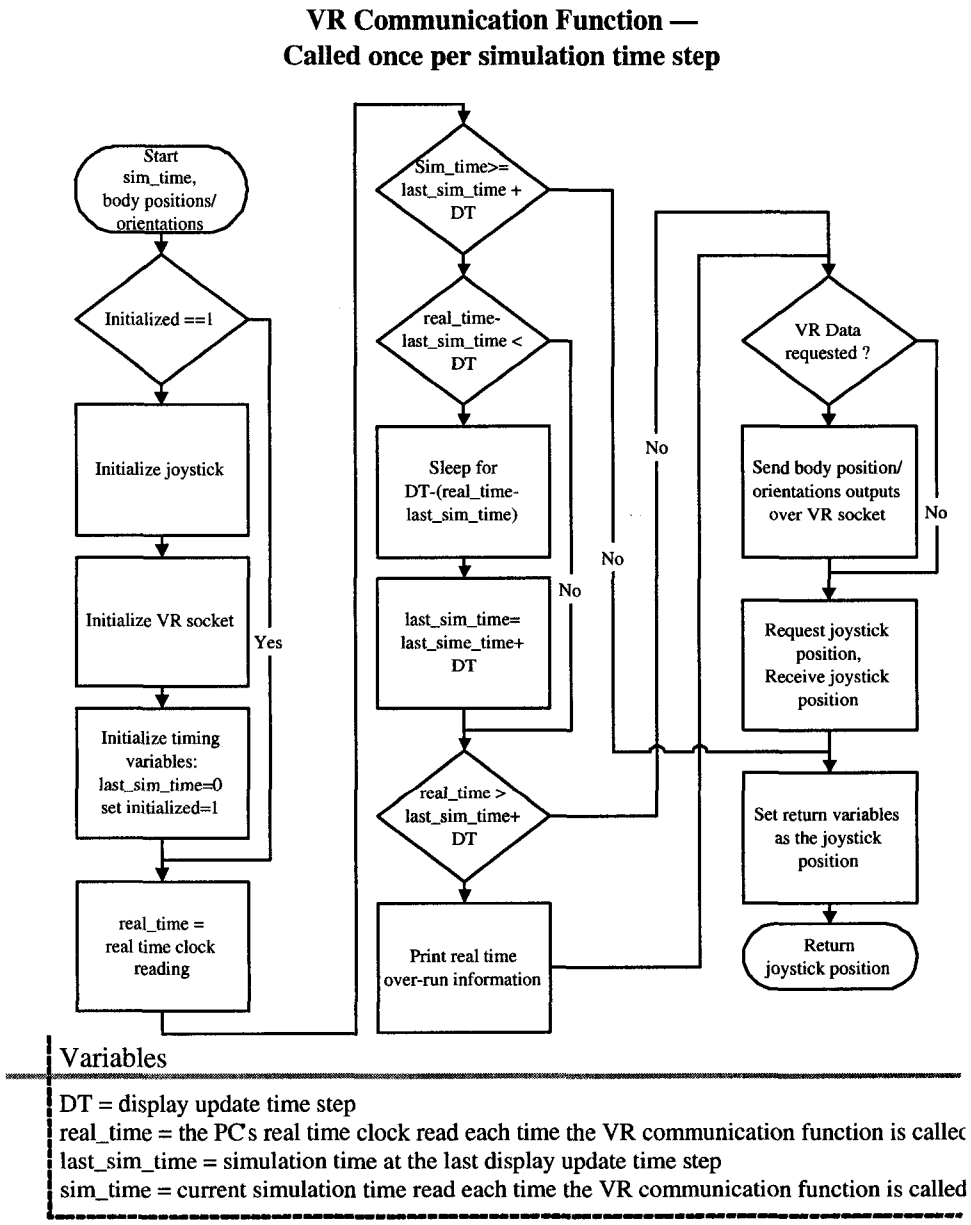

Figure 5.2 VR Communication function sub-program flow chart

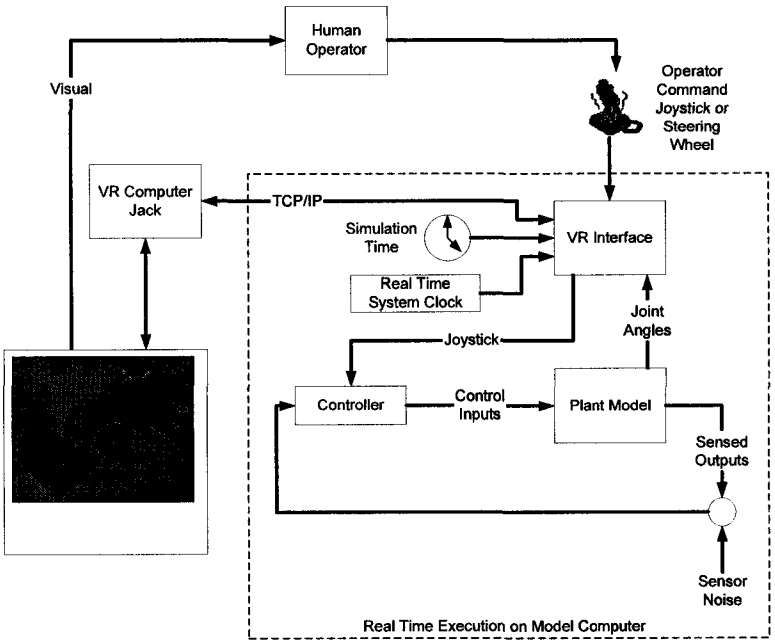

Figure 5.3 VR interface block diagram

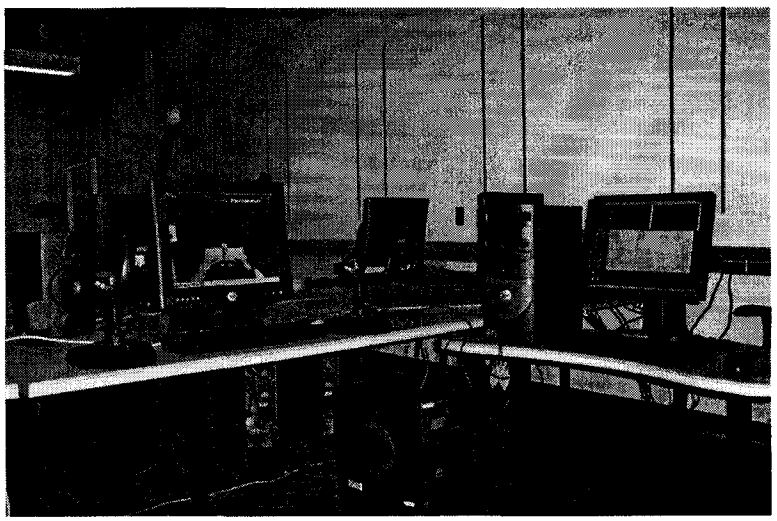

Figure 5.4 VR hardware setup running a simulation with steering and loader functions

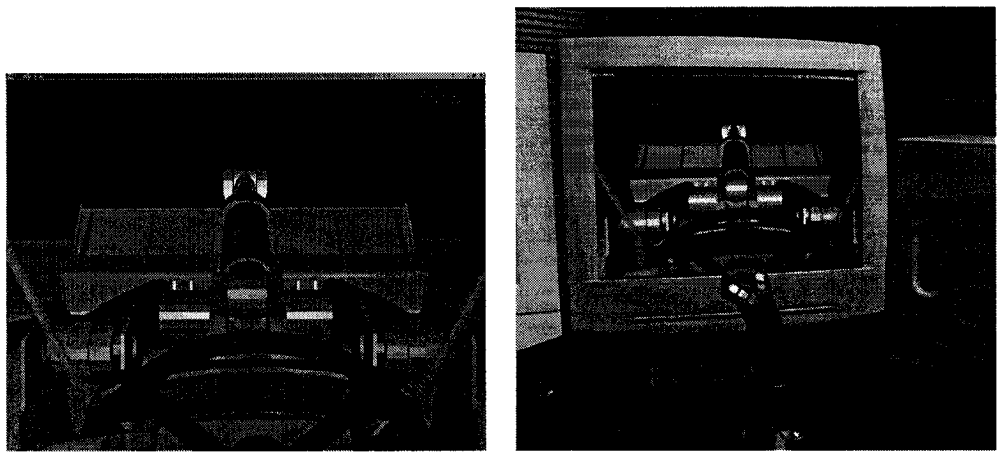

Figure 5.5 VR display from inside the operator's cabin

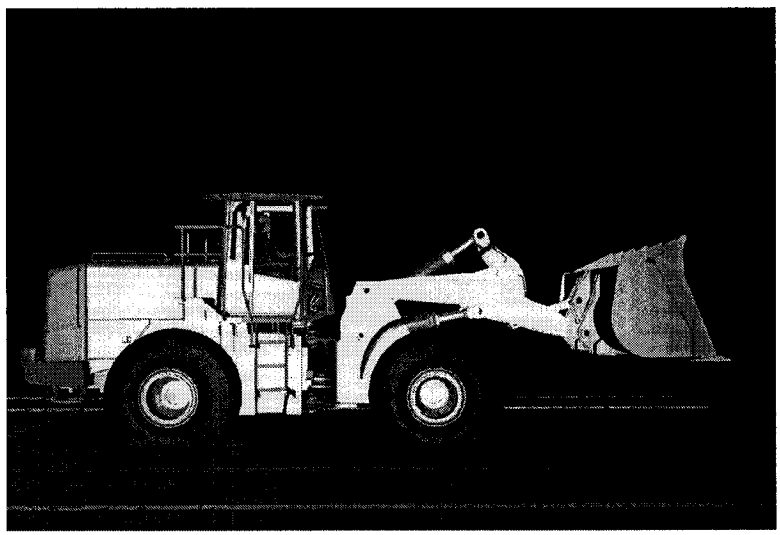

Figure 5.6 VR display from the side of the machine

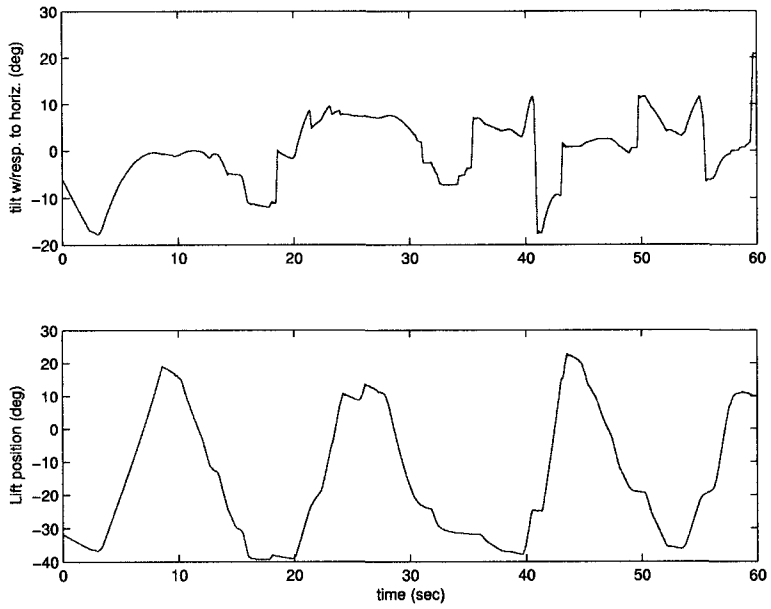

Figure 5.7 Output of the VR simulation controlled by a novice operator

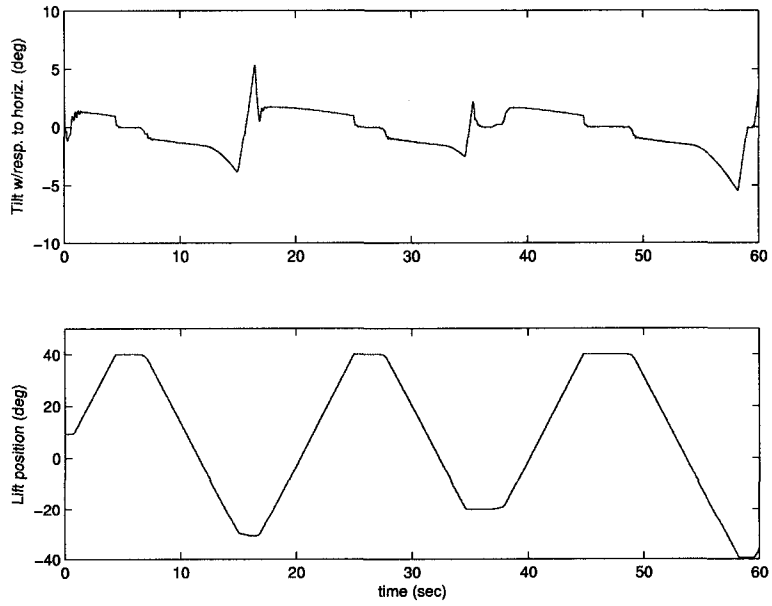

Figure 5.8 Output of the VR simulation with the level lift controller aiding the operator

CHAPTER 6. CONCLUSIONS AND FUTURE WORK

The research focus in this work was primarily on the development and validation of the real-time simulation capability for assessing open- and closed-loop performance of off-highway machinery using virtual reality environment and operator-in-the-loop interface. The overall scope of the research combines dynamic modeling, controller design (both linear and nonlinear), real-time simulation capability, operator controls, and VR interface. The idea was to develop a design tool that allows engineers to evaluate the design of construction machinery such as a wheel loader system without having to build a physical prototype which is often time consuming and costly. This research has demonstrated that the virtual prototyping concept can be effectively used to test the mechanical design, control design, and operator interface without having to build the physical machine. In particular, for this research, the test case of level lift control using human-in-the-loop configuration was used for the wheel loader in the virtual environment. The findings of this research are summarized in the ensuing sections of this chapter and some suggestions for future work are also presented.

6.1 Conclusions

The wheel loader system presented a challenging control design problem. The model of the wheel loader developed in this work was a fairly high fidelity model of the system. The resonant peaks in the frequency response of the open-loop system pose difficulties in the design of a robust controller. The nonlinearities and inherent dynamic coupling in hydraulics posed difficult challenges in obtaining robust linear design using traditional controllers such as PI control which is current industrial practice. It was demonstrated that the use of advanced control design concepts can provide significant improvement over existing controllers. The

implementation of these controllers in VR environment was accomplished to demonstrate their effectiveness.

The wheel loader model included a hydraulic system and linkage dynamics. The modeling effort resulted in a 13 state model. The entire model was created using MATLAB and Simulink. This allowed for a more convenient analysis and simulation process compared to using multiple packages designed for specialized components (i.e. hydraulics, linkages, etc.).

Linearization of the model allowed for analysis of the system and design of linear controllers. The model was linearized at an operating point representing typical level lift conditions. The linearization was unique in that the entire system was linearized at once rather than by combining linearized components from separate models as is commonly done in industry. An important result from analyzing the frequency response of the linear model was that high frequency peaks near 10 and 20 Hz could cause difficulties in obtaining a robust controller design. The linearized model was used for the linear controller designs which were verified through simulations on the nonlinear plant model.

Robust control design improved the robustness of the level lift control design. Compared to the PI control design, the stability robustness to an input uncertainty was improved using LQG and H_∞ control designs. Simulations showed superior resistance to under-damped oscillations with more advanced controller designs. The nonlinear feedback linearization based control design showed superior robustness compared to the linear control designs. The feedback linearization with an outer loop of H_∞ control gave an approximately 80% reduction in the peak of the maximum singular value plot of the robust stability condition. Adequate performance and robustness were also achieved with a proportional outer-loop controller as opposed to H_∞ controller.

Simulations showed that the response of the model was accurate and fast enough for real time execution. In addition to creating a model with an appropriate level of detail, the selection of a simulation time step was a critical factor in making sure that the simulation would run in real time. The simulation time step was selected based on analysis of the eigenvalues of the linear model. The step time was further reduced to ensure simulation accuracy with the

nonlinear model. Timing the simulation execution using a real time clock and comparing this to the simulation time showed that the model could run in real time.

The implementation of a VR simulation required the development of VR-specific modifications for the model. A joystick interface, timing system, and communication link were developed for the implementation. The joystick interface allowed the operator to directly control inputs to the model during a simulation using standard joystick hardware connected to the simulation computer. The timing system used the PC's real time clock to control the execution speed of the simulation to maintain synchronization of simulation time with real time. The communication link transferred linkage position information to the the VR display so that the operator could see the linkage position output of the simulation. All of these additions to the model made the real-time VR simulation possible.

The VR simulation enabled the designer to evaluate how the control system affects the operation of the machine with a human-in-the-loop interface. A clear improvement was seen in the ability to maintain the bucket levelled as the boom was raised and lowered by using the level lift control system to aid the operator. The simulation gave a realistic visualization of what it is like to operate a wheel loader linkage.

6.2 Future Work

There are several areas in which further improvements can be made and the fidelity of the VR simulation can be enhanced. A state estimator can be developed to estimate some of the unmeasured signals for the feedback linearization. In this work, cylinder pressures, the cylinder positions, and the supply pressure must be measured for the controllers based on feedback linearization. In contrast, only the cylinder positions were measured for the linear designs. Currently, pressures are difficult to predict.

The speed of the pump's margin pressure control response could be improved. Also, oscillations in the margin pressure could be reduced. To make these improvements, the output pressure of the pump could be controlled by electronically controlling the pump displacement rather than by relying on the current mechanical control system. Electronic pump control

included a system wide multi-variable control system could also improve position tracking performance. The simulations showed that the margin pressure often drops to low levels when high cylinder velocities are demanded. This causes a change in the pressure flow dynamics resulting in slower cylinder motion. While the margin pressure tracking performance is ultimately limited by the pump displacement, improvements could be made through controller design.

For future work, there are several ways the model, VR display, and controls could be improved. Addition of tire compliance dynamics would give the operator a more realistic view of how the machine's chassis reacts when the loader linkage is in motion. A drivable, entire vehicle model with digging capability would provide an even more realistic experience. A motion base could be developed so that the operator feels the accelerations of the machine which are a consequence of moving the loader linkage.

The most important step for the future work is to implement the controllers on real machinery. To do this, a few hurdles must be overcome. One is the conversion of the controllers to a discrete time form for implementation in a micro-controller. Standard techniques exist for accomplishing this[23]. The controller complexity may also need to be reduced using model reduction techniques[15] for practical implementation. Lastly, some additional functionality could be added to the joystick interface such as ability to switch modes such as turning the level lift controller on or off using a press button.

BIBLIOGRAPHY

[1] Grant, P., J.S. Freeman, R. Vail, and F. Huck, *Preparation of a Virtual Proving Ground for Construction Equipment Simulation.*, DETC98/DAC-5614, ASME Design Engineering Technical Conference, Atlanta, GA, 1998.

[2] Buzdugan, L., O. Balling, P. Lee, C. Balling, J.S. Freeman, and F. Huck, *Multirate Integration for Real-Time Simulation of Wheel Loader Hydraulics*, DETC99/VIB-8253, ASME Design Engineering Technical Conference, Las Vegas, NV, 1999.

[3] Bobrow J.E., F.C. Park, and S.R. Ploen, "A lie group formulation of robot dynamics," The International Journal of Robotics Research, 14(6), Pages: 609–618, 1995.

[4] Burl, J., *Linear Optimal Control*, Addison-Wesley, 1999.

[5] DiMaio, S.P., S.E Salcudean, C. Reboulet, S. Tafazoli, K. Hashtrudi-Zaad, "A virtual excavator for controller development and evaluation," Robotics and Automation, 1998. Proceedings, Pages: 52 -58 vol.1., 16-20 May, 1998.

[6] Fales, R., E. Spencer, A. Kelkar, "Robust Control Design for a Construction Machine Using LQG and H_∞ Based Methods," Submitted for review to: ASME Journal of Dynamic Systems, Measurement and Control, 2004.

[7] Nakamura, Y. and K. Yamane., "Dynamics computation of structure-varying kinematic chains and its application to human figures", IEEE Trans. on Rob. & Aut., 16(2), Pages: 124-134, 2000.

[8] Salcudean, S.E., K. Hashtrudi-Zaad, S. Tafazoli, S.P. DiMaio, and C. Reboulet, "Bilateral Matched-Impedance Teleoperation with Applications to Excavator Control," Control Systems Magazine, Vol.19, No.6, Pages: 29-37, Dec., 1999.

[9] Tafazoli, S., S.E. Salcudean, K. Hashtrudi-Zaad, P.D. Lawrence, "Impedance control of a teleoperated excavator," Control Systems Technology, IEEE Transactions on , Volume: 10 Issue: 3, Pages: 355 -367, May, 2002

[10] Zhang, R., A. Aleyne; E. Prasetiawan, "Modeling and H_2/H_∞ MIMO Control of an Earthmoving Vehicle Powertrain," ASME J. Dyn. Syst., Meas., Control, 124, Pages: 625-636, 2002.

[11] Yao, B., F. Bu, and G.C.T. Chiu, "Nonlinear adaptive robust control of electro-hydraulic systems driven by double-rod actuators," International Journal of Control, Vol.74, No.8, Pages: 761-775, 2001.

[12] Chen, C.T., *Linear System Theory and Design*, New York: Oxford University Press, 1999.

[13] Maciejowski, J.M., *Multivariable Feedback Design*, Workingham: Addison-Wesley, 1989.

[14] Merritt, H.E., *Hydraulic Control Systems*, New York: Wiley, 1967.

[15] Skogestad, S., I. Postlethwaite, *Multivariable Feedback Control Analysis and Design*, Chichester: John Wiley and Sons, 1996.

[16] Balas, G. J., J.C. Doyle, K. Glover, A. Packard, and R. Simth, *Mu (μ)-Analysis Toolbox, for Use with MATLAB*, Mathworks, Inc., MUSYN Inc., 2001.

[17] Fales, R., A. Kelkar, E. Spencer, F. Wagner, and K. Chipperfield, "Modeling and Control of a Construction Machine with a Human-in-the-Loop Assessment in Virtual Reality", IMECE2003-41597 ASME International Mechanical Engineering Congress and Exposition, Washington, DC, Nov., 2003.

[18] Jelali, M., A. Kroll, *Hydraulic Servo Systems: Modelling, Identification and Control*, London: Springer-Verlag, 2003.

[19] Kugi, A., *Nonlinear Control Based on Physical Models: electrical, mechanical and hydraulic systems*, London: Springer-Verlag, 2001.

[20] Ferreira, J.A., J.E. de Oliveira, V.A. Costa, "Modeling of Hydraulic Systems for Hardware-in-the-loop Simulation: a Methodology Proposal," International Mechanical Engineering Congress & Exposition Nashville, USA, 14-19 Nov., 1999.

[21] Schlegel C., M. Bross, and P. Beater, "HIL-Simulation of the Hydraulics and Mechanics of an Automatic Gearbox," 2nd International Modelica Conference, Oberpfaffenhofen, Germany, 18-19 March, 2002.

[22] W. R. Norris, "A Design Framework for Qualitative Human-in-the-loop System Development," Ph.D. Dissertation, University of Illinois Urbana Champagne, 2001.

[23] Phillips, C.L., H.T. Nagle, *Digital Control System Analysis and Design*, Englewood Cliffs, New Jersey: Prentice Hall, 1995.

[24] Freeman, J.S.,G. Watson, Y.E. Papelis, T.C. Lin, A. Tayyab, R.A. Romano, and J.G. Kuhl, "The Iowa Driving Simulator: An Implementation and Application Overview", SAE Paper 950174, 29 Dec., 1994.

[25] Chiriboga, J., M. Thein, E.A. Misawa, "Input-output feedback linearization control of a load-sensing hydraulic servo system," Control Applications, Proceedings of the 4th IEEE Conference on, Pages: 910 - 915, 28-29 Sept., 1995.

[26] W. Krus, "On Load Sensing Fluid Power Systems With Special Reference to Dynamic Properties and Control Aspects," Ph.D. Thesis, Linkoping University, 1988.

[27] B. Lantto, "On Fluid Power Control With Special Reference to Multiload Conditions in Load Sensing Systems," Ph.D. Thesis, Linkoping University, 1992.

ACKNOWLEDGEMENTS

I would like to thank Dr. Kurt Chipperfield, Denis Dorozhkin, Dan Robinson, Eric Spencer, Frank Wagner for their assistance, contributions, and suggestions during my dissertation work. Also, I would like to thank Dr. Tye Conlan and John Deere for supporting the project. I would also like to thank all of the people at the Virtual Reality Applications Center (VRAC) for all of their support of my work. Thanks go to my committee, Dr.'s James Bernard, Greg Luecke, Murti Salapaka, Brian Steward, and Judy Vance, for inspiration and helpful suggestions and advice. Most of all, I appreciate the helpful guidance of my major professor, Dr. Atul Kelkar.